Fall 1-13-2019

Development of a Novel Electroless Plating Approach for Coating Aluminum (Al) on Multi-Walled Carbon Nanotubes (MWCNTs) and Investigating their Use in Reinforcing Cast and Powder Compacted Aluminum Composites

Mohammed Elsharkawi
The American University in Cairo

THE AMERICAN UNIVERSITY IN CAIRO
الجامعة الأمريكية بالقاهرة

School of Sciences and Engineering

Development of a Novel Electroless Plating Approach for Coating Aluminum (Al) on Multi-Walled Carbon Nanotubes (MWCNTs) and Investigating their Use in Reinforcing Cast and Powder Compacted Aluminum Composites

A Thesis Submitted to

The School of Sciences and Engineering, Department of Mechanical Engineering, The American University in Cairo

In partial fulfillment of the requirements for the degree of
Master of Science in Mechanical Engineering

By

Mohammed Taha Elsharkawi
Bachelor of Mechanical Engineering

Under the supervision of
Dr. Amal Esawi
Professor, The Department of Mechanical Engineering
The American University in Cairo

December 2018

THE AMERICAN UNIVERSITY IN CAIRO
الجامعة الأمريكية بالقاهرة

School of Sciences and Engineering

Development of a Novel Electroless Plating Approach for Coating Aluminum (Al) on Multi-Walled Carbon Nanotubes (MWCNTs) and Investigating their Use in Reinforcing Cast and Powder Compacted Aluminum Composites

By
Mohammed Taha Elsharkawi

A thesis submitted in partial fulfillment of the requirements for the degree of
Master of Science in Mechanical Engineering

Under the supervision of:
Dr. Amal Esawi
Professor, Department of Mechanical Engineering
The American University in Cairo

December 2018

Dedication

To my beloved **Father** and **Mother**

Who provided me with endless support and love through the different stages of my life.

Abstract

Due to their superior mechanical properties, Aluminum-Carbon Nanotube (Al-CNT) composites have been widely investigated by various researchers using several processing techniques. One of the most successful techniques in creating Al-CNT composites is the ball milling technique followed by hot compaction and hot extrusion for powder consolidation. However, this technique has some drawbacks including the limited design flexibility of the produced parts, the high initial cost of milling equipment, and the damage of CNTs during milling that has been reported to take place due to the harsh impact of milling balls on CNTs leading to the formation of brittle Al_4C_3 phases in the aluminum matrix with the increase of milling time. Therefore, researchers have investigated simple, cheap and flexible casting techniques in producing Al-CNT composites. However, it was found that CNTs are not wettable in molten aluminum due to the big difference in surface tension between them. Besides, CNTs have a lower condensed phase density than aluminum. Therefore, they tend to form segregations in the aluminum matrix that hinder the mechanical properties of the entire composite. Therefore, some researchers have experimented coating CNTs with metals by electroless plating to modify their surface characteristics and make them wettable with molten aluminum. However, these metallic coats were found to have a misleading alloying effect on the aluminum matrix that made the investigation of CNTs addition on aluminum not viable. In the current study, a novel aluminum electroless plating approach was developed and made it possible to cover CNTs with a nano-crystalline layer of pure aluminum at room temperature. The Al-coated CNTs are used as a reinforcement phase for pure aluminum without introducing any alloying elements. Previously, aluminum electroless plating in aqueous solutions represented an impossible challenge due to the high electrode potential of aluminum (-1.66 E(V)) that lies outside the electrochemical window (EW) of water. Therefore, limited number of trials have been made towards developing room temperature ionic liquids (RTILs) of a wide EW suitable for aluminum electroless plating. Researchers have focused on expensive RTILs such as $AlCl_3$-EMIC that has a wide electrochemical window allowing aluminum to be deposited without decomposing the ionic compound. However, due to the high surface area to volume ratio of CNTs, they require a larger volume of the RTIL to be electroless plated. This could put Al-coated CNTs at a tremendously high cost of production. Therefore, the current study focused on finding an alternative cost effective RTIL for aluminum electroless plating by modifying $AlCl_3$-Urea battery electrolyte. This modification was done by adjusting the molar ratio of $AlCl_3$-Urea from 1.3:1 to 2:1 in addition to adding lithium aluminum hydride

(LAH) as a reducing agent. The electrochemical window of the new electrolyte was measured against a standard Ag/Ag+ electrode and reported to be wider than the requirement of aluminum plating. This modified RTIL was used to coat MWCNTs (~10 nm diameter) by aluminum in 3 steps starting by catalyzing CNTs using colloidal palladium-stannous (Pd-Sn) nanoparticles in a single step followed by an acceleration step in a group of acids to remove excess stannous hydroxide $Sn(OH)_2$ from the surface of Pd-Sn particles. Finally, electroless plating of Al on CNTs was done in the developed RTIL. Electron microscopy imaging revealed that CNTs had up to 160 nm increase in their thickness after deposition indicating the formation of Al-coat on their surfaces. Energy dispersive X-ray (EDX) analysis along with the X-ray diffraction (XRD) pattern confirmed the presence of crystalline Al on the surface of CNTs. The Raman analysis revealed that CNTs did not undergo any damage during the chemical coating process as the D-band to the G-band intensity ratio of Al-coated CNTs did not differ from the one reported for the as-received CNTs. The prepared Al-CNT powders were used to reinforce pure aluminum using both the casting and hot compaction techniques such that the overall percent of CNTs in the final composite were 2% by weight in each sample.

The XRD of bulk samples detected the presence of all the crystallographic planes of aluminum in addition to small spikes of Al_4C_3 in both cast and powder compacted samples. Raman analysis showed that a small increase in the D-band took place in both the cast and the hot compacted samples. However, the D-band was higher in the hot compacted sample than in the cast sample. Mechanical properties of the obtained Al-CNT composites were investigated for both the hot compacted-hot extruded samples and the cast samples. The coated layer of aluminum on CNTs resulted in excellent dispersion and wettability of CNTs in the cast sample reflected on the homogeneous mechanical properties obtained with a minimal standard error (SE) and on the SEM fractography imaging obtained for each sample. The mechanical testing showed an increase of 353.4 %, 338.7 %, and 266.1 % in the tensile strength, Vickers hardness, and nanoindentation hardness of the reinforced cast sample in addition to an increase of 164.8 %, 147.2 %, and 165.8 % of the same properties for the hot compacted-hot extruded reinforced samples respectively. These promising results will open the road for producing low cost, design flexible, and fast to produce Al-CNT composites with enhanced mechanical properties.

Acknowledgement

In the beginning, I would like to start my thesis by being thankful to my lord and my creator "Allah" for giving me the power and passion to innovate in my research work. I thank him for putting me in situations where I met all the wonderful people who facilitated the process of learning at the American University in Cairo (AUC).

I would like to express my deep thanks to Prof. Dr. Amal Esawi the supervisor of my thesis work. I am deeply indebted to her for giving me the guidance, constructive feedback, and motivation during supervising on my work. I remember the nights she stayed too late to revise my work and give me feedback. I am truly thankful to her for facilitating my research work through putting a part of her research budget in providing me with a full access to the research equipment I needed in the mechanical engineering labs as well as the Yousef Jameel Science and Technology Research Center (YJ-STRC) at the AUC.

I would like to thank Prof. Dr. Adham Ramadan and Prof. Dr. Pakinam Askalani from the chemistry department for teaching me how to be persistent in learning. They made complex subjects fun to learn with their exceptional teaching skills. They made me believe that despite of having a mechanical engineering background, I can definitely learn and get use of other fields of science in producing an extraordinary work in my own field.

Also, I am truly indebted to the office of the dean of graduate studies and research at the AUC for providing me with the laboratory instruction fellowship as well as the graduate merit fellowship needed to cover my tuition fees. I am also truly grateful to them for the research and conference grants they gave to me.

As an external source of funding, I would like to express my sincere appreciation to Al-Alfi foundation for covering my tuition fees in Fall 2016 and spring 2017.

Aside from the academia, I would like to thank Engineer Magdy Elkady from the Plating of Plastics (POP) industry for making my eyes open on the industrial catalyzation systems that I applied in my research and came out innovative, cost effective and time saving.

Finally, there is nothing I can do to express my gratitude towards my parents. You have put all your effort in making a better version of me through the good times and the bad. You have given me an unconditional support and love. Thank you for everything.

Mohammed Elsharkawi

2018

Table of Contents

List of figures

List of tables

List of Equations

List of abbreviations

Abbreviation	Meaning
MMCs	Metal Matrix Composites
Al-CNT	Aluminum Carbon Nanotube
CNTs	Carbon nanotubes
HIP	Hot Isostatic Pressing
SPS	Spark Plasma Sintering
MWCNT	Multi-Wall Carbon Nanotube
SWCNT	Single-Wall Carbon Nanotube
EW	Electrochemical Window
Rochelle salt	Potassium sodium tartrate tetrahydrate
RTIL	Room Temperature Ionic Liquid
EMIC or $[Emim]^+ [Cl]^-$ or $[C2mim]^+ [Cl]^-$	1-ethyl-3-methylimidazolioum chloride
DIBAH	Diisobutylaluminum Hydride
LAH	Lithium Aluminum Hydride
THF	Tetrahydrofuran
wt.%	Weight percent
Vol%	Percent by volume
MF	Microfiltration
IPA	Isopropanol
SEM	Scanning Electron Microscopy
SPM	Scanning Probe Microscopy
TEM	Transmission Electron Microscopy
EDX	Energy Dispersive X-ray
XRD	X-Ray Diffraction
CVD	Chemical Vapor Deposition
DC	Direct Current
A	Amperes
SE	Standard Error

1. Introduction

In the last decade, the research demand on producing Al-CNT composites has grown rapidly due to their superior mechanical properties and potential use in light weight aerospace and automotive applications.

The use of CNTs in composite materials have been hampered by the presence of van der Waals forces that keeps CNTs agglomerated and makes their dispersion in different matrices a challenging task.[1] Therefore, different approaches were used to improve the dispersion of CNTs in the aluminum matrix. Most of the researchers have focused on producing Al-CNT composites by powder metallurgical approaches such as high energy ball milling followed by hot compaction and hot extrusion for the consolidation of the produced composite Al-CNT powders.[2]–[8] Despite of the excellent dispersion these techniques have achieved for CNTs in the aluminum matrix, many drawbacks could be noticed on the produced Al-CNT composites including a reduction in the quality of CNTs represented in the formation of Al-carbides not only on the surface of CNTs but also inside the aluminum matrix.[9]–[11] These carbides have led to an undesirable drop in the fracture toughness of Al-CNT composites.

Processing of Al-CNTs in the powder form also involved a high investment cost, limited part size and complexity, high cost of raw aluminum powder compared to wrought pure aluminum, and high cost of tools and dies.[12], [13] Therefore, researchers have kept an eye open on implementing Al-CNT composites via much simpler and cost effective techniques such as metal casting. However, molten aluminum was found to possess a surface tension that is 19 time higher than CNTs causing a poor wettability of CNTs when introduced in molten aluminum.[14] Therefore, researchers have investigated the electroless plating of CNTs by copper, nickel-phosphorous (Ni-P), or silver to improve their wettability and dispersion in the molten aluminum.[15]–[19] However, these foreign metallic elements were found to impart an alloying effect on the pure aluminum matrix which might mislead the investigation of CNTs as a reinforcement for pure aluminum.[15] To suppress these alloying effects, the current research has focused on providing pure aluminum coating on CNTs prior to their dispersion as a reinforcement phase in molten aluminum and well as in aluminum powder. Previously, researchers have carried aluminum electroless plating on different substrates using 1-ethyl-3-methylimidazolium chloride-aluminum chloride (EMIC-$AlCl_3$) as a room temperature ionic liquid (RTIL) in addition to diisobutylaluminum hydride (DIBAH) in toluene as a liquid

reducing agent.[20]–[22] However, the high cost of EMIC as an ionic liquid does not enable the use of this approach in coating CNTs (high surface area to volume ratio) that require bigger volumes of the prepared ionic liquid to be completely coated with aluminum. Therefore, a new novel low cost aluminum electroless plating technique was invented by using $AlCl_3$-Urea RTIL that is at least 41 times lower in the cost than $AlCl_3$-EMIC. The reducing agent used was Lithium Aluminum Hydride (LAH). The brand new electrolyte has enabled the conformal coating of aluminum on CNTs prior to their introduction in aluminum matrices and investigating the improvement of mechanical properties in the final composite.

2. Literature background

2.1 History of Carbon Nanotubes

The invention of carbon nanotubes (CNTs) is credited to the Japanese researcher Sumio Lijima in 1991 after synthesizing hollow carbon nanotubes using the arc discharge method.[23] At that time, an increased awareness of this novel structure started to spread worldwide pointing on the potential novel properties and applications that can be discovered for CNTs. In 1992, researchers at MIT theoretically investigated the electric properties of single walled CNTs.[24]–[26] And in 1993, single-walled CNTs were characterized and discovered.[27] In addition, a method of producing them via transition metal catalysis was introduced.[28]

Afterwards, wide investigations of the physical properties of CNTs have taken place. These investigations have shown a great potential in the use of these novel nanostructures in electronic devices, metal composites, polymer composites, and biological applications.

2.2 Structure, bonding, and chirality of CNTs

Naturally occurring carbons such as diamond and graphite have totally different properties even though they are both consisted of carbon. Diamond is known as a transparent material possessing excellent electric insulation characteristics, while graphite is known as an opaque material with superior electric conductivity.[29] These differences conclude that the way carbon atoms are arranged and bonded in a lattice determines the key features of carbon materials. Unlike diamond and graphite, CNTs and graphene sheets are human made carbons that were designed and synthesized for the purpose of possessing special characteristics that are tailored for different applications.[30]

Carbon has six electrons as shown in Figure 2-1. In its ground state, two of these electrons (core electrons) are located in the 1*s* state near the nucleus. These two electrons are strongly bonded to the nucleus and they never participate in any chemical reaction.

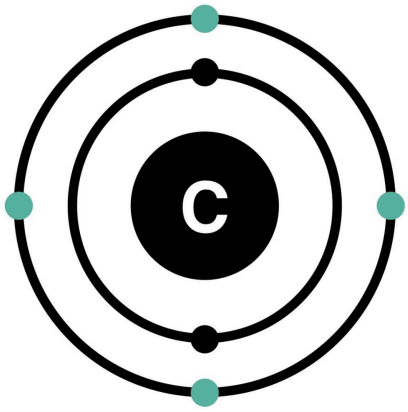

Figure 2-1 An illustration of electrons in a carbon atom.[31]

The other four electrons of a carbon atom are valent electrons located in the $2s$ and $2p$ orbitals. In the excited state of carbon, one electron from the $2s$ orbital moves to occupy the $2p_z$ orbital.[32] When two carbon atoms combine in a lattice, carbon atoms hybridize to reach a stable state and form molecular orbitals. In the case of graphene, carbon atoms are covalently boned by sp^2 hybridization.[33] Figure 2-2 illustrates the electron configuration during the sp^2 hybridization of a carbon atom.

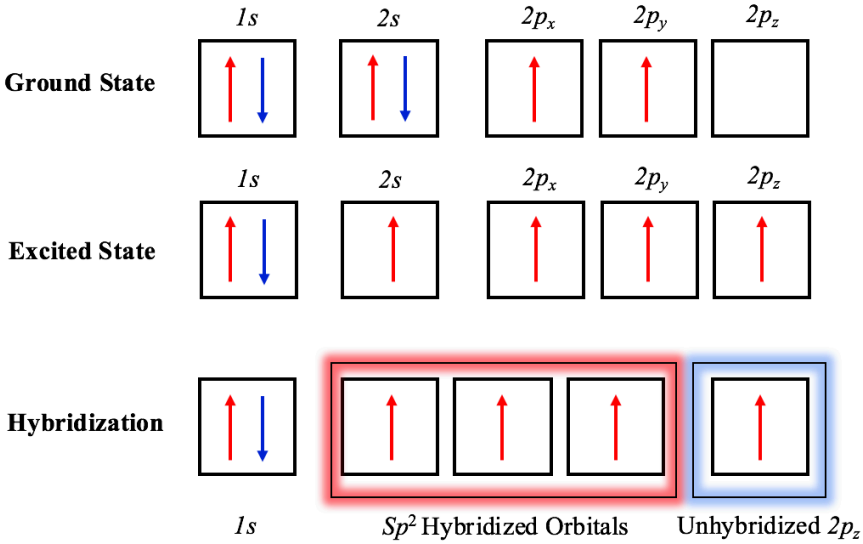

Figure 2-2 Electron configuration of carbon in the ground state, excited state, and after hybridization.[32]

When two sp^2 hybridized atoms overlap, a covalent σ bond is formed.[34] In a honeycomb lattice, three σ-bonds are formed for each carbon atom as a result of the hybridization with three of the nearby carbon atoms as represented in Figure 2-3. In addition, one π-bond is formed as a result of the electron existing in the unhybridized $2p_z$ orbital. The π-orbitals existing over each carbon atom overlap with the neighboring π orbitals. These free delocalized π-electrons give graphene superior electric conductivity.

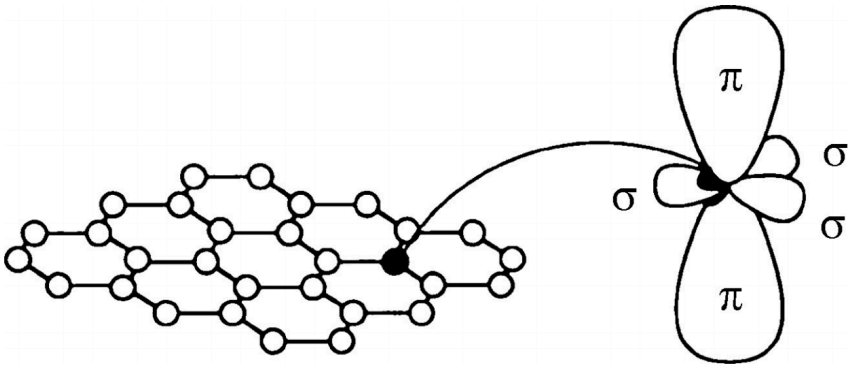

Figure 2-3 σ and π orbitals of a carbon atom in a honeycomb lattice of graphene.[34]

A single wall carbon nanotube (SWCNT) can be formed by rolling a graphene sheet to form a seamless cylinder as illustrated in Figure 2-4.[35]

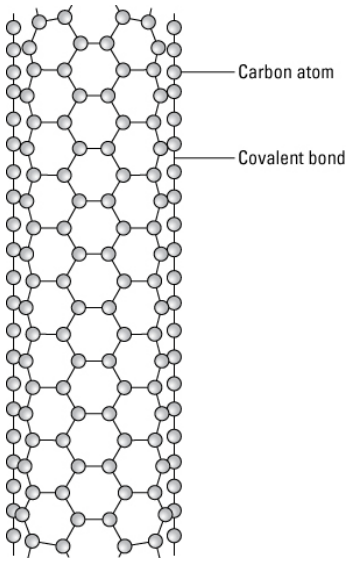

Figure 2-4 A representation of rolling a graphene sheet to form a SWCNT.[35]

There could be many configurations of rolling a graphene sheet to form a CNT as shown in Figure 2-5. When a graphene sheet is rolled towards the chiral axis $\vec{C}$, a nanotube is formed with a circumference that is equal to the length of $\vec{C}$ given in Equation 2-1.

$$\vec{C} = n\vec{a}_1 + m\vec{a}_2 \qquad \text{Equation 2-1}$$

Where $\vec{a}_1$and $\vec{a}_2$ are the vectors of the lattice translation, while (n, m) are integers.[3]

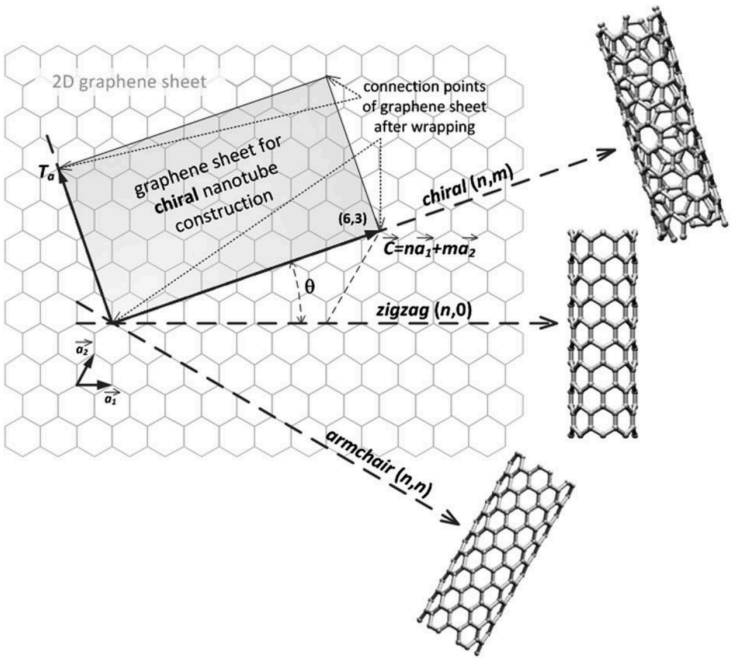

Figure 2-5 The concept of CNTs formation from a sheet of graphene along the chiral victor $\vec{C}$.[36]

The diameter of a CNT depends on the values of (n, m) as given in Equation 2-2.[3]

$$D = \frac{a\sqrt{n^2 + m^2 + nm}}{\pi} \qquad \text{Equation 2-2}$$

Where a is the lattice vector that has a value of 2.46 Å. When $n = m$, "Armchair" CNTs are formed. While "Zigzag" CNTs are formed when either m or n is equal to zero.[3] For better visualization, Figure 2-6 compares the different orientations of graphene lattices before and after being rolled in order to highlight the different configurations of CNTs. The CNT axis is the axis around which a graphene sheet is rolled.

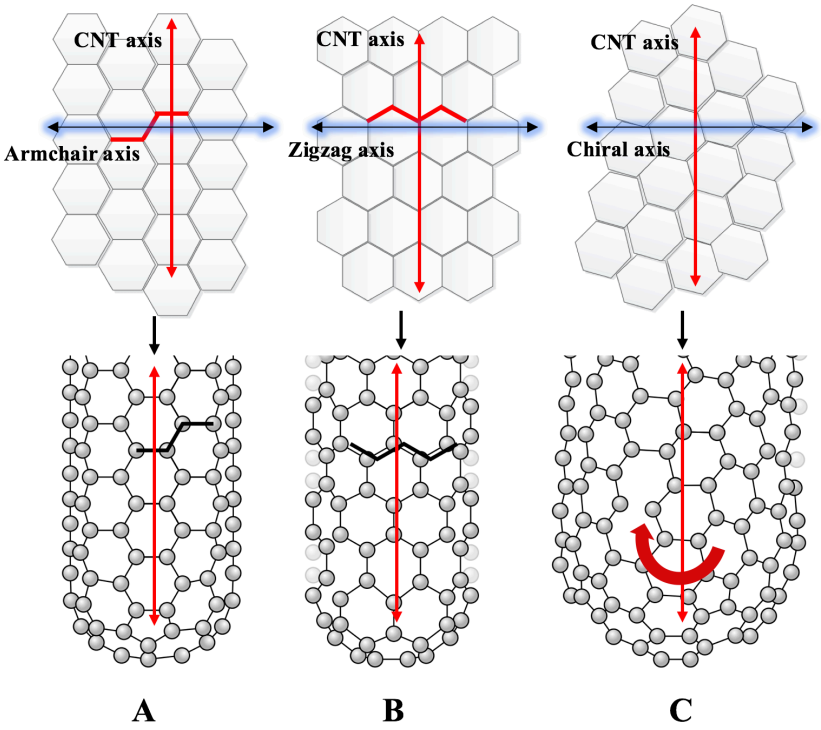

Figure 2-6 Different configurations of a CNT A) armchair B) zigzag C) chiral.[35], [37]

When multiple concentric SWCNTs coexist inside each other, a multi-wall carbon nanotube (MWCNT) is formed as shown in Figure 2-7.

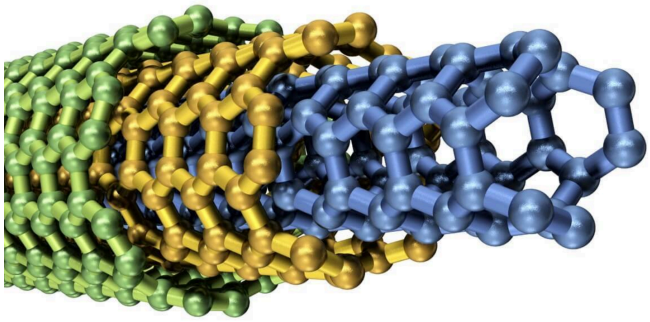

Figure 2-7 An illustration of MWCNT.[38]

The diameter of SWCNTs is few nanometers while that of MWCNTs is several tens of nanometers. MWCNTs typically have lengths in the micron range. A simple example for a MWCNT is a Double-Wall CNT (DWCNT) as illustrated in Figure 2-8.

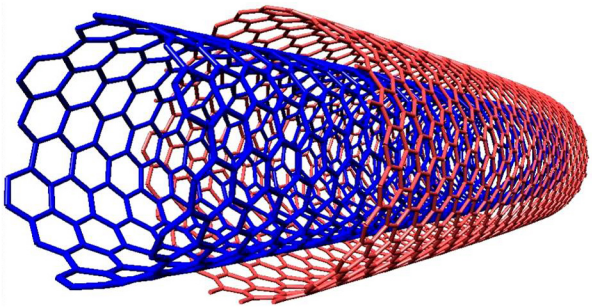

Figure 2-8 Double-Wall Carbon Nanotube (DWCNT).[39]

2.3 Properties and applications of CNTs

Due to their structural integrity, CNTs possess extraordinary mechanical, electrical, optical, and thermal properties that make them attractive in many applications.

2.3.1 Mechanical properties

The strong σ bonds between carbon atoms in CNTs render them with the highest Young's modulus and tensile strength ever found.[40] When a tensile load was applied on different MWCNTs placed between AFM tips as shown in Figure 2-9, tensile strengths of 11-63 GPa and Young's moduli in the range of 270-950 GPa were observed.[41]

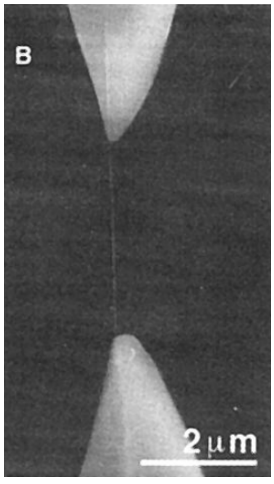

Figure 2-9 A MWCNT between two AFM tips.[41]

In 2007, a study showed that the Young's modulus of MWCNTs produced by arc discharge is 955 GPa.[42] In 2008, another study demonstrated the dependence of Young's modulus and tensile strength of MWCNTs on their outer-shell chirality. A tensile strength up to 110 GPa

and a modulus of elasticity up to 1.1 TPa were observed.[43] CNTs are not only strong but also light. In 2009, the density of condensed phase CNTs was measured and reported for the first time at 1.74 ± 0.16 g/cm^3.[44] To establish a fair comparison between the strength of CNTs and other materials, the density of each material has to be taken into consideration. Figure 2-10 compares CNTs, Kevlar, carbon fiber, mild steel, and pure aluminum based on their specific strength (ultimate strength/density) values. The figure concludes that CNTs have a specific strength that is around 19 times higher than carbon fiber and 2500 times higher than aluminum. This makes CNTs superior as a reinforcement for polymer matrix composites (PMCs) and metal matrix composites (MMCs).[3], [45]

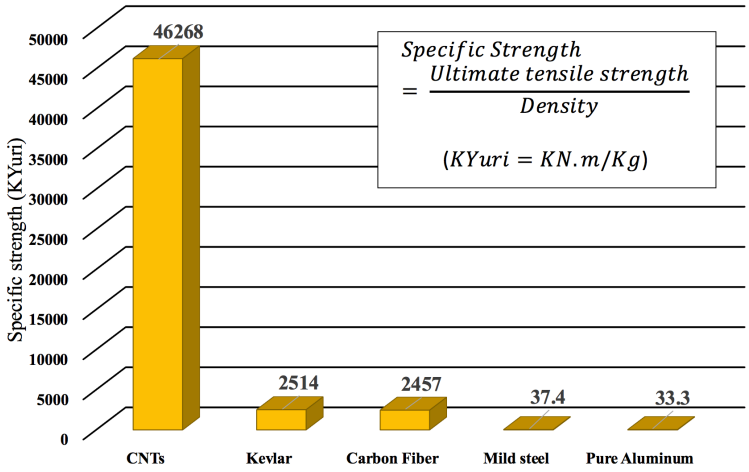

Figure 2-10 Strength to density ratio of CNTs compared to Kevlar, carbon fiber, mild steel, and pure aluminum. [41], [46]–[49]

The high aspect ratio (length to diameter) of CNTs makes them stiff. This means that CNTs have a high elasticity. When a compression force was applied on CNTs using AFM tips, CNTs were bent and after the force was released, they went back to their original shape.[50] The percentages of elongation at break for zigzag and armchair CNTs were reported to be 16% and 24% respectively.[51] The combination of these properties makes CNTs applicable as a probe material for scanning probe microscopy (SPM).[52], [53]

2.3.2 Electrical properties

CNTs possess a superior electric conductivity of around 1850 Scm^{-1} measured at a current density of 10^7 A/cm^2.[54] The conductivity of CNTs was reported to be a function of their diameter and chirality. All armchair CNTs and other types of CNTs of $n - m = 3K$ have a metallic electric behavior. While the other types are semiconducting.[3] The most conductive type of CNTs is the SWCNT ropes that happen to have a resistivity of 10^{-4} Ohm.cm.[55] SWCNTs can handle a current density up to 4×10^9 A/cm^2.[56] Therefore, CNTs are

considered good electron field emitters. CNTs were also found suitable for flat panel displays because of their high electrical conductivity, nano-size, structural integrity, and chemical stability.[57], [58]

Certain types of SWCNTs have defects. These defects make them applicable as transistors.[59], [60] In the same manner, combining two or more CNTs together may form a good transistor. When a CNT has a metallic and semiconducting nature (a part of it is metallic and the other part is semiconducting), a rectifying diode can be formed.[61]

2.3.3 Optical properties

The absorption of laser and the Raman response of CNTs makes them easy to characterize in a non-destructive manner. CNTs are characterized by two important Raman peaks. The intensity of these peaks determines different information about the level of crystallinity and disorders in CNTs. This means that non-tubular structures of carbon can also be detected. The Raman peaks are also useful in determining the chirality of CNTs. The G-band is a characteristic peak for the C-C vibrational modes in sp^2 hybridized carbons such as graphene and CNTs. Whereas, the D-band is a characteristic peak for the defects introduced in the structure. Therefore, the ratio between the intensity of the D-band (I_D) to the intensity of the G-band (I_G) determines the disorder and defects of CNTs.[62]–[64] In research related to composite materials, CNTs are functionalized by acids to introduce more defects and increase their dispersion in different matrices.[65]–[67] Figure 2-11 illustrates the difference in the G-bands and the D-bands of CNTs before and after functionalization. The D-band increases after acid attacking of CNTs indicating the increase of defects.[68]

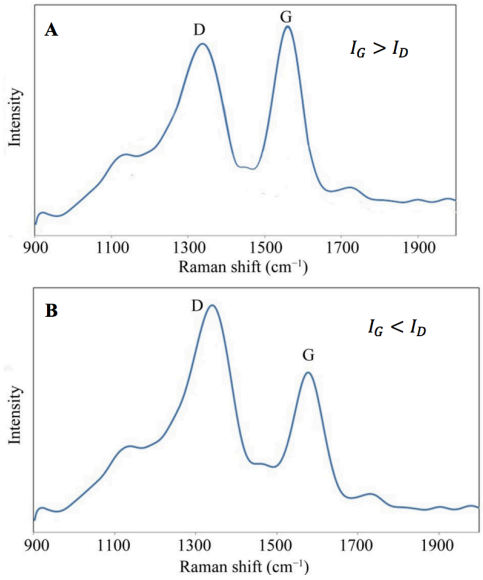

Figure 2-11 Difference in G-bands and D-bands of CNTs A) before acid functionalization and B) after acid functionalization.[68]

2.3.4 Thermal properties

Individual SWCNTs are known for their high thermal conductivity along their axis. The room temperature thermal conductivity of individual SWCNTs was reported to be 3000 $W.m^{-1}K^{-1}$.[69] On the other hand, the radial direction of SWCNTs exhibits a much lower thermal conductivity of 1.52 $W.m^{-1}K^{-1}$.[70] When CNTs were assembled in the form of fibers or films, their overall thermal conductivity was reported to be 1500 $W.m^{-1}K^{-1}$.[71] Defects decrease the thermal conductivity of CNTs as they introduce phonon scattering and shorten the mean free path.[72] The superior thermal conductivity of CNTs leads to their consideration as heat sinks for microchips.[73]

Due to the sp^2 hybridization of carbon atoms that results in strong covalent bonding, CNTs have low thermal expansion coefficient. In addition, CNTs were proven to be thermally stable at 2800 $°K$ in vacuum and at 700 $°K$ in air.[74]

2.3.5 Chemical properties

When the behavior of CNTs as a hydrogen adsorbent was studied, it was discovered that SWCNTs exhibit an extraordinary reversible adsorption of hydrogen on their surface. This phenomenon grabbed the attention to the possibility of using CNTs as a high capacity storage tank for hydrogen.[75]

2.4 Synthesis of CNTs

Several synthesis techniques have been investigated to produce sizable amounts of CNTs in a scalable manner. The most reported methods in producing CNTs include arc discharge, electrolysis, chemical vapor deposition (CVD), hydrothermal/sono-chemical techniques, and laser ablation as illustrated in Figure 2-12.

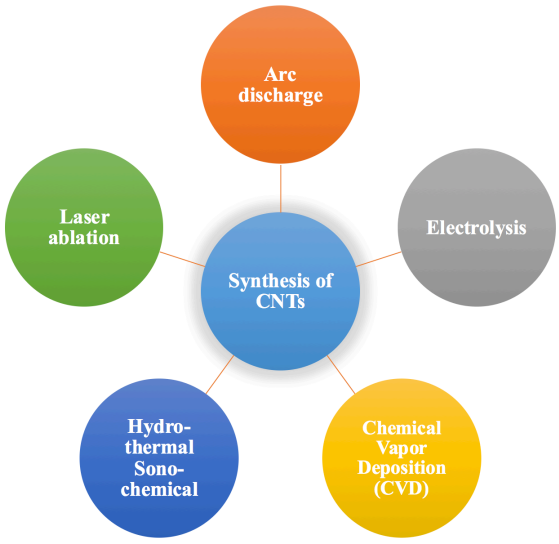

Figure 2-12 Synthesis techniques of CNTs.[36]

2.4.1 Arc discharge method

During an experiment to produce fullerenes via arc discharge, it was unintentionally discovered that both DWCNTs and MWCNTs can be produced by this technique.[23] The arc discharge apparatus consists of a vacuum chamber inside which two graphite electrodes are placed vertically as shown in Figure 2-13.

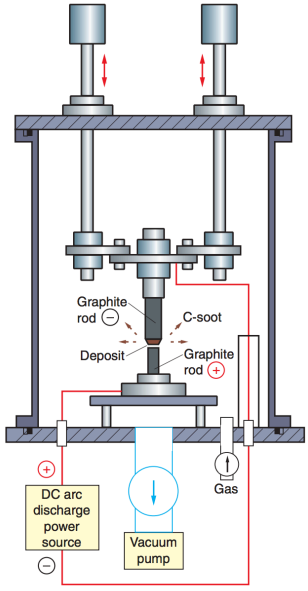

Figure 2-13 Arc discharge apparatus for the production of CNTs.[76], [77]

To synthesize CNTs by arc discharge, a vacuum chamber was evacuated and filled with an inert gas. Afterwards, a DC current of 100 A was applied between two graphite electrodes that were vertically placed in the chamber. Fullerenes were produced in the form of a soot inside the chamber due to the consumption of the anode. However, part of the anode was evaporated and deposited on top of the cathode electrode. This deposit is known as the cathode deposit inside which CNTs exist.[78] The CNTs were found to exist in region B of the deposit as shown in Figure 2-14. While region A is the cathode tip, Region D is a hard layer of graphite, layer C shows the part of the deposit facing the anode, and d is the overall thickness of the deposit.

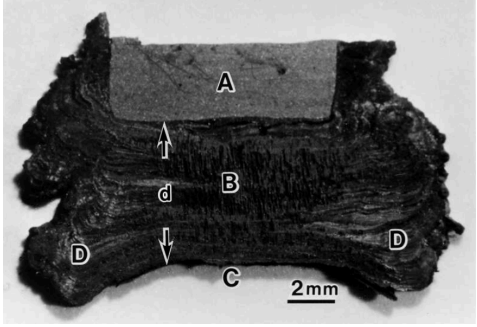

Figure 2-14 The cathode deposit of an arc discharge approach.[78]

SEM micrographs showed the existence of carbon nanotubes and graphite particles as shown in Figure 2-15

Figure 2-15 Carbon nanotubes and graphite nanoparticles grown by arc discharge.[78]

The arc discharge method was found to produce high quality double-walled CNTs and multi-walled CNTs of different diameters as shown in *Figure 2-16*. The length of the produced CNTs was observed to reach up to 50 μm.

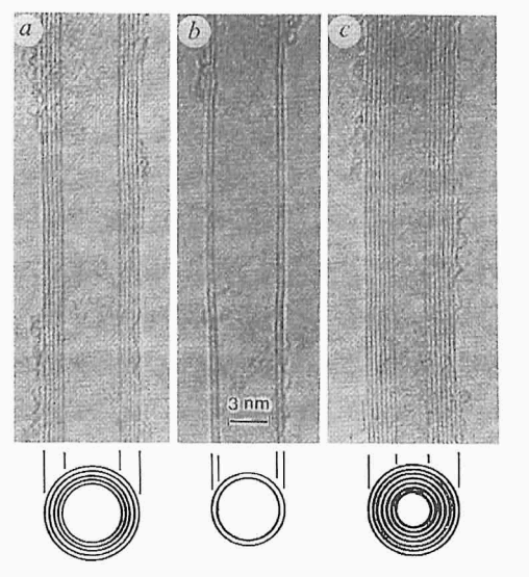

Figure 2-16 TEM micrographs of Double-Wall and Multi-Wall CNTs discovered originally by Lijima in 1991.[23]

2.4.2 Chemical Vapor Deposition (CVD)

Chemical Vapor Deposition (CVD) is the most common technique used for producing CNTs in large quantities at a low cost. It relies on chemical reactant gases that are introduced inside a vacuum chamber inside which a heated substrate coated by catalytic nanoparticles is placed. CNTs grow on top of the catalytic nanoparticles while the byproducts of the reactants are purged outside the reaction chamber. A typical CVD reactor for CNTs is shown in Figure 2-17

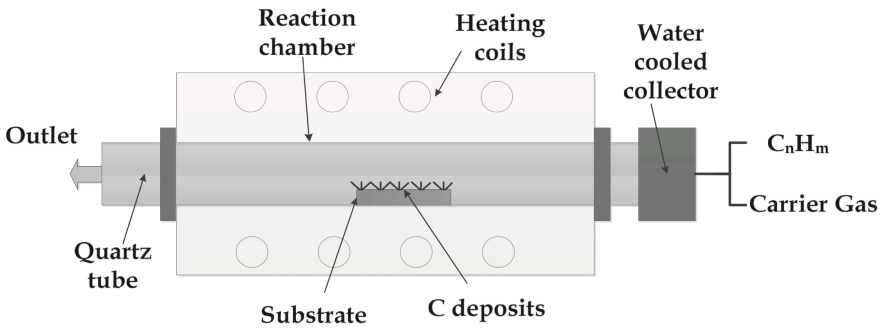

Figure 2-17 A typical setup for CVD growth of CNTs.[37]

The synthesis of CNTs takes place over a substrate that is heated in a range of 550-750 ℃. The main reactant gases used for the catalytic CVD of CNTs are acetylene (C_2H_2) or ethylene (C_2H_4) mixed with argon(Ar) or nitrogen(N_2) as carrier gases. During the reaction on top of the heated catalyzed substrate, carbon decomposes on the edges of the catalytic particles growing CNTs that can be formed under the catalytic particles (Base growth) or on top of the catalytic particles (Tip growth).[79], [80] Figure 2-18 (A-B) illustrates the difference between base and tip grown CNTs. The diameter of the catalytic particles (such as Fe or Co) is a key factor in determining the diameter and type of the nanotube whether it is going to be a SWCNT or a MWCNT as demonstrated in Figure 2-18 (C).[37]

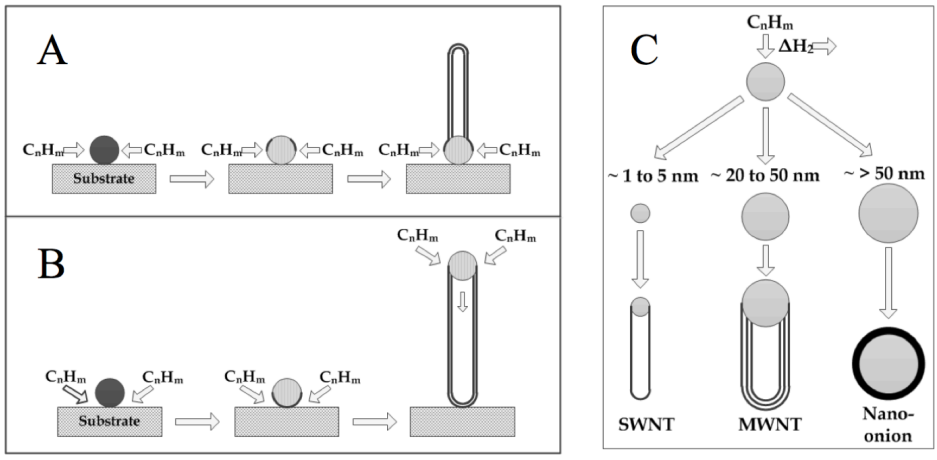

Figure 2-18 Growth mechanisms of CNTs by (A) base growth, (B) tip growth, and (C) effect of the catalyst particle size on the structure of CNTs.[37]

The CVD technique produces MWCNTs with a good quality. However, CVD produced CNTs sometimes suffer from poor graphitization. Figure 2-19 shows an SEM image of MWCNTs produced by CVD.

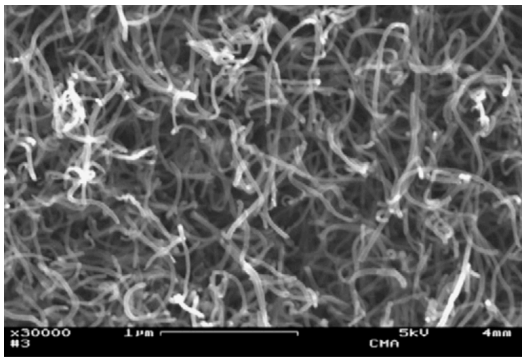

Figure 2-19 SEM image of grown MWCNTs by CVD using 10% C_2H_2/N_2.[81]

2.4.3 Laser ablation method

This technique uses a high power YAG type laser to vaporize carbon from a graphite target placed in a quartz tube inside a furnace that is heated at 1200℃ as represented in Figure 2-20. The ablated carbon is collected on a water cooled collector at which CNTs start to grow.[82]

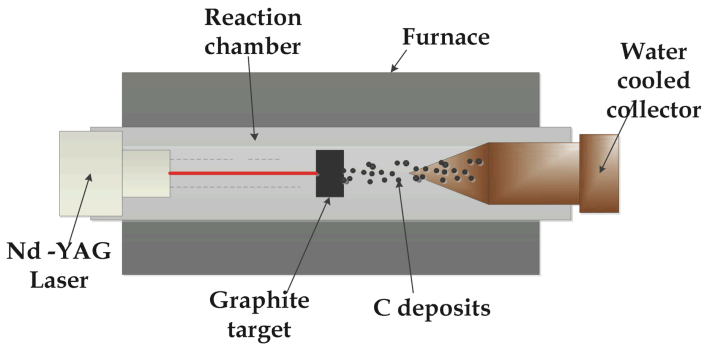

Figure 2-20 Synthesis of CNTs by laser ablation.[37]

Small amounts of Ni and Co are added to the graphite target to promote the growth of CNTs on the water cooled collector.[55] This technique produces ropes of bundled SWCNTs as shown in Figure 2-21.

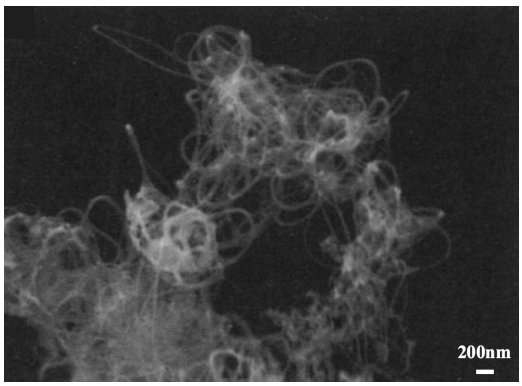

Figure 2-21 An SEM image representing a high yield of SWCNTs produced by laser ablation.[55]

2.4.4 Electrolysis technique

This method was discovered and patented in 1995.[83] It relies on the electrolysis of molten salts. The synthesis starts by passing a DC current of 30A through a carbon electrode that is placed in molten lithium chloride (LiC) at 600℃ inside a graphite crucible that acts as an anode as shown in Figure 2-22.

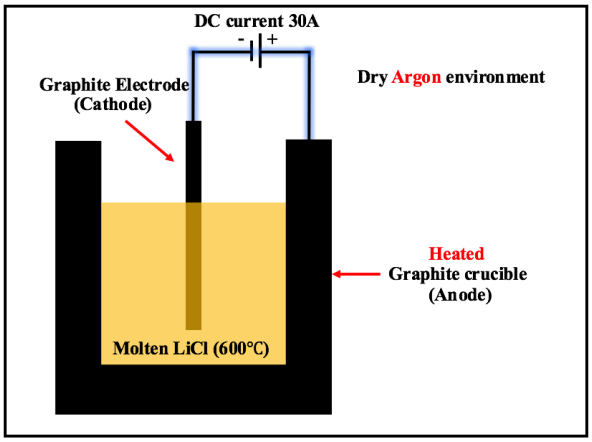

Figure 2-22 Production of MWCNTs by electrolysis.

The mechanism of growing CNTs by electrolysis starts with the dissolution of carbon from the graphite anode along with the reduction of lithium ions to form Lithium Carbide (Li_2C_2) as illustrated in Equation 2-3. The formation of $Li_2C_2$is the main reason of forming CNTs in the molten salt by the extrusion and segregation of carbon atoms to form hexagonal graphitic arranged nanotubes.[84]

$$2Li^+ + 2e^- + 2C_{graphite} \rightarrow Li_2C_2 \qquad \text{Equation 2-3}$$

The main drawback of this technique is that the extraction process of CNTs grown in the molten salt is time consuming. However, MWCNTs grown by this technique were found similar to CVD grown CNTs in some of their characteristics. A length of 0.5 microns and diameters of 3-10 nm were observed.[83] Figure 2-23 shows a TEM image of a MWCNT grown by the electrolysis technique.

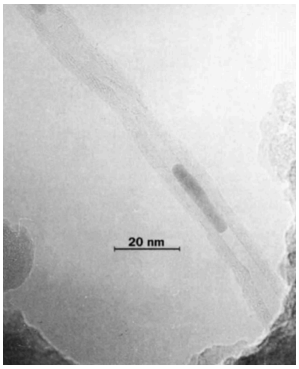

Figure 2-23 TEM image of MWCNT grown by electrolysis.[83]

The synthesis of MWCNTs can also be done from Carbon Dioxide (CO_2) dissolved in molten salts via an electrolytic technique. By the reduction of CO_2 in molten ionic salts such as $KCl, NaCl, LiCl, or\ LiBr$, CNTs can be grown on top of catalytic particles embedded in the salt. Figure 2-24 shows a TEM image of the produced CNTs by this technique. These CNTs were found clustered and grown with different angles unlike the CNTs grown with the CVD technique.[85]

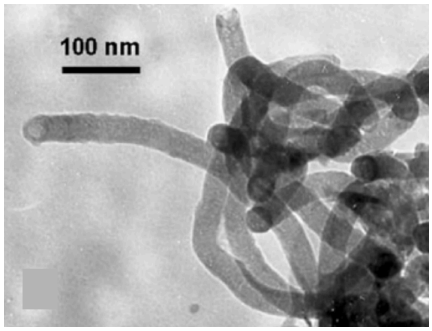

Figure 2-24 TEM image of the produced CNTs from CO_2 reduction in molten salts.[85]

2.4.5 Sonochemical/Hydro-thermal technique

In this technique, a mixture of hydrocarbons and a catalyst is prepared in an aqueous solution. The solution has to be sonicated for a certain amount of time (sonochemical). Then, the solution is placed in a chemical resistant Teflon-lined stainless steel autoclave and heated in a furnace for a certain amount of time (Hydrothermal).[86], [87] A typical sonochemical solution for synthesis of CNTs is composed of a 20 ml of dichloromethane ($C_2H_2Cl_2$), 0.5 grams of cobalt chloride ($CoCl_2$), 0.5 grams of lithium (Li) dissolved in 15ml of sodium hydroxide ($NaOH$). The solution is sonicated at 40 KHz for half an hour at room temperature. Finally, the mixture is put in an autoclave at 160℃ for 24 hours as shown in Figure 2-25.[86]

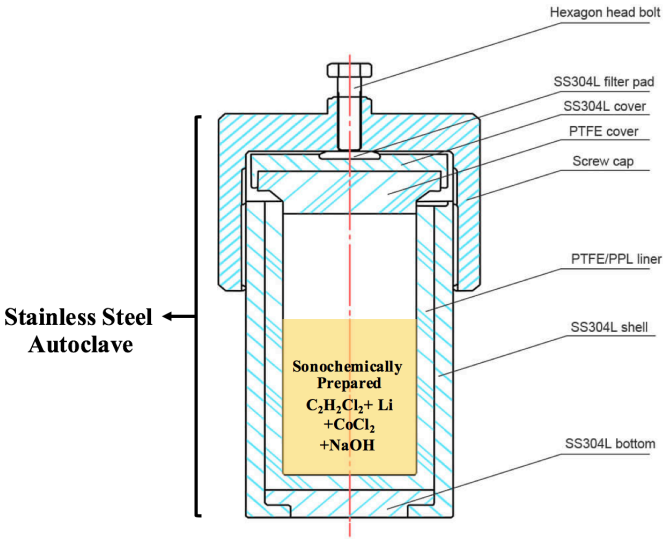

Figure 2-25 Experimental setup for the hydrothermal synthesis of CNTs.[88]

The hydrothermal processing results in a black paste that has to be washed with ethanol and diluted acids to remove any traces of the catalyst added during processing. The high resolution TEM imaging shown in Figure 2-26 confirms the growth of MWCNTs by the hydrothermal approach.

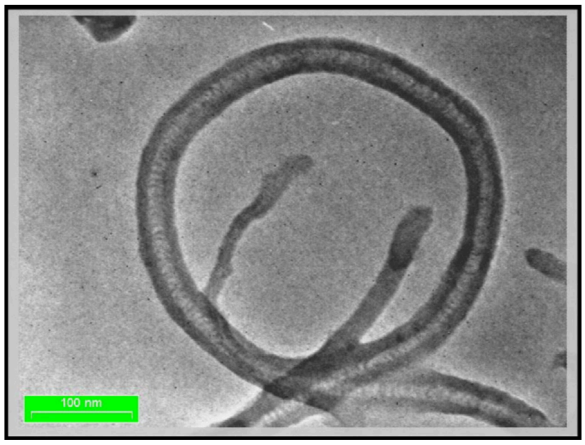

Figure 2-26 High resolution TEM image of MWCNT grown by the hydrothermal approach.[86]

To conclude on these different techniques of producing CNTs, the best quality of CNTs can be obtained from the arc discharge method. However, large amounts of decent quality MWCNTs can also be produced by CVD in a cost effective manner. These MWCNTs can be used for composite applications. Therefore, and despite of their quality that is lower than CNTs produced by arc discharge, CVD grown MWCNTs are the most commonly used type of CNTs in composite applications.

2.5 Carbon nanotube reinforced aluminum composites

Aluminum is an abundant metal in the nature. It possesses superior characteristics such as light weight, corrosion resistance, thermal conductivity, low electric resistivity, ductility, and formability. Therefore, several industries have been using it in their products including and not limited to vehicles, aircrafts, electronics, household items, and food packaging. However, aluminum in its pure form has low hardness and strength. Therefore, the development of effective techniques in improving the mechanical properties of aluminum has been considered an important challenge long time ago.

CNT reinforced aluminum composites have been produced with different techniques in the last decade due to the high strength of CNTs that is expected improve the mechanical properties of aluminum especially the modulus of elasticity.[1]–[7], [9]–[11], [15], [17], [45], [89]–[106] Both powder metallurgy and casting were investigated for producing Al-CNT composites. The

most successful approach used to disperse CNTs in aluminum was done by creating composite particles of aluminum and CNTs using high energy ball milling to disperse the CNTs within the Al powders followed by a consolidation step via hot isostatic pressing (HIP), hot compaction, or spark plasma sintering (SPS). Melting approaches was also investigated. However, these processing techniques have faced several challenges, as will be described in 2.6.

2.6 Challenges in manufacturing Al-CNTs composites

There are numerous problems related to the fabrication of Al-CNT composites for each processing technique. These challenges are addressed as follows:

2.6.1 Dispersion of CNTs in aluminum powders

Achieving a uniform distribution of CNTs within the aluminum matrix is the most important issue in fabricating Al-CNT composites. Carbon nanotubes have the tendency to agglomerate due to the Van der Waal's forces between them. These forces come as a result of the high surface area of CNTs ($200m^2/g$) as well as the interaction between π-electrons on their surfaces. Figure 2-27 shows clustered MWCNT (as received).

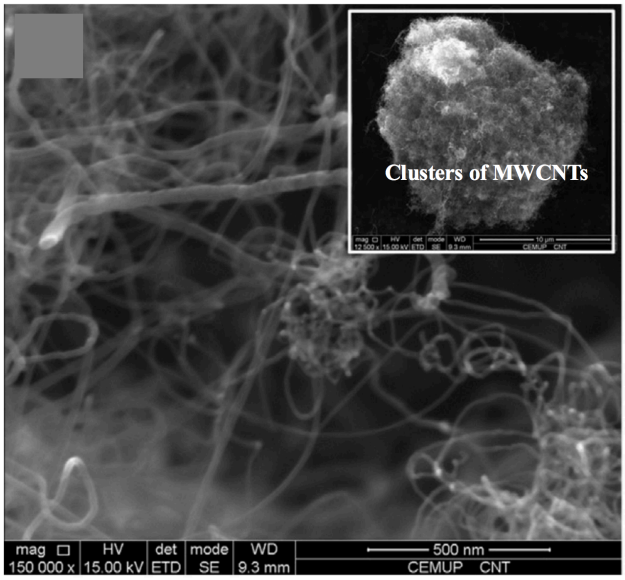

Figure 2-27 Clusters of as received CNTs formed by Van der Waal's forces.[11]

In order to exploit the outstanding mechanical properties of CNTs, uniform dispersion of CNTs in the aluminum matrix is required. Clusters of CNTs both increase the porosity and reduce the elasticity modulus as well as the overall mechanical properties for the final Al-CNT composite. The higher the percentage of CNTs in the matrix, the higher their tendency to form clusters.[89] Conventional mixing techniques were used to disperse CNTs in the aluminum matrix. One of these techniques involved stirring of 10% by volume of CNTs mixed with aluminum powder

in ethanol for around 30 min at 300 RPM. [90] Another technique involved mixing 1% by weight of CNTs with aluminum by a turbula shaker followed by mixing in a planetary mill.[91] These techniques have been found ineffective in dispersing CNTs inside the aluminum matrix as clustered CNTs were found in the fracture surface of Al-CNT composites produced by both techniques as illustrated in Figure 2-28.

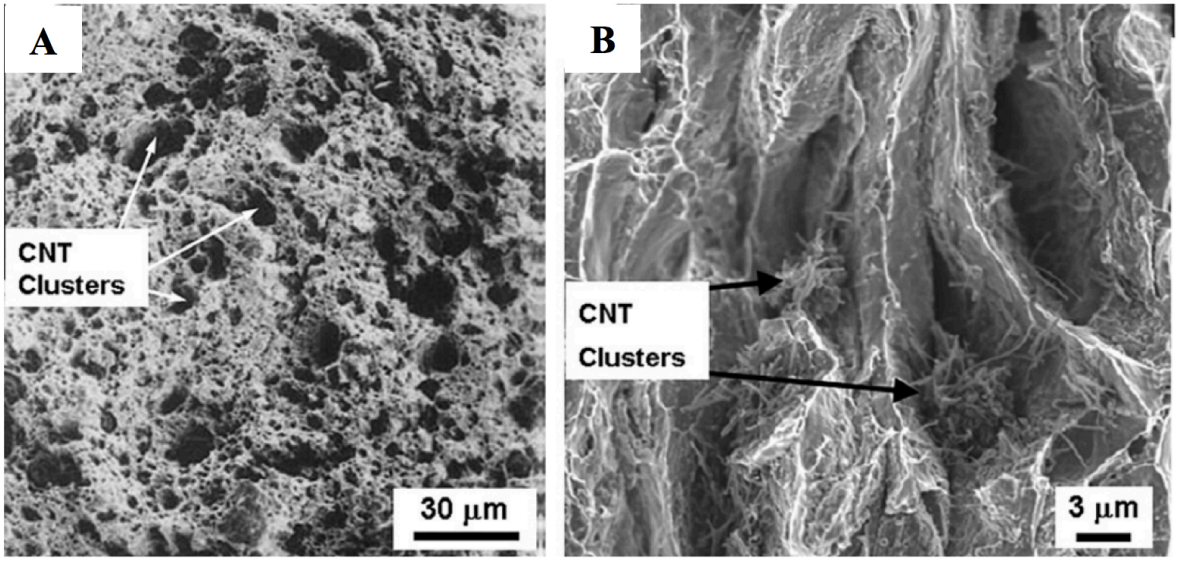

Figure 2-28 SEM images of the fracture surface showing the formation of clustered CNTs in A) 10% by volume CNTs in Al composite B) 1% by weight CNTs in Al composite.[90], [91]

The failure in dispersing CNTs in aluminum using the conventional low energy mixing techniques has led scientists to investigate the use of novel powder metallurgical techniques that will be discussed in detail in section 2.7.

2.6.2 Porosity of Al-CNTs produced by powder techniques

Porosity of Al-CNT composites is a common problem that comes as a result of multiple factors. Any clusters of CNTs remaining in prepared Al-CNTs powder will show up in the final processed composite resulting in porosity that reduces the tensile strength. The Porosity may also be initiated as a result of a poor metal to metal contact between the powder particles to be consolidated.[107]–[110] This happens as a result of oxide layers that form on the surfaces of Al-CNT particles. These aluminum oxide layers prevent metal to metal contact between composited Al-CNT particles and each other, and hence increase the porosity of the final composite. This problem can be overcome by using some deformation techniques such as hot extrusion or hot rolling that breaks these oxide layers to allow better metal to metal contact.

2.6.3 Damage of CNTs and formation of brittle Al-carbides

Many research articles have addressed the problem of aluminum carbides formation in Al-CNTs composites.[4], [9]–[11], [90], [92], [93] These carbides were found in different regions of the composite such as the interface between the aluminum matrix and CNTs, the tips (open ends) of CNTs, as well as the aluminum matrix itself in the form of fully transformed aluminum carbides.[9]–[11] The defects in CNTs cause the formation of different phases of aluminum carbide in the matrix that are characterized by being brittle.[111] Most of the researchers have explained the formation of Al_4C_3 due to the reaction between aluminum and both distorted carbon (defective carbon) on the body of CNTs, amorphous carbons, as well as on the tips of CNTs. The defective carbons tend to form Al_4C_3 in order to reach a stable state.[4], [92], [93] The higher the quality of CNTs, the lesser the defects and the lesser the formation Al-carbides.[90] There was not any reactions observed between molten aluminum and high quality CNTs (Free of defects).[93] Processing techniques such as high energy ball milling (Mixing technique) were found to reduce the quality of CNTs by imparting damage and defects in CNTs. A significant increase in $I_D: I_G$ ratio of ball milled CNTs with aluminum powder was reported by researchers especially with the increase of milling time indicating the increase of defects in CNTs.[5]

The diameter and morphology of CNTs also affect the formation of carbides. The smaller the diameter of CNTs, the higher the interfacial area between them and the aluminum matrix and hence, more aluminum carbides are formed in the composite. [94] Some researchers have explained that aluminum carbides are formed by the interaction between the outer shell of MWCNTs and the aluminum matrix.[95] Nonetheless, the formation of Al_4C_3 around CNTs and on their tips was found beneficial in improving the interfacial adhesion between CNTs and the aluminum matrix as well as helping in the load transfer between CNTs and the matrix.[93], [96] Furthermore, the presence of aluminum carbides was found to interrupt the dislocation movement in aluminum matrix resulting in increased strength.[112], [113] When Al-CNT powders were used in thermal spraying, aluminum carbides formed on CNTs were proven to reduce the contact angle of CNTs with molten aluminum from 135° to 55°.[97]

Case studies of aluminum carbides formation in Al-CNT composites

In 1998, a group of scientists prepared Al-CNT composites via hot pressing of Al-CNT powders. These powders were prepared by mixing CNTs with aluminum by a hand grinder. When the microstructure was investigated, aluminum carbide phases such as AlC and AlC_2 were reported as shown in Figure 2-29. These Al-C phases were found around CNTs as a result of the reaction between Al and amorphous carbons (defective) on the surface of CNTs.[9]

Figure 2-29 Aluminum carbide phases in 1% by weight CNT reinforced aluminum.[9]

There was not any evidence of the reported aluminum carbide phases. Even the reported ratios of Al:C based on Energy Dispersive X-Ray (EDX) cannot give enough evidence that carbon is chemically bonded with aluminum. Another study investigated aluminum carbide formation in samples prepared by hot pressing Al-CNT powders at 500-640°C.[11] Al-CNT powders were prepared by dispersing CNTs in ethanol, sonicating the powder, and mixing it with aluminum using a turbula mixer. Figure 2-30 illustrates the formation of Al_4C_3 on a CNT using TEM imaging.

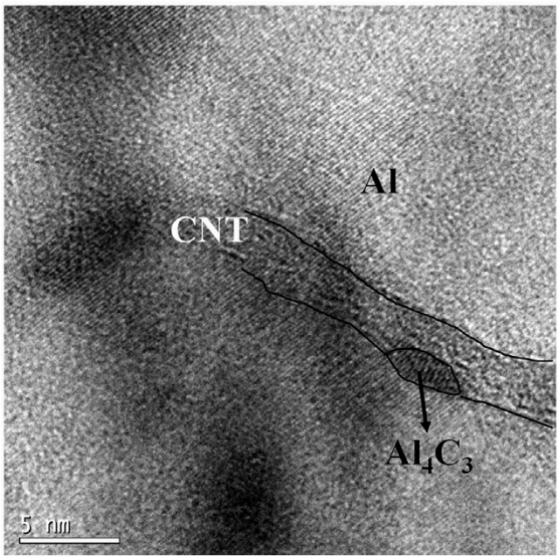

Figure 2-30 High resolution TEM image of a CNT and Al_4C_3 formed on its surface.[11]

Fully transformed aluminum carbides were also found inside the aluminum matrix as shown in Figure 2-31.

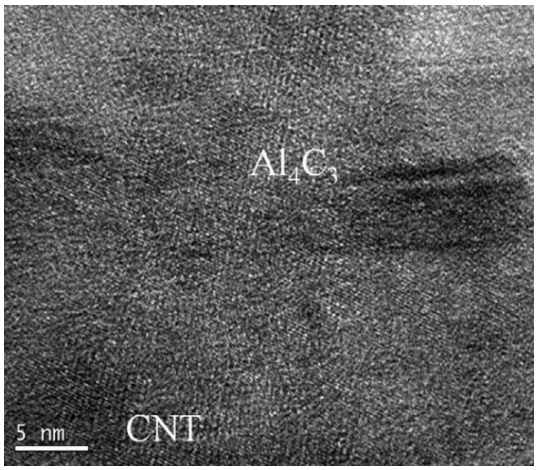

Figure 2-31 Fully transformed aluminum carbide phase inside the aluminum matrix.[11]

This proves that even without using ball milling, some aluminum carbide phases can form around CNTs and inside the matrix due to the interfacial interaction between Al and CNTs at high temperature.[93] Further studies conducted selected area electron diffraction (SAED) indexing on Al-CNTs prepared by hot pressing followed by hot extrusion in order to spot the formation of Al_4C_3. These carbides were found cylindrically shaped around CNTs and dumbbell shaped on top of CNTs as shown in Figure 2-32.

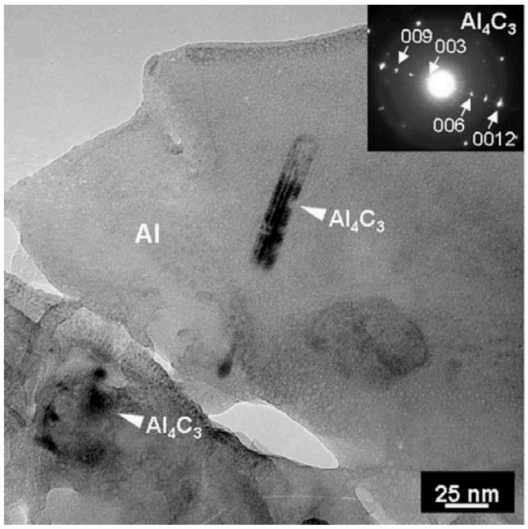

Figure 2-32 High resolution TEM imaging and SAED indexing of Al_4C_3 on CNTs.[10]

Several conclusions can be drawn based on the previous studies. The most important of which is that aluminum carbides were formed in all the hot pressed powders regardless of the quality of CNTs used and the dispersion techniques used to mix CNTs with aluminum. However, the use of high energy ball milling increases the defects in CNTs and accordingly leads to increased carbide formation.

2.6.4 Dispersion, wettability and interfacial phenomena of CNTs with aluminum

When the fabrication of Al-CNT composites was attempted by melting techniques such as casting, poor wettability between molten aluminum and CNTs was observed and attributed to the high surface tension of molten aluminum compared to CNTs.[14], [114] When MWCNTs were introduced in molten aluminum by casting, clusters and segregations of CNTs were detected in the matrix as shown in Figure 2-33.[15]

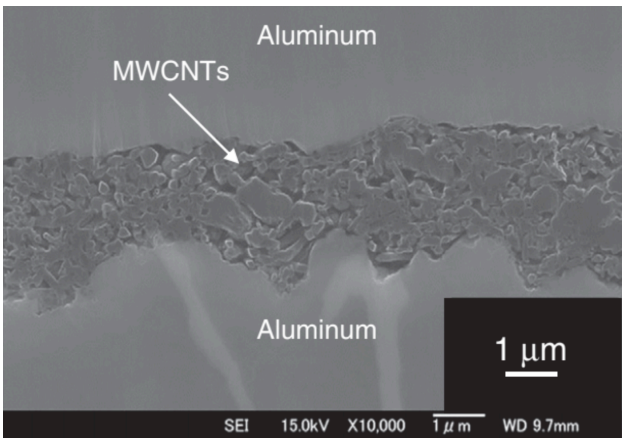

Figure 2-33 A cross-section of an Al-CNT sample showing poor dispersion and wettability of MWCNTs in cast aluminum.[15]

For a better illustration of the phenomenon, the contact angle between a liquid droplet and the surface of CNTs is defined in Figure 2-34.

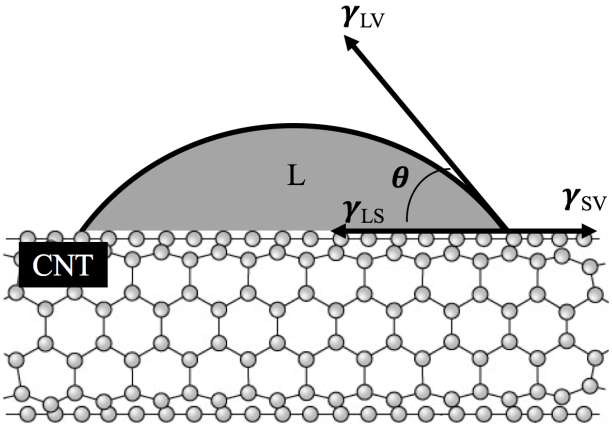

Figure 2-34 An illustration of the contact angle definition between a liquid droplet and CNT.[3]

The contact angle θ is defined as the angle between the liquid-vapor interface and the liquid-solid interface. The surface tension between the liquid droplet and CNTs directly affects the contact angle θ as governed by Equation 2-4.

$$\cos\theta = \frac{\gamma_{SV} - \gamma_{LS}}{\gamma_{LV}} \qquad \text{Equation 2-4}$$

Where γ_{SV}, γ_{LS}, and γ_{LV} are the solid-vapor, liquid-solid, and liquid-vapor surface energies respectively. The smaller the contact angle on the metal-CNT interface, the better the wettability. The contact angle also has a reflection on the work of adhesion W_A between the liquid metal and CNT as illustrated in Equation 2-5.

$$W_A = \gamma_{LV}(1 + \cos\theta) \qquad \text{Equation 2-5}$$

Molten aluminum exhibits the poorest wettability with CNTs among all metals as indicated in Table 2-1. The surface tension of CNTs (γ_{SV}) was reported to be 45.3 $mN.m^{-1}$.[114] This implies that aluminum is 19 times higher in surface tension than CNTs.

Table 2-1 Surface tension and wettability of metals with CNTs.[14]

Element	Surface Tension (mN/m)	Wetting with CNT
S	61	Yes
Cs	67	Yes
Rb	77	Yes
Se	97	Yes
Te	190	No
Pb	470	No
Hg	490	No
Ga	710	No
Al	860 at 750℃[115], [116]	No

The big difference in surface tension between molten aluminum and CNTs makes the contact angle between them higher than 90° resulting in poor wettability. Therefore, surface modification of CNTs by coating them with a metallic interphase should be implemented to reduce the contact angle and hence, improve the wettability as demonstrated in Figure 2-35.

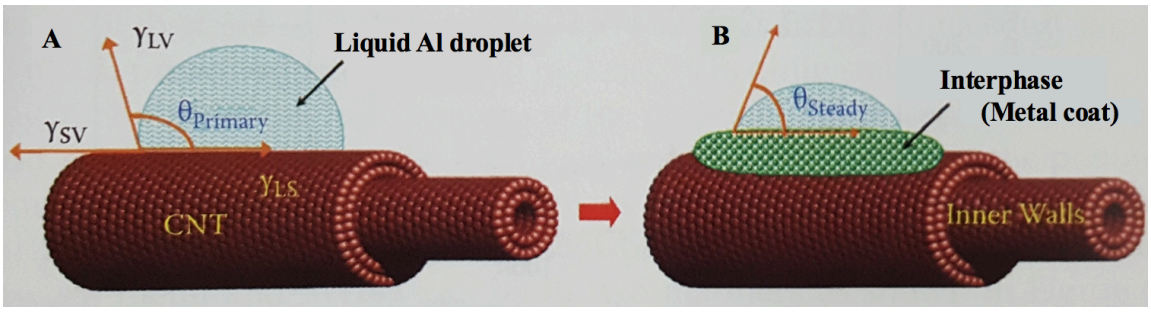

Figure 2-35 Contact angle between Al and CNTs A) without applying a metallic coat, and B) with applying a metallic coat.[97]

It was proven by experiment that coating carbon structures such as graphite with a metallic coat such as copper can reduce the contact angle between molten aluminum and graphite significantly.[117] Figure 2-36 (A-B) shows a droplet of molten pure aluminum that has a contact angle of 140° (poor wetting) with the surface of a graphite substrate. After coating the substrate with copper by the electroless plating process that will be discussed in detail in section 2.8, the contact angle between aluminum and graphite instantaneously dropped to 55° as shown in Figure 2-36 (C). By reaching a steady state after 30 min, the contact angle was recorded to be 58° as shown in Figure 2-36 (D).

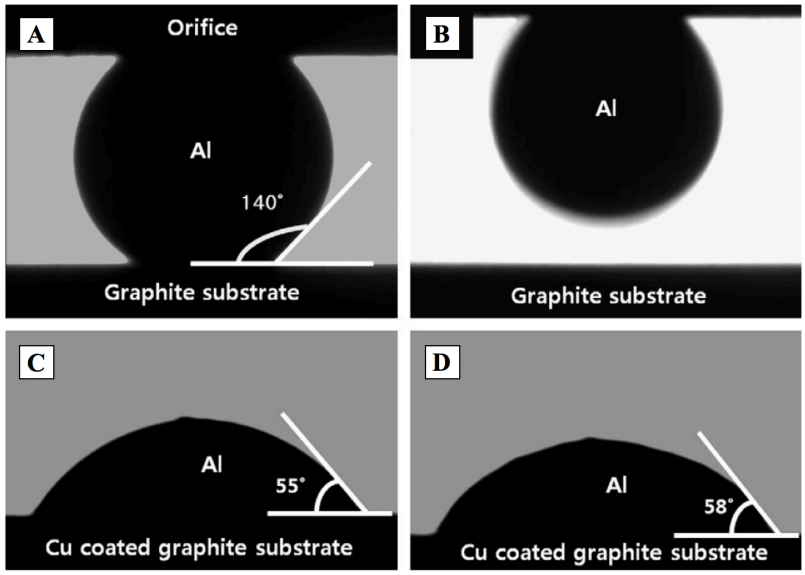

Figure 2-36 CCD camera images of (A-B) un-wetted pure aluminum droplet with the surface of a graphite substrate, C) aluminum droplet wetted with copper coated graphite substrate, and D) steady contact angle of after 30 minutes. [117]

Similar to graphite, the wettability between aluminum and CNTs was improved by coating CNTs with different metals such as Cu, Ni or silver via electroless plating as will be discussed in detail in Section 2.8.

2.7 Processing techniques to tackle Al-CNT challenges

The methods by which Al-CNT composites are processed can significantly influence the mechanical properties of the final composite. Most of the processing techniques are focused on insuring a uniform dispersion of CNTs in the aluminum matrix. Many constraints were put on processing methods in order to keep CNTs with their original form without destruction. Harsh processing conditions at elevated temperatures may alter the structural integrity of CNTs and cause chemical reactions between CNTs and the aluminum matrix resulting in carbide formation.[4], [92], [93]

The processing techniques of Al-CNT composites are split into two main routes. The most common route is the powder metallurgical route represented in a group of techniques designed to embed and disperse CNTs in the aluminum powder by forming composite particles of Al-CNTs that can be consolidated by sintering to form a bulk sample. The second route is the melting route that faces tremendous problems represented by the difference in density between CNTs and molten aluminum in addition to the poor wettability between them. Scientists have managed to overcome some of the present challenges in producing Al-CNT composites by both the powder metallurgical and melting approaches, as discussed in the following sections. Powder metallurgy is a technique for processing composite materials by mixing the reinforcing phase with the matrix phase in their solid state to form composite powders that can be consolidated at high temperature. There could be many ways of mixing CNTs with the aluminum powder. Conventional mixing techniques such as turbula shaking or ultrasonic mixing were found ineffective in obtaining a uniform dispersion of CNTs in the Al powders.[90], [91] Therefore, processing techniques such as mechanical ball milling was adopted to promote the dispersion of CNTs in aluminum by applying mechanical forces that mechanically interlocks CNTs in the aluminum matrix.[5], [6], [95], [118], [119]

- **High energy ball milling**

In this technique, pure aluminum powders and CNTs were placed in a stainless steel jar that is filled with stainless steel balls. The jar was then covered and placed in a planetary ball mill in which it rotates causing high energy collisions of the stainless steel balls with both CNTs and the aluminum powder.

The high energy ball milling was found to produce a uniform dispersion of CNTs in the aluminum matrix. In 2007, two important studies were carried out to show the effectiveness of ball milling in distributing CNTs in the aluminum powder. Up to 48 hours of milling were investigated.[119], [120] When aluminum powders and CNTs were mixed in a turbula mixer, agglomerates of CNTs were found in the mixture indicating the poor dispersion of CNTs in the matrix as represented in Figure 2-37 (A). When ball milling was used, aluminum flakes covered with CNTs were formed after short time of milling as shown in Figure 2-37 (B). These flakes were then cold welded into particles and refined by increasing the milling time as illustrated in Figure 2-37 (C-D). From these results, it can be concluded that ball milling results in an excellent dispersion of CNTs in aluminum powder. In addition, the ball milling time directly affects the morphology of the produced particles.

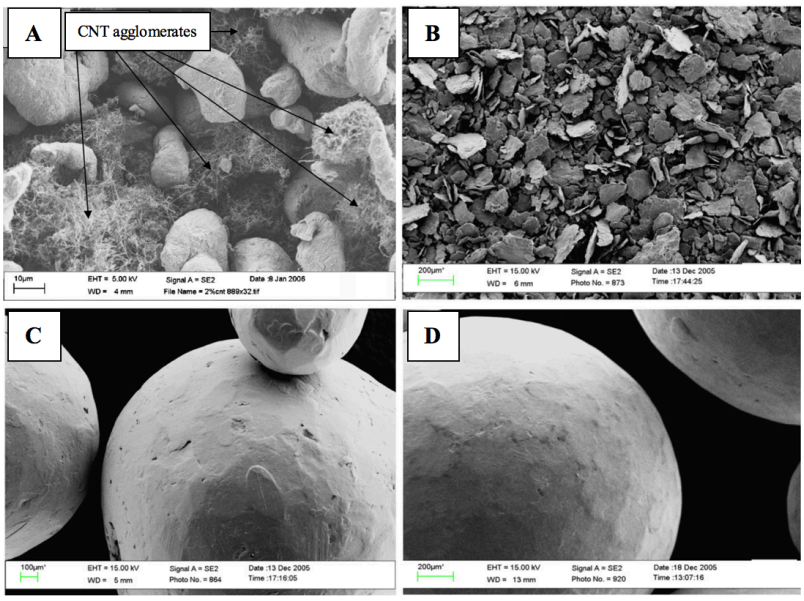

Figure 2-37 SEM imaging of A) clustered CNTs after turbula mixing with aluminum powder without milling, B) composite flakes of Al-CNTs after milling for 1 hour, C) composite particles of Al-CNTs after milling for 24 hours, and D) Al-CNT particles after 48 hours. [120]

The produced Al-CNT particles by ball milling require post processing for the purpose of consolidating the milled powder to form a bulk specimen. Different techniques of consolidation were used including powder compaction combined with sintering and other deformation techniques.

- **Powder compaction and sintering**

Processing techniques used to consolidate Al-CNT powders into a final product have a tremendous impact on the properties of the final composite. Processing affects the final density of the composite. The higher the density of the composite, the better the CNT-matrix adhesion and therefore, a better load transfer from the matrix to CNTs could be achieved.[89]

The powder compaction is the most important step to conduct after the preparation of Al-CNT powders. The compaction temperature should be controlled to avoid recrystallization and grain growth of the fine Al-CNT structures as well as avoiding the loss in some of the metastable characteristics during heating process.[12] Common methods of powder consolidation are cold/hot compaction followed by hot extrusion, hot compaction followed by hot rolling or hot forging, Hot Isostatic Pressing (HIP) followed by hot extrusion, and spark plasma sintering (SPS). For Al-CNT composites, powder pressing alone does not result in a great improvement of the mechanical properties. Therefore, deformation techniques have to be implemented to induce an increase in the dislocation density of aluminum and improve its tensile

characteristics. Hot extrusion was used in many studies as a final processing step for Al-CNT composites. In this process, a compacted-sintered Al-CNT sample is pushed through a die in order to induce a reduction in the cross sectional area by a certain reduction factor that is called the extrusion ratio (ER). Extrusion leads to a considerable increase in the final density of the sample. It was found that the larger the ER, the higher the degree of deformation that aligns CNTs along the direction of extrusion as shown in Figure 2-38. This deformation also helps in disintegrating CNT clusters in the aluminum matrix.

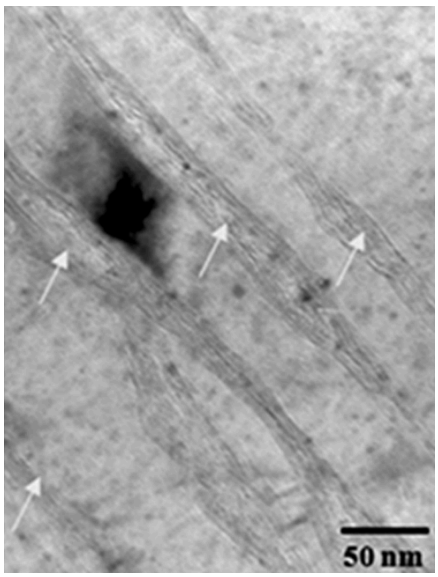

Figure 2-38 TEM image that shows an alignment of CNTs after hot extrusion of 4.5% CNTs in aluminum. [98]

Using larger ER was also found to induce better contact between CNTs and the aluminum matrix. This excellent contact helps in Al-CNT load transfer and hence improves the mechanical properties.[89]

Aluminum powders are known for their poor sintering ability due to the formation of oxide layers (melting point above 2000℃) on their surface. This aluminum oxide layer prevents metal to metal contact during sintering.[107]–[110] Both extrusion and pressure used in the hot compaction of the powder were found useful in breaking these oxide layers on Al-CNT particles allowing better metal to metal contact during consolidation and hence increasing the density of the composite and reducing porosity.[121]

Hot extrusion cannot be considered the golden key for improving the mechanical properties of Al-CNT composites. Failure in dispersing CNTs in the aluminum powder will lead to poor mechanical properties even after compaction and extrusion.

The best results in the mechanical properties of Al-CNT composites can be credited to mechanical ball milling followed by sintering techniques due to the excellent dispersion it provides for CNTs in the aluminum matrix. Structure refinement due to milling is also a major contributor towards the strength improvement. However, this comes at the expense of ductility since the excessive work hardening experienced by the material during mechanical milling has been reported to cause notch sensitivity and severe loss in ductility. In addition, the limited design flexibility and the high processing costs limit the use of this technique on an industrial scale except for some specialized applications. Therefore, scientists tried to fabricate Al-CNT composites by the casting technique to reduce cost and increase shape flexibility.

2.7.1 Melting techniques: Casting

Casting is a popular technique in manufacturing metallic parts. The most intricate features both internal and external can be easily cast. Small as well as large heavy metallic parts can be easily mass-produced in a much simpler and cost effective fashion compared to powder sintering techniques. However, there are some considerations that have to be taken into account when fabricating Al-CNT composites using the casting technique. These considerations are:

1- Insuring adequate wetting between aluminum and CNTs.
2- Obtaining a good dispersion of CNTs in molten aluminum.
3- Insuring the thermal stability and structural integrity of CNTs at the high melting temperature of aluminum.

Due to the poor wetting between aluminum and CNTs, casting has been very challenging as a processing technique of Al-CNT composites. In order to reinforce the aluminum matrix with CNTs through casting routes, different casting methodologies have been employed such as stir casting and induction melting. The introduction of CNTs into molten aluminum has been done in different fashions including the direct and indirect addition of CNTs to molten aluminum. The direct addition of CNTs involves the use of them without being coated by any dispersing or wetting agent. While the indirect introduction involves coating of CNTs with a metal or a polymer that can help in their dispersion and improve their wettability in the matrix.

- **Squeeze casting**

Squeeze casting is a technique that relies on the pressure infiltration of molten metals into a reinforcement prepreg or a preform.[122] Figure 2-39 illustrates the fabrication steps of composites by this technique. At the beginning of the process, the metal matrix is melted over a reinforcement preform that is placed in a die. Afterwards, the pressure infiltration is done by

forcing the molten metal into the preform using a press. The formed composite is then cooled and ejected outside the die by the use of an ejector pin.[123]

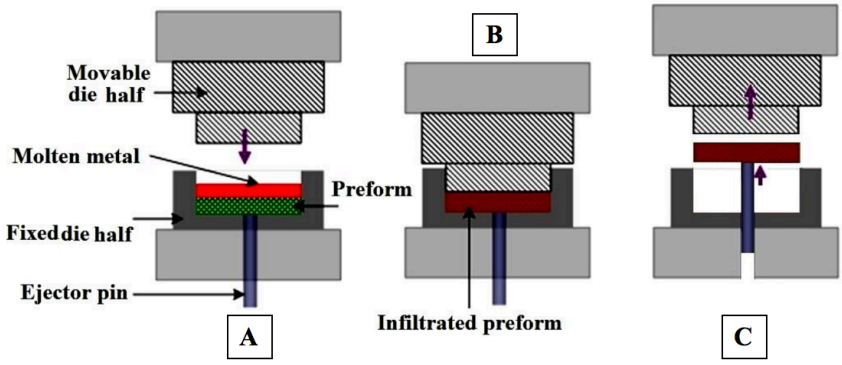

Figure 2-39 Steps for squeeze casting of Al-CNT composites A) poured molten metal on CNT preform in a die, B) infiltrating the preform by aluminum via squeezing, and C) ejecting the formed composite.[123]

To fabricate Al-CNT composites using squeeze casting, scientists prepared a CNT prepreg consisting of MWCNTs binded with a binder as shown in Figure 2-40 (A).[124] Molten aluminum was then pressure infiltrated through the prepreg to form the final Al-CNT composite. Figure 2-40 (B) shows a cross-section in the fabricated Al-CNT composite that indicates the presence of well distributed CNTs that are wetted with the aluminum matrix.

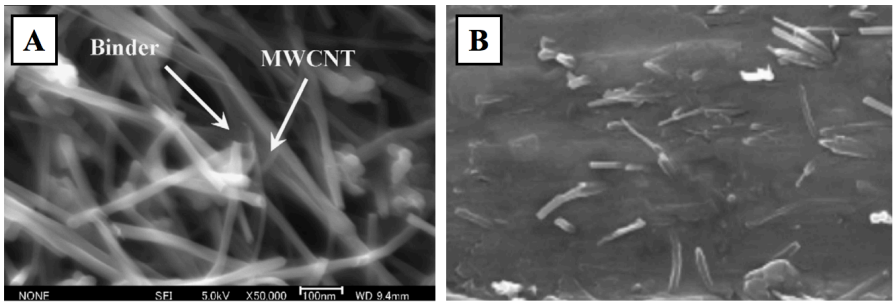

Figure 2-40 SEM image of A) MWCNT prepreg and B) imbedded CNTs in the aluminum matrix after squeeze casting of aluminum on MWCNT prepreg.[124]

It can be concluded that by applying a pressure between molten aluminum and CNTs, the wettability between CNTs and aluminum could be improved.

- **Melt infiltration**

Unlike squeeze casting, the melt infiltration is a pressureless infiltration process of molten aluminum into a CNT preform. It might seem impossible to infiltrate molten aluminum into CNTs without pressure due to the small pores in the preform. However, scientists could overcome this by preparing Al-Mg-CNTs preform by mixing pure aluminum and pure magnesium powders with CNTs using the ball milling technique at 700 RPM for 7 hours. The

prepared mixture was then pressed as a preform that was then placed in a crucible inside an electric furnace. Afterwards, a slab of an aluminum alloy was melted at 800℃ on top of the preform to cause the infiltration in a nitrogen environment as shown in Figure 2-41. During the infiltration process, it was believed that the nitrogen reacted with Mg forming MgN_2 that was believed to improve the wettability and infiltration of the aluminum alloy into the preform.[125]

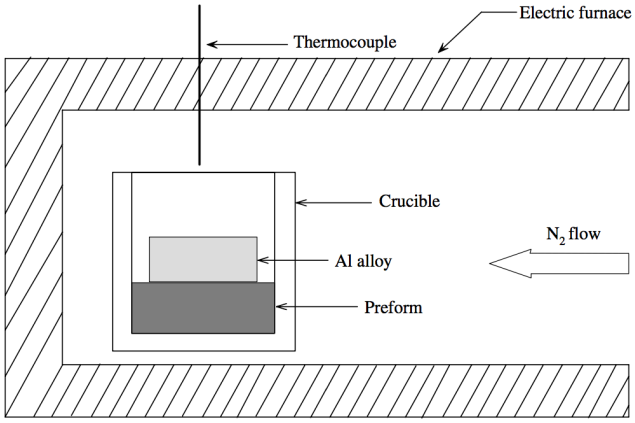

Figure 2-41 Schematic diagram of melt infiltration fabrication of Al-CNT composites.[125]

Up to 10% by volume of CNTs were successfully imbedded in the aluminum matrix by this technique. Figure 2-42 shows the fracture surface of the produced sample. The success of the infiltration process could clearly be seen as CNTs were clearly dispersed in the matrix.

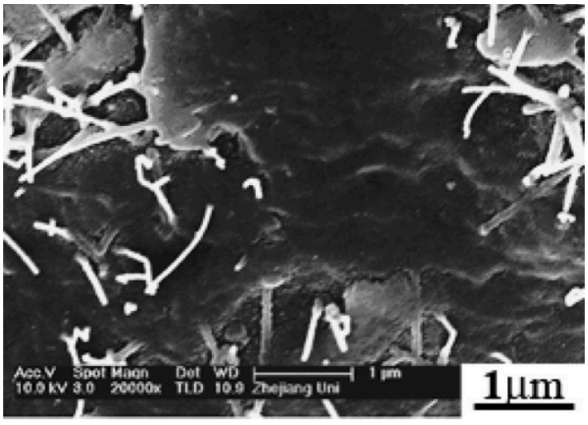

Figure 2-42 SEM image of the fracture surface of the infiltrated Al-CNT sample.[125]

The squeeze casting and melt infiltration techniques resulted in excellent wettability of CNTs with aluminum besides the ability of dispersing bigger amounts of CNTs. However, these techniques were only done in dies and could not produce a pourable composite. Therefore, other researchers investigated several techniques that enabled the pouring of molten Al-CNT mixture into molds for the ease of fabrication.

- **Compocasting**

This technique relied on forming composite powders of nickel phosphorous (Ni-P) coated aluminum particles that has Ni-P coated CNTs on top of them.[126] Coating CNTs with Ni-P was believed to improve their dispersion and wettability when injected in molten A356 aluminum alloy. To prepare these composite particles, pure aluminum powder shaped as indicated in Figure 2-43 (A) were mixed with CNTs. The mixture was then activated with palladium nanoparticles and coated by Ni-P using an electrochemical technique known as the electroless plating as will be discussed in detail in section 2.8. The electroless plating resulted in producing composite nanoparticles of aluminum that is coated by Ni-P and has Ni-P coated CNTs on their surface as represented in Figure 2-43 (B-C).

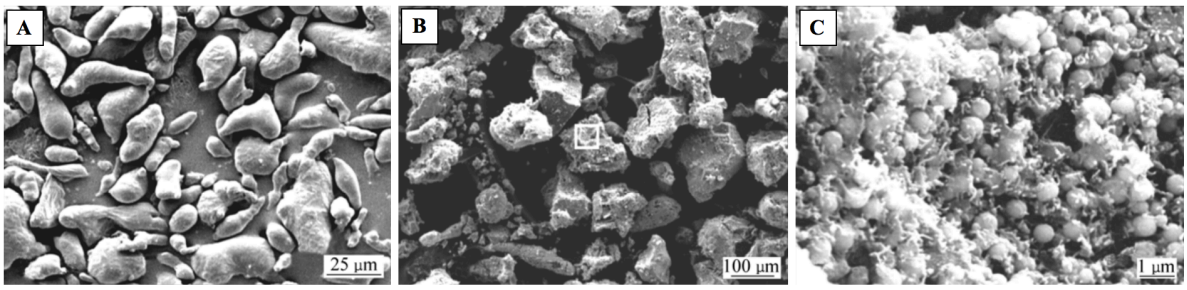

Figure 2-43 SEM images of A) aluminum powder B) aluminum powder after Ni-P electroless plating with CNTs, and C) high magnification of the fabricated Ni-P coated CNTs on aluminum powder.[126]

The prepared composite powders were then injected in molten A356 aluminum alloy under continuous stirring as shown in Figure 2-44. The melt was then poured into a mold and prepared for testing.

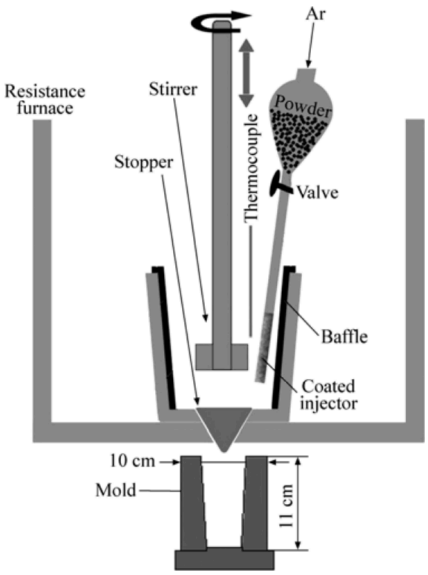

Figure 2-44 Apparatus for Compocasting.[126]

There was not any high resolution imaging observed for the produced samples. However, a Brinell hardness of 75 HBN was achieved in the 2 % CNT sample compared with the unreinforced A356 alloy that has 60 HBN.

- **Stir Casting**

In this processing technique, pure aluminum slabs were melted inside a muffle furnace followed by the direct addition of MWCNTs during mixing with a stirring rod. The mixture was then poured into a mold and left to solidify. In spite of the low cost of fabricating Al-CNT composites by this technique, most of the research attempts to produce Al-CNT composites by stir casting using the direct addition of CNTs in molten aluminum were hampered by a reduction in the tensile strength of the composite especially for Al samples reinforced by 2 wt. % CNTs compared to samples of a lower content of CNTs.[127] The dispersion of CNTs in the aluminum matrix was found to be less uniform due to the low density of CNTs that makes them float on top of the cast once poured into molds in the absence of stirring. The poor wettability of aluminum and CNTs also played a great role in reducing the tensile strength of the composite. Therefore, scientists avoided the direct introduction of CNTs into molten aluminum when fabricating Al-CNT composites by the casting technique. This was done by following indirect approaches. One of these approaches was done by creating a master composite of Al-CNT composite powders using the ball milling technique followed by hot extrusion as shown in Figure 2-45. This master composite was then added to molten A356 aluminum alloy to fabricate Al-CNT composites by stir casting.[104]

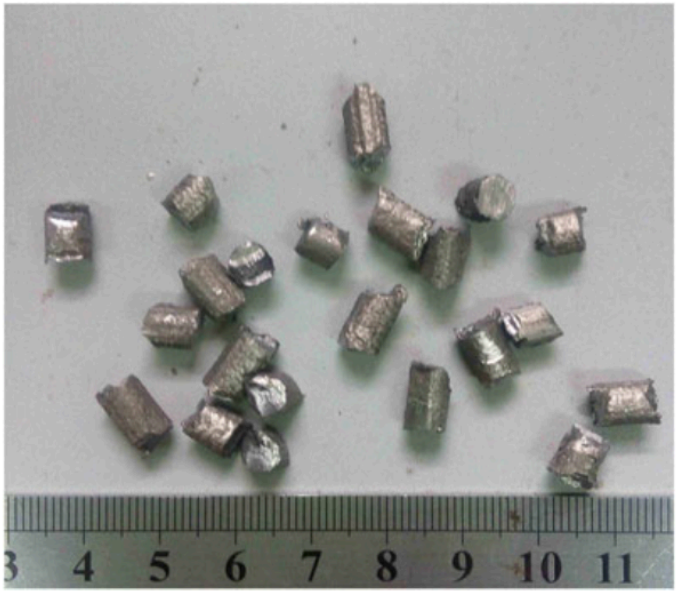

Figure 2-45 Hot extruded Al-CNT master composite at 390℃.[104]

By introducing CNTs in molten aluminum using the master composite technique, a better dispersion of CNTs in molten aluminum could be achieved as shown in Figure 2-46 that shows the well dispersed pulled-out CNTs (0.2% by wt.) in molten A356 aluminum alloy.

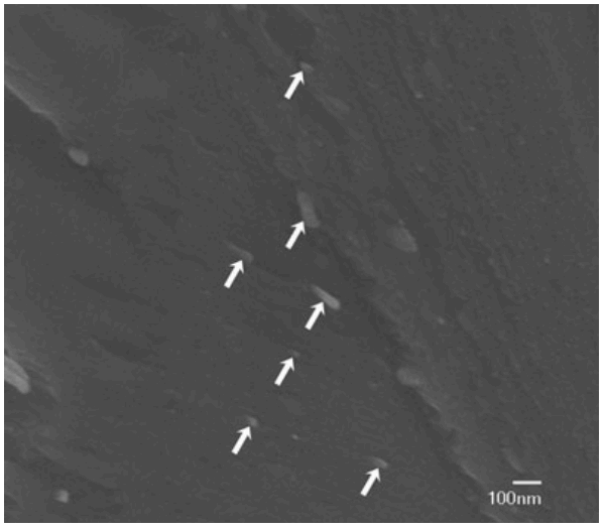

Figure 2-46 Fracture surface of 0.2 wt. % CNTs in A356 composite sample showing pulled out CNTs.[104]

It is apparent that this study relied on dispersing small amounts of CNTs in the aluminum matrix. This resulted in a slight increase in the ultimate tensile strength of the 0.2 wt. % CNTs sample as represented in Table 2-2. By increasing the weight percent of CNTs to 0.4%, a drop in the tensile strength of the Al-CNT composite was noticed indicating the failure of this technique in dispersing higher amounts of CNTs in molten aluminum.

Table 2-2 Mechanical properties obtained for the cast Al-CNT samples by the master composite technique.[104]

Specimens	A356	0.2 wt% CNTs	0.4 wt% CNTs
UTS (MPa)	172.0 (±8.3)	193.0 (±7.4)	176.7 (±12.5)
Elongation (%)	4.23 (±1.21)	4.69 (±1.44)	3.39 (±1.92)

An alternative approach to indirectly introduce CNTs in molten aluminum was done by gradually adding 500g of pure Al powder, 10g of pure magnesium (Mg) powder, MWCNTs (10-20g) to 100g of natural rubber (NR).[102] This mixture was then stacked as slabs and compressed at 80℃ in a mold. Pure aluminum slabs were added on top of the previously fabricated composite slabs and melted at 800℃ to form the final Al-CNT composite. This technique succeeded in dispersing up to 1.6 % by volume of CNTs in molten aluminum.

However, the fracture surface of the samples revealed that some of the carbon nanotubes are not wetted in the aluminum matrix as represented in Figure 2-47.

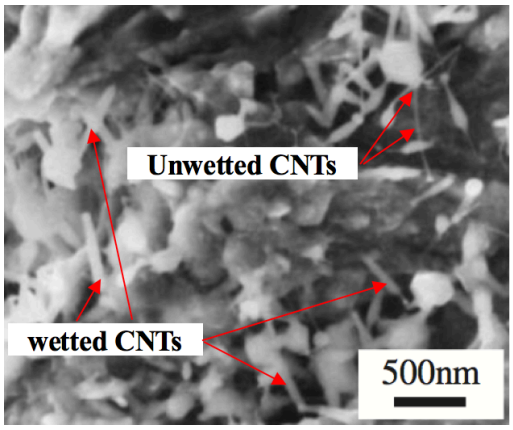

Figure 2-47 Fracture surface of Al-CNT composite produced by the NR mixing method.[102]

A significant increase in the tensile strength was obtained for both the 0.8 % by volume and 1.6 % by volume of CNT-reinforced samples compared to pure aluminum samples as shown in Figure 2-48. However, since pure Mg powder was added to the mixture, the mentioned increase in the tensile strength of the samples cannot be only explained as a result of the addition of CNTs.

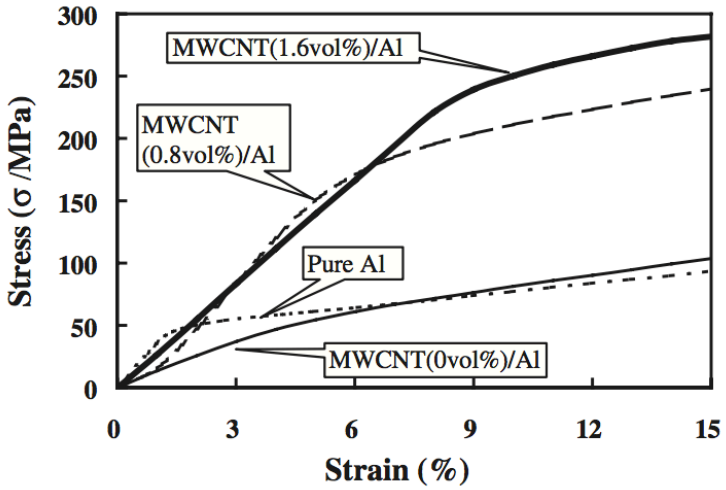

Figure 2-48 Stress-strain diagram of the compression test for Al-CNT samples of 0.8 vol. % and 1.6 vol. % of CNTs in them.[102]

In another research work, the indirect introduction of CNTs in molten aluminum was carried out by coating CNTs with certain materials to act as a wetting agent for CNTs prior to being introduced in molten aluminum. The coated CNTs act as a feedstock that is wettable and dispersible in molten aluminum unlike pristine CNTs that are hard to introduce in the aluminum matrix. For example, CNTs were coated by silicon carbide (SiC) via mixing silicon particles

with CNT flakes and annealing this mixture at 1300℃ for 1 hour as represented in Figure 2-49.[128]

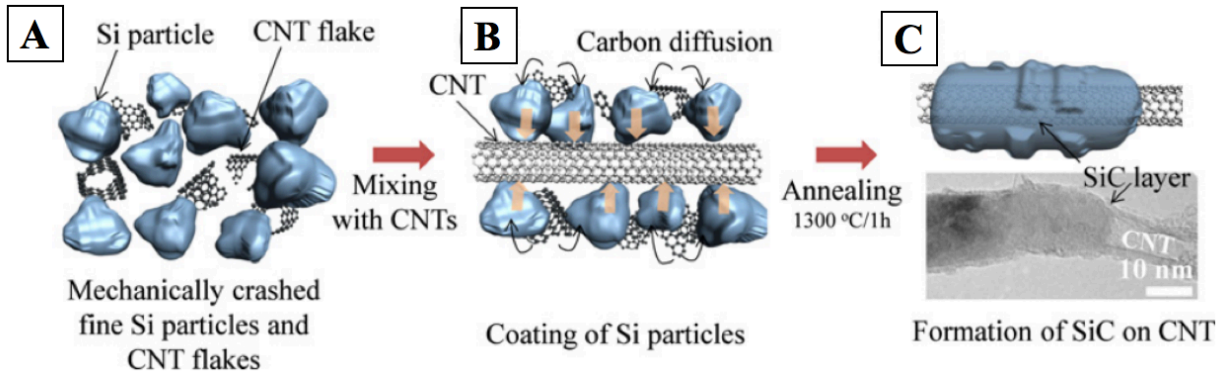

Figure 2-49 Procedures for silicon carbide coating on CNTs with A) mixing Si particles with CNT flakes, B) carbon diffusion in Si particles, and C) formation of SiC on CNTs after annealing at 1300℃ for 1 hour.[128]

The annealing resulted in the diffusion of carbon into silicon forming SiC around CNTs. Figure 2-50 (A) concludes that silicon carbide was melted around CNTs resulting in embedding CNTs into SiC structures rather than conformably coating each individual CNT. High resolution TEM imaging besides SAED indexing, showed CNTs enclosed by SiC as represented in Figure 2-50 (B).[128]

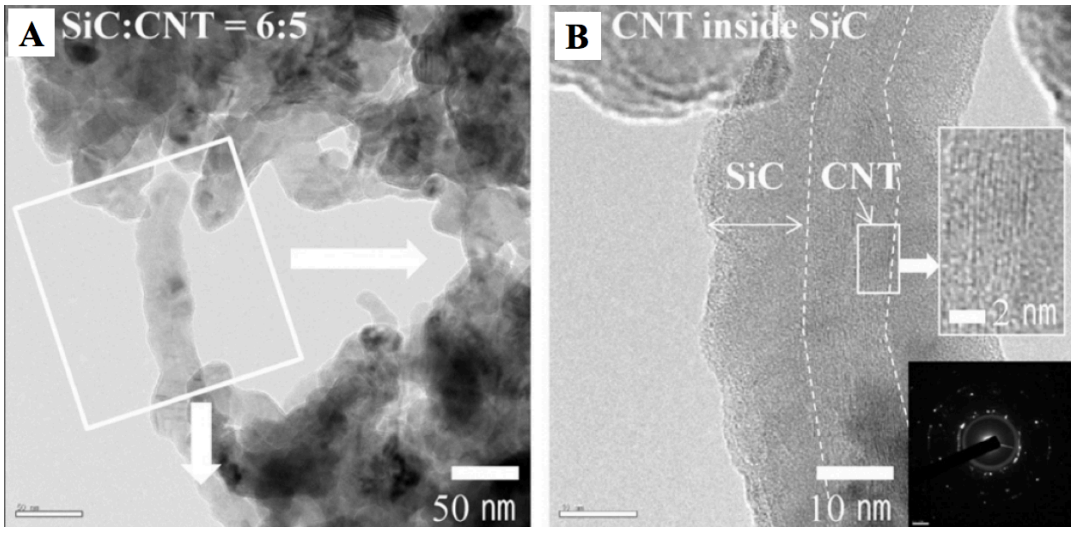

Figure 2-50 TEM imaging of A) SiC formed around a CNT with SiC:CNT ratio of 6:5, and B) a CNT embedded in SiC structure with the SAED indexing on the bottom right corner.[128]

The SiC-coated CNTs were then mixed with pure aluminum powder by ball milling. The mixture was then used as a feedstock reinforcement phase for A356.2 aluminum alloy. This was done by melting the A356.2 alloy and adding the feedstock reinforcement to it during

stirring. Figure 2-51 shows that both partially embedded and fully embedded CNTs were found in the structure of the aluminum alloy.

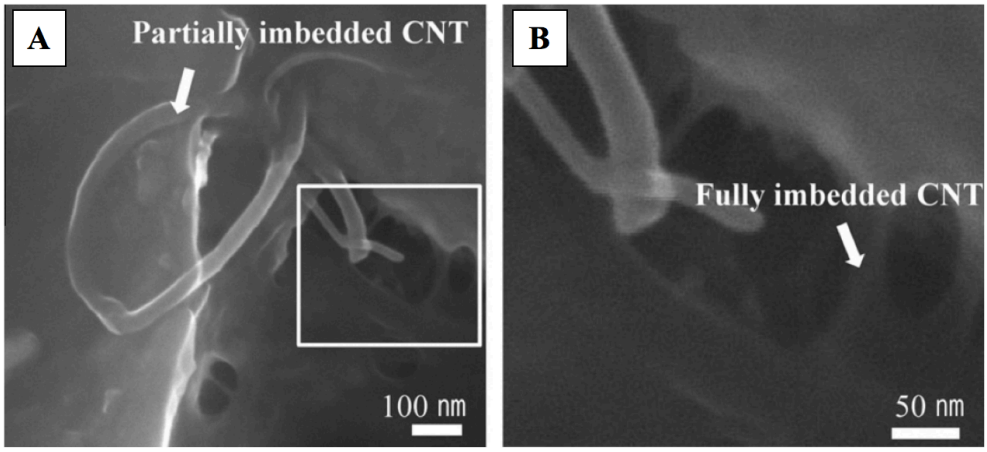

Figure 2-51 SEM imaging of SiC coated CNTs that are A) fully embedded, and B) partially embedded in the aluminum matrix.[128]

The SiC coating approach of CNTs was found complex and time consuming especially with the high processing temperature required for silicon to react with CNT flakes and form SiC around CNTs. Therefore, most of the recent research has focused on coating CNTs with metals that can be processed at low temperature using electrochemical techniques. Metals such as nickel, copper, and silver were found perfect for decorating CNTs prior to being embedded in molten aluminum. These metals can be deposited using a stand-alone low cost electroless plating approach that will be discussed in detail in section 2.8.

- **Induction melting**

The induction melting utilizes the electromagnetic stirring action to disperse CNTs in the aluminum matrix.[101], [129] In 2016, scientists managed to develop a process that uses an air induction furnace in fabricating Al-CNT composites. The fabrication of the composite was done by mixing MWCNTs with fluxes using a mortar and pestle before being used as a feedstock in the casting process. The main function of fluxes was to reduce the melting temperature of aluminum and protect the composite from oxidation in the air without affecting the overall chemical composition of the matrix.[129] To prepare the composite, the procedures shown in Figure 2-52 were conducted by introducing pure aluminum slabs into a cruicible in which the induction melting takes place. When aluminum was partially melted at 660 ℃, the mixture of fluxes and MWCNTs was added to the cruicible. At 760℃, aluminum fully melts and the self stirring action of the magnetic flux starts to take place dispersing CNTs in the

matrix. The rapid heating induced by induction melting was found useful in protecting CNTs from degradation.[101]

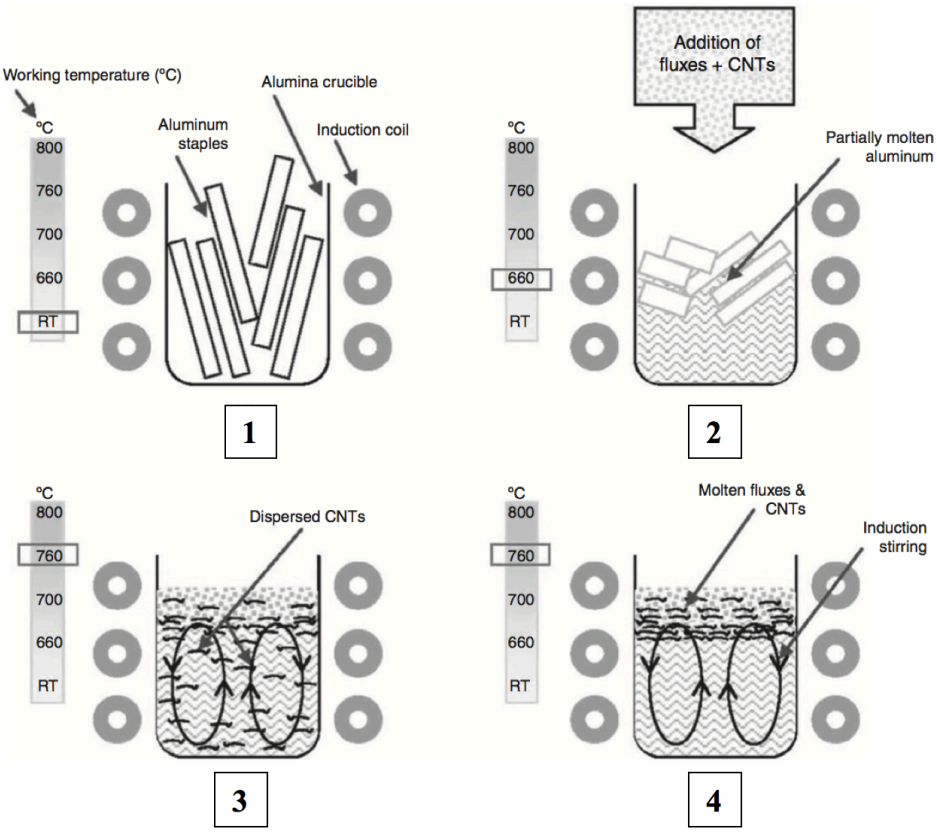

Figure 2-52 Procedures for fabricating Al-CNT composites by air induction heating.[101]

The excess fluxes on the surface of the composite were removed before the mixture was poured into molds and prepared for tensile testing. Figure 2-53 (A) shows the presence of CNTs embedded in the matrix by TEM imaging. MWCNTs were also present in the fracture surface of the 0.2 % CNT-Al sample as represented in Figure 2-53 (B).

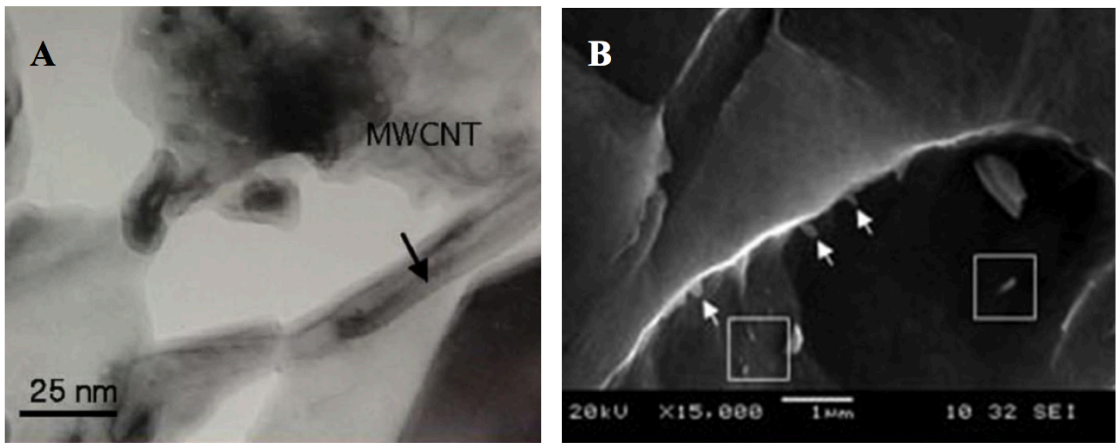

Figure 2-53 A) TEM image of MWCNTs embedded in the aluminum matrix, and B) SEM image of pulled out CNTs in the fracture surface of the composite.[101]

The mechanical testing resulted in a net increase in the elastic modulus, yield strength, tensile strength, percentage of elongation, and hardness by 5%, 77%, 52%, 44%, and 45% respectively as illustrated in Table 2-3. The increase in the percentage elongation was explained by the mismatch in the coefficient of thermal expansion between MWCNT ($\sim 1K^{-1}$) and aluminum ($\sim 23.6K^{-1}$). The increase in lattice strain could be the reason for the increase in strength by increasing the dislocation density. However, this study has avoided the use of CNTs at high percentages in the aluminum matrix. Therefore, a lack of such an investigation maybe questionable when using induction melting at high percentages of CNTs.

Table 2-3 Results of mechanical testing for the induction melted Al-CNT composites.[101]

MWCNTs (vol.%)	Elastic modulus (GPa)	Yield strength (MPa)	Tensile strength (MPa)	Elongation (%)	Hardness (HV)
0	64 ± 1.5	65 ± 5	82 ± 4	2.15 ± 0.35	27 ± 4
0.1	65 ± 2.1	105 ± 4	112 ± 3	2.35 ± 0.40	34 ± 4
0.2	67 ± 2.9	115 ± 5	125 ± 3	3.10 ± 0.55	39 ± 5
Net change (%)	~5	~77	~52	~44	~45

To compare the casting techniques with the powder metallurgical approaches for the production of Al-CNT composites, the mechanical processing of Al-CNT composites by ball milling not only involved harsh processing steps leading to the breakage of CNTs and create aluminum carbides (depending on the milling parameters used) but also increased the sources of contamination from the used stainless steel balls and jars in addition to the long milling time.[99], [130], [131] Table 2-4 addresses the pros and cons of casting compared to the ball milling and powder sintering technique in producing Al-CNTs.

Table 2-4 A comparison between casting and sintering of ball milled powders in producing Al-CNT composites.

Comparison	**Casting**	**Ball milling +sintering**
Ease of production	✓	✗
Mass production	✓	✗
Heavy parts production	✓	✗
Cost effectiveness	✓	✗
Intricate shapes	✓	✗
Excellent dispersion of CNTs	✗ The poor dispersion of CNTs in molten Al was avoided by the indirect	✓ CNTs are dispersed in aluminum by mechanical forces.

	introduction methods of CNTs in the matrix.	
Excellent wetting of CNTs in aluminum	✕ wettability of CNTs in molten Al is poor. It can be improved by metal coating of CNTs using electrochemical techniques.[15], [17], [105], [128], [132]	**Not-applicable** As the Al-CNT powders are consolidated from their solid state, the wettability did not represent an a problem.
Improvement of tensile strength	✓	✓
2 wt.% CNTs	~280 MPa[102] (Mixed MWCNTs with Al and Mg in NR followed by melting of aluminum slap on top of the mixture at 800℃)	~243 MPa[118] (Ball milling + pressureless sintering at 550℃ + hot extrusion at 500℃) ~184MPa[133] (Ball milling + cold compaction (2 Ton/Cm^2 + Sintering at 580℃ for 90 min + cold extrusion)
1 wt. % CNTs	~265 MPa[128] SiC coated CNTs added to molten 356.2 Aluminum alloy.	~245 MPa[6] Ball milled Al-CNT powders were compacted and hot extruded at 500℃
0.2 wt. % of CNTs	~125 MPa[101] (mixed CNTs with a flux + casting in pure Al) ~193 MPa[104] (Ball milled CNTs added to A356 molten aluminum alloy)	–

Good ductility of the composite	✓	✕ % elongation is reduced as a result of strain hardening of Al
% strain	~15%[102] (for the 2 wt. % CNTs)	$\sim 5.7 - 7.9\%$[7] (for the 2 wt. % CNTs)

Table 2-4 has shown the potential of the casting technique in producing Al-CNT composites of a tensile strength that is comparable to those produced by powder metallurgy. The casting approach induced a better improvement of the tensile strain for Al-CNT composites. The poor dispersion and wettability of CNTs in molten aluminum was easily solved by adopting techniques that rely on the indirect introduction of CNTs in the matrix. However, these techniques add extra cost and complexity to the Al-CNT composites hindering the merit of the casting technique as a low cost technique. Therefore, a new strategy to tackle the problems of casting Al-CNTs has been followed by different researchers via using simple and low cost electroless plating approaches for coating CNTs with metals for the purpose of making them wettable in molten aluminum. This approach could combine the advantages of low cost and simplicity in imparting a great surface modification of CNTs prior to casting them in pure Al.

2.8 Electroless plating

Electroless plating is an electrochemical technique that is similar to electroplating in inducing an electrochemical reduction of metal ions on top of the part to be plated. The main difference between both techniques is that in electroless plating, the metal ions are being reduced in an autocatalytic manner via a reducing agent without the need for connecting the part to be plated to an external power source.[134] The main prerequisite for electroless plating is that the surface to be coated has to be catalytic in nature. If not, catalytic nanoparticles have to be applied on the surface prior to the electroless plating.[135]–[137] These catalytic nanoparticles help in the kick start process of the reduction for metal ions on top of the surface to be coated. The reduced metallic ions nucleate on the surface of the substrate and promote the growth of the initial metallic film. Once the first layer is grown, an autocatalytic reduction process of the metal ions on top of the grown metallic layer starts to take place as a result of the electrons donated by the reducing agent. The thickness of the deposit can be controlled by controlling the deposition time. The electroless deposition is advantageous over electroplating in

producing uniform coats by insuring constant current density all over the surface as illustrated in Figure 2-54.

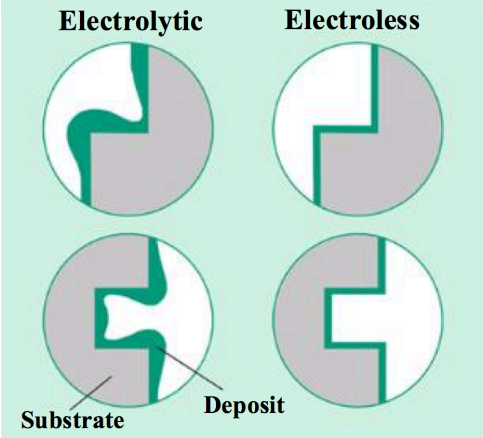

Figure 2-54 Film uniformity in electrolytic Vs. electroless plating.[138]

2.8.1 Catalyzation systems for substrates

As mentioned earlier, the catalyzation step of surfaces is mandatory prior to electroless plating especially when surfaces to be electroless plated are not catalytic in nature. Palladium nanoparticles are the most commonly used catalyst in electroless plating.[15]–[21], [132], [135], [136], [139], [140], [140]–[147], [147]–[150] Palladium has eighteen valent electrons but the most important feature of palladium is the location of the highest energy electrons in the d shell that is the furthest from the nucleus which means that these electrons are loosely bound to the nucleus. Besides, palladium is known for the ease of addition or removal of electrons from the $d_{x^2-y^2}$ subshell that happens as a result of the smaller energy barrier between d_{xy} and $d_{x^2-y^2}$ subshells as represented in Figure 2-55.

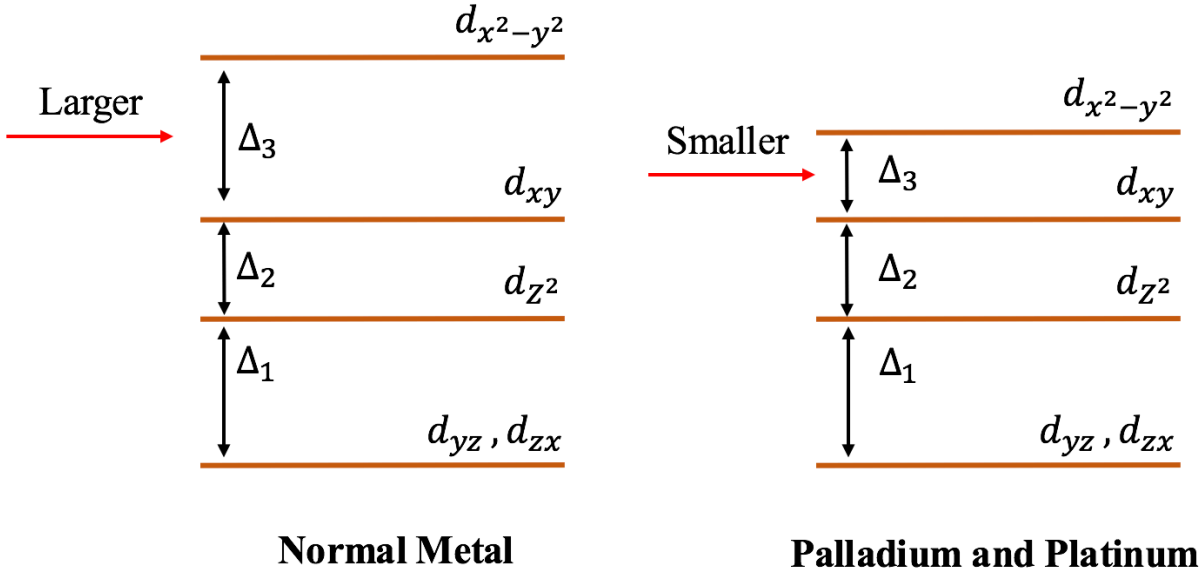

Figure 2-55 Normal metals vs. palladium in d_{xy} and $d_{x^2-y^2}$ electron transitions.[151]

Palladium nanoparticles are usually deposited by a two-step process. The first step involves the sensitization of substrates in an acidic stannous chloride solution ($SnCl_2$) in which tin ions (Sn^{+2}) attach themselves to the surface of the substrate. The second step is the activation step where the sensitized substrate is cleaned with distilled water and soaked into a palladium chloride solution ($PdCl_2$) in which Pd^{+2} ions are reduced as a result of Sn^{+2} ions attached on the surface of the substrate as illustrated in Equation 2-6.[139]

$$Sn^{+2}(s) + Pd^{+2}(aq) \rightarrow Sn^{+4}(s) + Pd^{0}(s) \qquad \text{Equation 2-6}$$

Figure 2-56 indicates that the end result of the two-step activation process is the growth of palladium particles on top of Sn^{+4} sites located on the surface of the substrate.

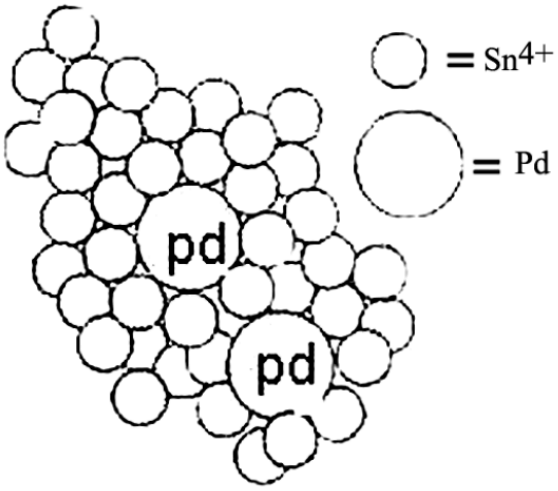

Figure 2-56 Lifted up palladium particles enclosed by stannous chloride.[140]

The previous two-step approach has undesirable drawbacks; namely, the hygroscopic nature of $SnCl_2$ that makes it liable to decomposition once exposed to moisture and humidity. Therefore, the sensitization process needs to be carried out in an inert atmosphere and preferably in a glove box. The second shortcoming of this approach is the lack of control over the quality of Pd particles. The diameter of Pd nanoparticles produced by this technique varies from 2 nm to 50 nm and hence, it is hard to obtain reproducible result via this approach. Finally, the volume of each solution needs to be optimized over different surface areas of substrates which is time consuming and practically difficult especially when the objects to be plated possess high surface area to volume ratio such as in the case of CNTs. Therefore, a one-step approach was developed by a group of researchers to tackle the previous problems.[137] It relies on the formation of a stable colloidal palladium-tin (Pd-Sn) solution that can be used in ambient conditions for any substrate. The colloidal Pd-Sn particles are an alloy of Sn and Pd of 1:7 elemental ratio. The average Pd-Sn particle size is 2-3 nm. The one-step approach

activates the substrate by adsorbing Pd-Sn nanoparticles to its surface. However, stannous hydroxide $Sn(OH)_2$ forms on top of the catalytic particles. Therefore, an accelerating step has to be carried out to remove excess $Sn(OH)_2$ from the surface and improve its catalytic activity as illustrated in Figure 2-57. Common accelerating media are NaOH, HCl, H_2SO_4, NH_4OH, and NH_4BF_4 in water.[135]

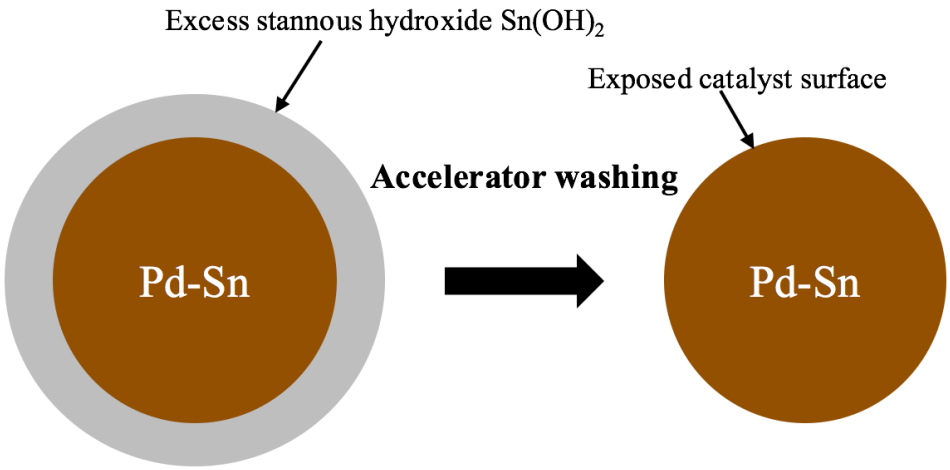

Figure 2-57 Effect of acceleration on increasing the catalytic activity of Pd-Sn particles.[137]

2.8.2 Electroless copper plating

Copper can be easily deposited from aqueous electrolytes at temperatures as low as room temperature and as high as 80°C.[100], [132], [143]–[146], [149], [152]–[154] During electroless copper plating, two reactions take place simultaneously. These two reactions are split into an anodic partial reaction that involves the oxidation process of a reducing agent to release electrons and a cathodic partial reaction that involves the reduction of metal ions by gaining electrons generated in the anodic reaction.[134], [143], [155] Copper ions are used as a source of copper. These ions can be released by dissolving copper sulfate ($CuSO_4$) in water. The most widely used reducing agent for copper electroless plating is formaldehyde, the electrochemical reduction potential of copper can be easily satisfied by oxidizing formaldehyde using sodium hydroxide (NaOH).

2.8.3 The mixed potential theory

For electroless plating, both anodic and cathodic partial reactions take place simultaneously. The anodic partial reaction is an oxidation reaction that is intended for the production of electrons. At the same time, these produced electrons are used in the reduction process in the cathodic partial reaction. The mixed potential theory represents the simultaneous change of the electro potential for both reactions at the same time.[155]

There are three types of potentials in an electroless plating reaction. These potentials are classified as follows:

1- Potential of the reducing agent oxidation reaction (E_{red})

In copper electroless plating, formaldehyde is used as a reducing agent. It gives electrons by being oxidized via (OH^-) groups generated by the addition of sodium hydroxide (NaOH). The oxidation results in the formation of formic acid besides the electrons stripped from the formaldehyde as illustrated in Equation 2-7.[141] Losing electrons means that the energy state of the reaction is in a spontaneous increase with the increase of the oxidation rate as implied in Figure 2-58.

$$2HCHO\ (low\ energy) + 4OH^- \rightarrow 2HCOO^-(high\ energy) + H_2 + 2H_2O + 2e^- \qquad \text{Equation 2-7}$$

2- Potential of metal ions reduction reaction (E_m)

This potential is associated with the reduction of copper ions using the electrons donated from the oxidation reaction of formaldehyde. The reduction of copper ions results in copper in its metallic form. Therefore, the reaction is driven from a high energy state (Cu^{2+}) to a low energy state (Cu) as illustrated in Equation 2-8.

$$Cu^{2+}(high\ energy\ state) + 2e^- \rightarrow Cu\ (low\ energy\ state) \qquad \text{Equation 2-8}$$

3- Mixed potential (E_{mp})

Both the anodic and the cathodic partial reactions take place simultaneously. The more electrons are produced, the more copper ions are reduced. The mixed potential is the equilibrium potential at which the deposition of copper starts to take place on top of the catalyzed surface to be plated as represented in Figure 2-58. This deposition takes place when the deposition current is equal to the oxidation current as well as the reduction current as illustrated in Equation 2-9.[142]

$$I_{dep} = I_m = I_{Red} \qquad \text{Equation 2-9}$$

Where I_{dep} is the current at which the copper deposition takes place, I_m is the current at which metal deposition starts to take place as a result of the reduction of copper ions, and I_{Red} is the current withdrawn from the reducing agent oxidation reaction. Equation 2-10 shows that the mixed potential deposition current (I_{dep}) can be used to calculate the deposition rate according to Faraday's law.[143]

$$\text{Deposition rate (mg/cm}^2\text{/hour)} = 1.18 * I_{dep} \qquad \text{Equation 2-10}$$

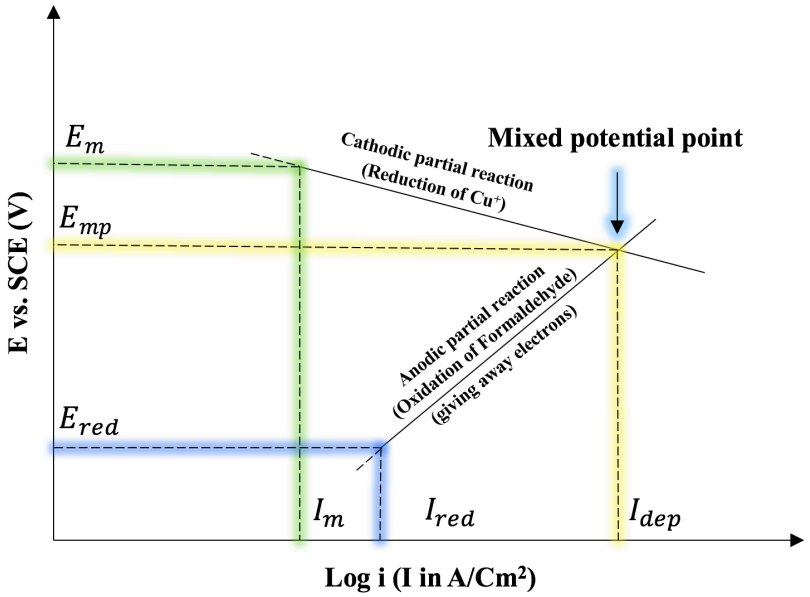

Figure 2-58 Evan's mixed potential diagram for copper electroless deposition.[155]

2.8.4 Factors affecting the deposition rate of copper

The deposition rate of copper in electroless plating is affected by many parameters including the PH level, the deposition temperature, and the catalytic activity of the surface to be plated.

1- pH level of the electroless solution

The copper deposition rate is affected by the pH level. The presence of OH^- groups is essential for the oxidation reaction of formaldehyde. The increase in OH^- groups in the ionic solution renders the entire solution basic. As a result, the pH level increases. In a recent study, the increase of pH level in the solution was found to increase the deposition rate of copper as indicated in Figure 2-59. This increase in the deposition rate was found obvious as more electrons are produced for the reduction process of copper ions.

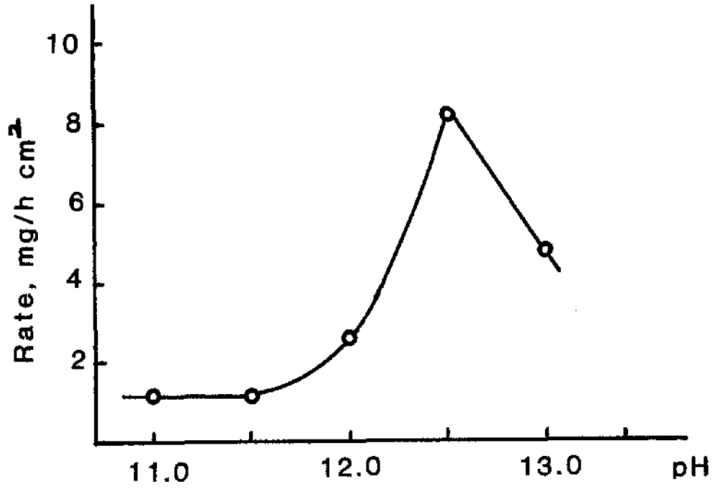

Figure 2-59 Effect of the pH level on the copper electroless deposition rate.[152]

When the pH level exceeds 12.6, it results in a tremendous drop in the deposition rate due to the consumption of OH^- ions in the hydrolysis reaction of formaldehyde to form methylene glycol anions as represented by Equation 2-11. These anions react with more OH^-groups to produce formate ions as indicated in Equation 2-12.[144]

$$HCHO + OH^- \rightarrow CH_2(OH)O^- \qquad \text{Equation 2-11}$$

$$CH_2(OH)O^- + OH^- \rightarrow CHOO^- + H_2O + e^- \qquad \text{Equation 2-12}$$

2- Electroless solution temperature

When the electroless plating solution is heated, the mobility of copper ions increases and hence, the deposition rate increases as represented in Figure 2-60. Heating also accelerates the rate of formaldehyde oxidation which results in generating more electrons to be used in reducing copper ions.

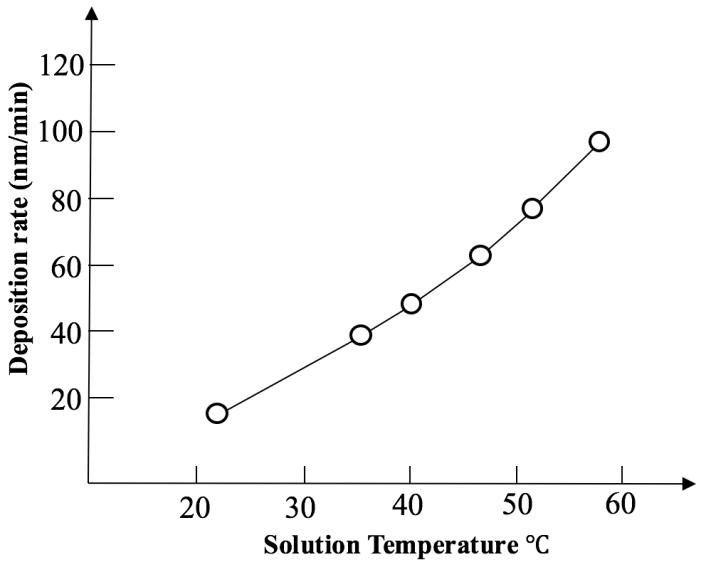

Figure 2-60 The correlation between electroless solution temperature and copper deposition rate.[153]

3- Substrate catalytic activities

The electroless deposition of copper was found difficult on surfaces that are not catalytic due to the kinetic barrier between copper ions and non-reactive surfaces. In order for copper to be deposited, a catalytic surface is needed to kick-start copper deposition that depends mainly on nucleation and thin film growth. The deposition rate of copper depends partially on the catalytic activity of the surface to be plated. In particular, the size of catalytic nanoparticles of the surface controls the kick start deposition rate. For palladium, the smaller the particle size, the higher the surface area to volume ratio. This results in better catalytic reduction of copper ions with more electrons that are present on the surface of the catalytic particles.

There are three major steps for the growth of copper films using the electroless deposition method as represented in Figure 2-61. The success in electroless copper deposition mainly depends on the presence of highly catalytic palladium nanoparticles on top of the surface to be plated. At the beginning of the reaction, copper ions get reduced as a result of the electrons shared by the catalyst (conducting the electrons generated by the reducing agent) in a step that is called the kick-start deposition. This results in the growth of a thin copper film on top of palladium particles. Afterwards, thicker copper coats can be achieved by an autocatalytic copper deposition process that mainly depends on the reduction of copper ions as a result of the electrons donated by the reducing agent.

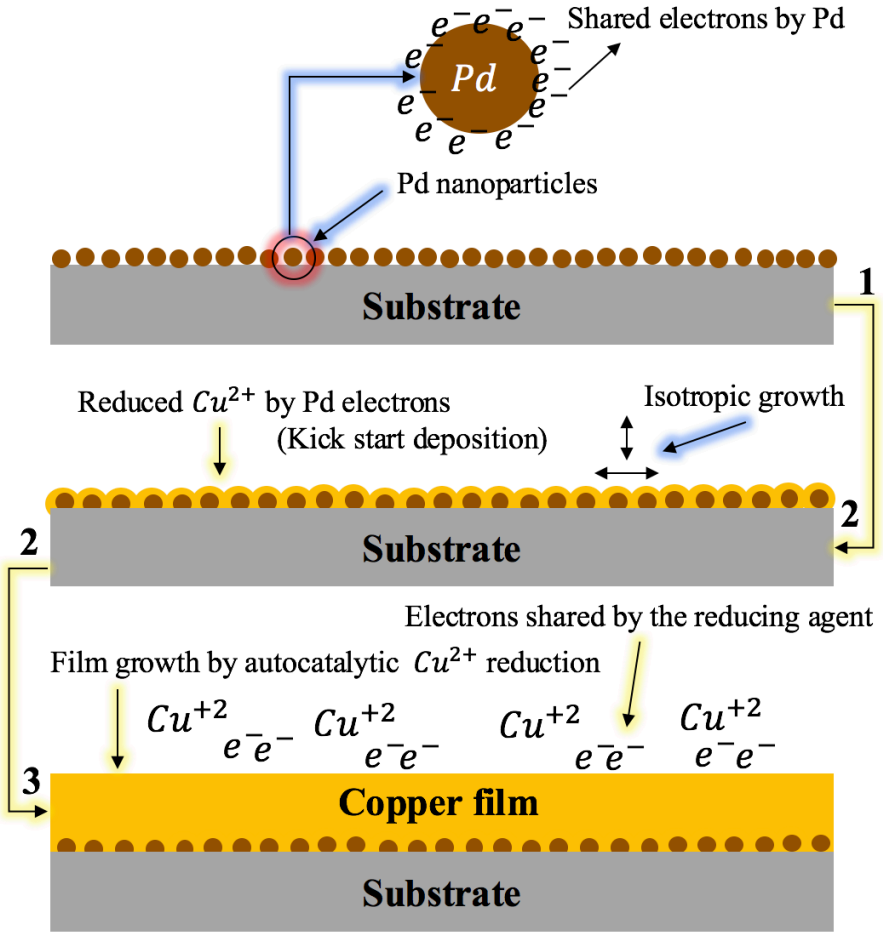

Figure 2-61 Mechanisms of copper electroless plating in presence of palladium as a catalyst.

The quality of the copper film from the point of view of surface coverage was found to be dependent on the concentration of the catalyst applied on the surface prior to plating. This can be interpreted as a result of the dependence of copper deposition rate on the concentration of palladium on the surface of the substrate. When more catalyst was used, the deposition rate increased tremendously as represented in Figure 2-62.

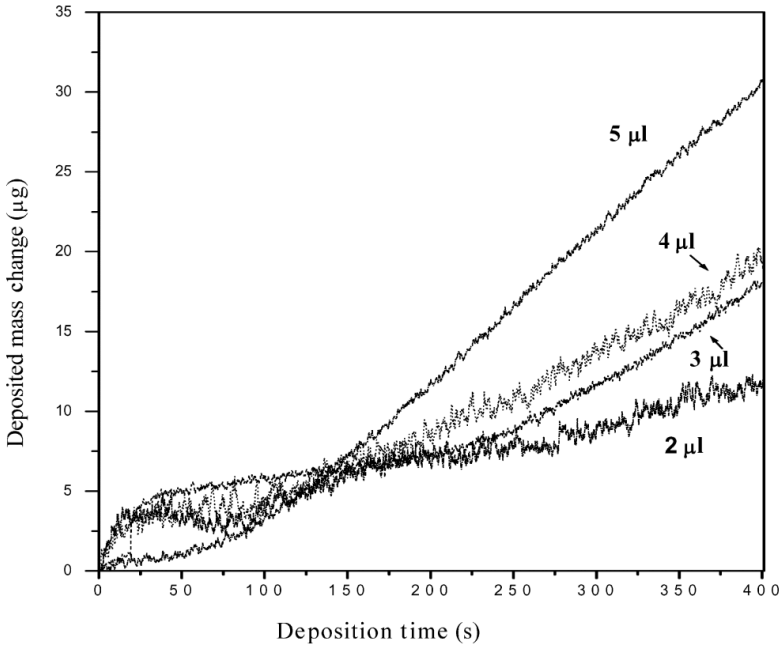

Figure 2-62 Increase of the deposition mass change as a result of the increase in the amount of Pd. [145]

Low catalyst concentrations were found to result in poor film growth as represented in Figure 2-63 (A-C). Using a decent amount of the catalyst on the surface results in an excellent coverage of the plated surface by copper as clearly seen in Figure 2-63 (D).

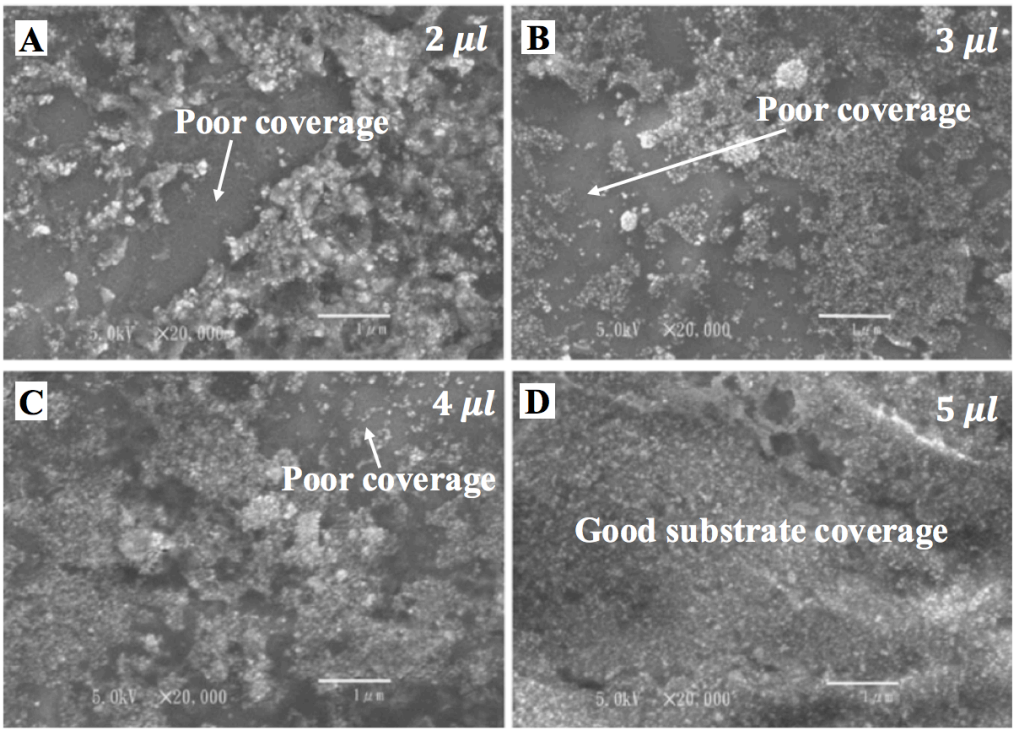

Figure 2-63 SEM imaging indicating the surface coverage by copper on palladium catalyzed substrates via A) 2μl, B) 3μl, C) 4μl, and D) 5μl Pd-solutions.[145]

2.9 Synthesis of metal coated CNTs by electroless plating

Electroless plating was found the ideal cost effective solution of coating CNTs with metals for the purpose of improving their dispersion and wettability in molten aluminum matrices. The surfaces of CNTs are not catalytic. Therefore, a catalyst has to be applied in order to render their surfaces reactive before putting them in the electroless plating bath.[17] Palladium nanoparticles are known for their catalytic activity. Therefore, they are widely used in activating surfaces prior to the electroless deposition.[136], [137], [146] Palladium helps in initiating the nucleation of the first metallic layer on the plated surface. Metals such as copper, nickel and silver was successfully plated on CNTs from aqueous electrolytes due to their electrochemical reduction potential that lies in the electrochemical window of water.[15]–[19], [100], [132], [147]–[150]

A lot of research has been done on metallizing CNTs with different metals for different applications. Previously, a film of grown CNTs on a substrate was coated by nickel using electroless plating. CNTs were catalyzed with palladium in a two-step process by the sensitization of CNTs in an aqueous $SnCl_2$/HCl solution at 20 ℃ for 30 min followed by the activation of CNTs in $PdCl_2$/HCl at 20 ℃ for another 30 min considering the rinsing of the film in DI water after each step. Afterwards, the electroless deposition of nickel was carried out in a nickel sulfate ($NiSO_4$) aqueous bath containing sodium hypophosphite (NaH_2PO_2) as a reducing agent. This reaction is governed by Equation 2-13. The deposition resulted in conformal Ni coats on CNTs as represented in Figure 2-64.[156]

$$Ni^{2+} + H_2PO_2^{-} + H_2O \rightarrow HPO_3^{2-} + 3H^{+} + Ni \quad \text{Equation 2-13}$$

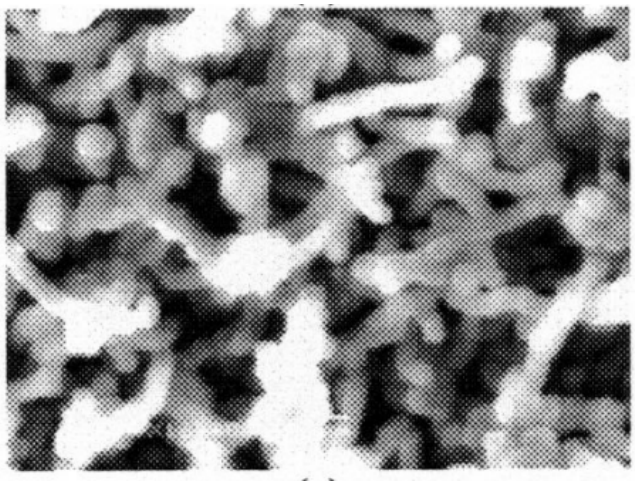

Figure 2-64 SEM image of nickel electroless plated CNT film.[156]

In another study, Nickel was also plated on CNTs in their powder form in a similar process as the previous study. The coating also led to conformal coating as proven by the TEM imaging

shown in Figure 2-65. This coat was intended for the study of the magnetic properties of Ni-CNTs.[16]

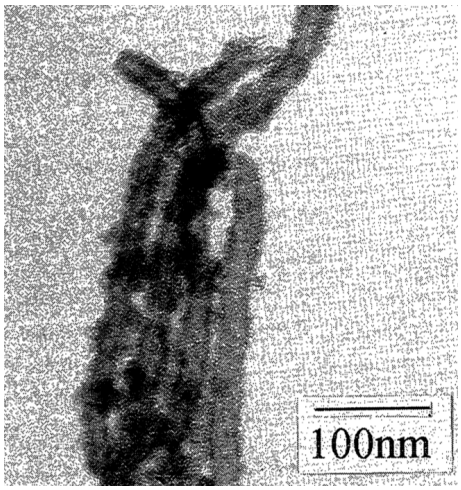

Figure 2-65 TEM image of nickel coated CNTs.[16]

Ni-coated CNTs were also used in other applications such as producing Al-CNT composites via the casting technique.[15] To improve the wettability between aluminum and MWCNTs, a coat of Ni-P was applied on the surface of MWCNTs by electroless plating. The plating resulted in a conformal coat of Ni-P on the surface of CNTs as shown in Figure 2-66. These Ni-P coated CNTs were added to molten aluminum and the effect of Ni-P on the wettability was investigated as will be discussed in section 2.9.1.

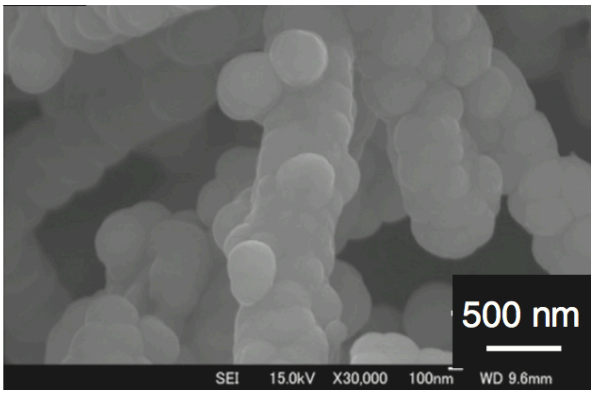

Figure 2-66 High resolution SEM imaging of Ni-P coated CNTs.[15]

In a study intended for using Ag-CNT composites in electronic applications, silver was coated on palladium activated CNTs by electroless deposition. The plating bath consisted of an aqueous solution of silver nitrate and formaldehyde as a reducing agent. The plating was done at 20 ℃. A continuous film of silver was obtained on the surface of CNTs as shown in Figure 2-67. The prepared Ag-CNT powder was intended for the use in Ag-CNT composites used in electronic applications.

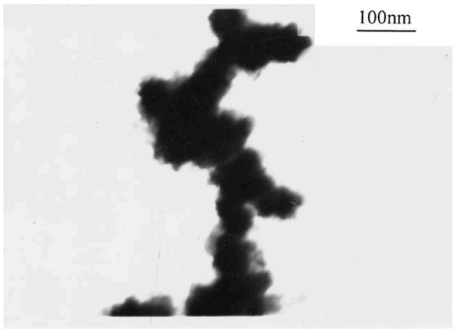

Figure 2-67 TEM imaging of a silver coated CNT via electroless deposition.[18]

Researchers have also tried coating CNTs with copper prior to being mixed with aluminum powder.[100], [154] The activation of CNTs was done by the two-step approach mentioned in 2.8.1. The electroless copper plating was done in a copper sulfate aqueous solution using formaldehyde as a reducing agent. The process resulted in a structure of copper that has embedded CNTs rather than coating individual CNTs with copper as illustrated in Figure 2-68.

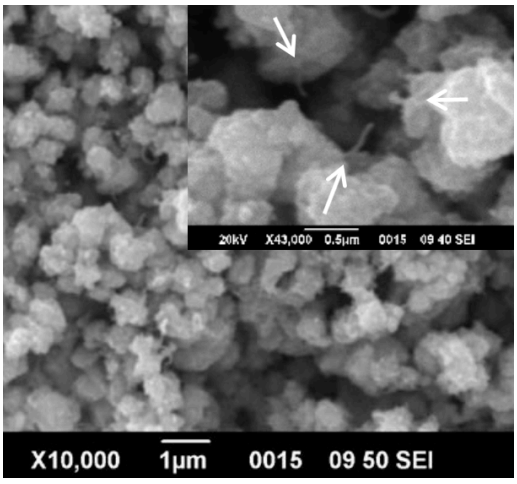

Figure 2-68 SEM image of Copper coated CNTs showing CNTs embedded in aggregated copper structures. [100]

2.9.1 Improving wettability of aluminum with CNTs by electroless plating

The poor wetting phenomenon between aluminum and CNTs addressed in section 2.6.4 has driven a lot of researchers to adopt the electroless plating of CNTs with different metals as an approach to increase the density of CNTs and create a wettable interface between CNTs and molten aluminum. Previously, the coat of nickel-phosphorous (Ni-P) shown in Figure 2-66 was provided on CNTs for improving their dispersion and wettability in pure cast aluminum.[15] The indicated poor wetting in Figure 2-69 (A) could be resolved by the applied Ni-P coat on CNTs as indicated in Figure 2-69 (B).

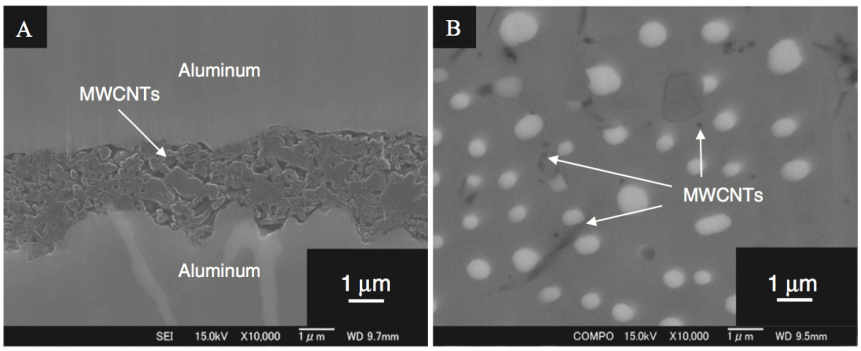

Figure 2-69 Cross-sectional SEM images of Al-CNT wettability A) before Ni-P coating B) after Ni-P coating. [15]

A serious drawback of using Ni-P can be seen in the alloying effect detected between nickel and aluminum as a result of the dissolution of Ni-P into the molten aluminum indicated in Figure 2-70 (A) and formation of Al-Ni intermetallic compounds besides phosphorous oxides as illustrated in Figure 2-70 (B).

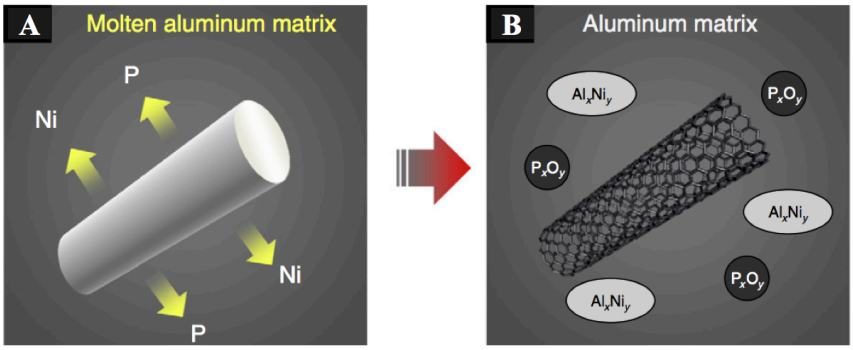

Figure 2-70 Alloying of Ni-P with the aluminum matrix by A) the dissolution of Ni and P in the aluminum matrix B) the formation of Al-Ni intermetallic compound (Al_xNi_y) in addition to phosphorous oxide (P_xO_y).[15]

The previous alloying effects in the aluminum matrix were reported to change the mechanical and electrical properties of the aluminum matrix and to give misleading results especially when the focus is on studying the effect of CNTs addition on improving the mechanical properties of pure aluminum. Therefore, providing a pristine aluminum coat on CNTs before embedding them in molten aluminum would be ideal to avoid any unintended alloying effects that might be involved in the structure of the aluminum matrix. Due to the several electrochemical challenges in the aluminum electroless plating field as will be discussed in detail in section 2.10, there have not been much research done in coating CNTs with aluminum. however, a research that indicated the potential of using aluminum coats on CNTs to improve their wettability with aluminum was carried out by electroplating a CNT film with aluminum

followed by applying a coat of aluminum powder on their surface that was then sintered at 700℃ as represented in Figure 2-71.

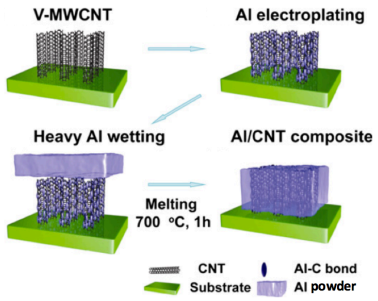

Figure 2-71 Process of heaving aluminum wetting with CNTs by electroplating followed by sintering the aluminum powder on top of the plated film.[105]

By electroplating the CNT film with aluminum in an electrolyte composed of $AlCL_3$-LAH in tetrahydrofuran (THF) and benzene, a conformal aluminum coat was obtained as shown in Figure 2-72. This process involved the use of an external power source that connects the CNTs film as a cathode and a pure aluminum substrate as an anode.

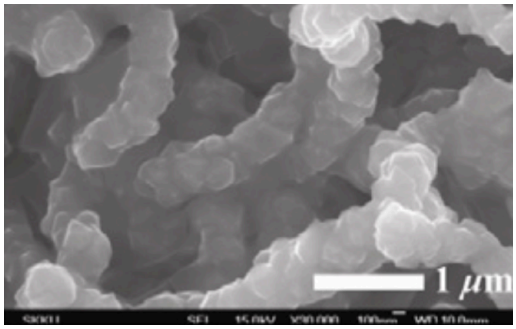

Figure 2-72 SEM image of aluminum electroplated CNTs film.[105]

When pure aluminum powder was used to coat the surface of Al-plated CNTs, aluminum wetting was achieved after sintering the entire film at 700℃ as shown in Figure 2-73 (A-B) that compares between CNTs without being Al-plated and CNTs after being Al-plated and wetted with the aluminum powder.

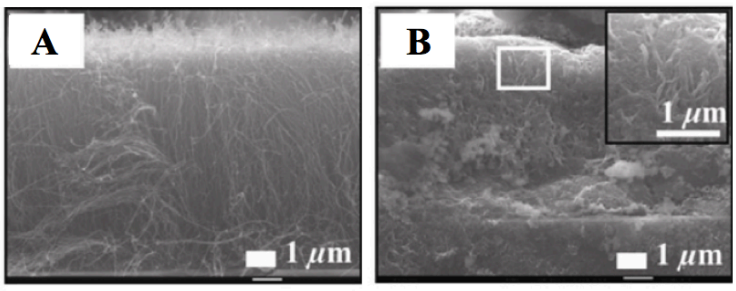

Figure 2-73 SEM imaging of A) CNT film without Al plating B) Al-coated CNT film after Al-wetting.[105]

For Al-CNT composites produced by casting, CNTs are used in their powder form. This implies that individual CNTs cannot be connected to an external power source for plating in addition to the need of well-dispersing them in the plating bath. Therefore, the aluminum electroplating approach cannot be used for CNT powder.

The focus of the current study is to develop a cost effective electroless plating process of aluminum that can be compatible with CNTs of high surface area to volume ratio. Aluminum electroless plating was not previously addressed in the literature to coat CNTs. However, it was performed on different substrates including glass and copper.[20], [21] There are many challenges that make aluminum electroless plating difficult. These challenges are addressed in 2.10.

2.10 Electroless plating of aluminum

Aluminum electrodeposition is challenging because aluminum has a standard reduction potential of -1.66 E(V) in an aqueous solution.

Due to the narrow electrochemical window (EW) of water, the electrochemical energy intended for the electrochemical reduction of aluminum is ruined by the electrolysis of water whenever it is desired to deposit aluminum from an aqueous solution.[20]

The location of the electrode potential of aluminum outside the oxidation and reduction potential limits of water shown in Figure 2-74 makes it difficult for scientists to develop a water based solution for aluminum electroless plating.

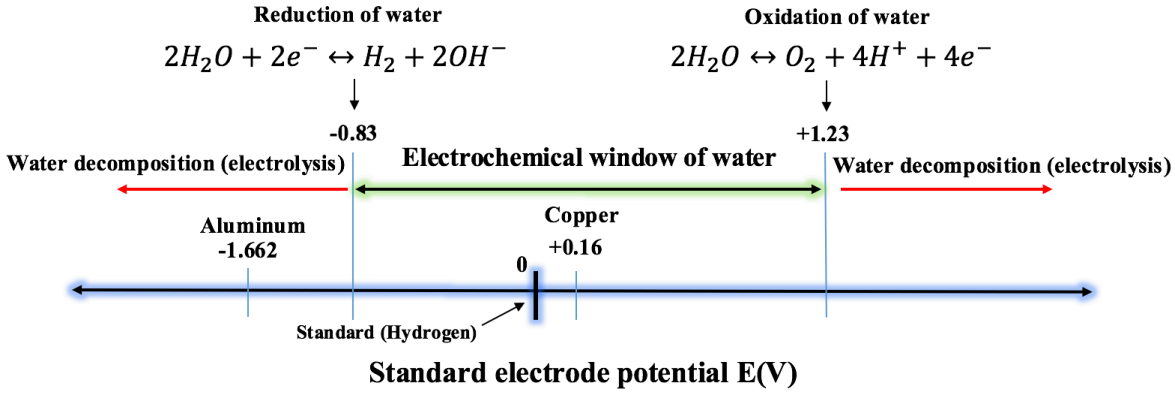

Figure 2-74 Positions of copper and aluminum electrode potentials compared to the electrochemical window of water. [20], [21], [157]

Therefore, scientists have developed a non-aqueous approach for electrodepositing aluminum using ionic liquids. Ionic liquids are ionic compounds of a melting temperature below 100°C and some of them melt at room temperature.[20], [21], [158]–[160] These ionic liquids are known for their wide electrochemical window.[161]

2.10.1 Ionic solutions Vs. Ionic liquids

There are common features between ionic liquids and ionic solutions such as the low energy consumption, low pollutant emission, low operating cost, and high electric conductivity. However, ionic liquids possess a number of attractive features over the normal ionic solutions. These features such as the wide electrochemical window and adjustable Lewis acidity make the ionic liquids dominant when plating active metals such as aluminum.[158]

2.10.2 Room Temperature Ionic liquids (RTILs) used in aluminum electroless deposition

There are several ionic liquids that are developed for the purpose of electrodepositing aluminum. Most of these ionic liquids are based on chloroaluminate melts such as 1-ethyle-3-methyl imidazolium chloride- aluminum chloride (EMIC-$AlCl_3$). The reaction between EMIC and $AlCl_3$ results in the formation of a strong positive electrophile in addition to an $AlCl_4^-$ anion as illustrated in Figure 2-75. This combination results in a wide electrochemical window that varies from 2.8-4.4 V depending on $AlCl_3$: EMIC molar ratio.[162]

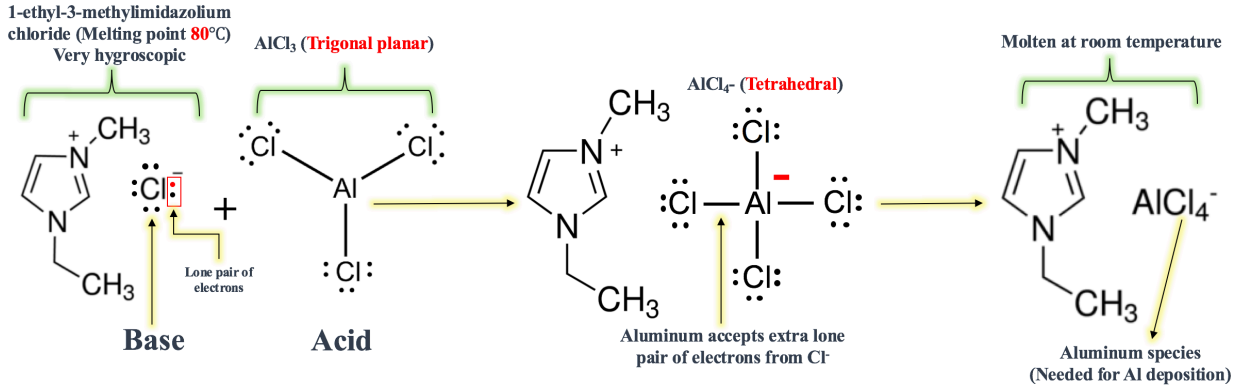

Figure 2-75 EMIC-$AlCl_3$ reaction.[163]

The change in the molar ratio between $AlCl_3$ and EMIC plays a big role in adjusting the Lewis acidity of the ionic liquid. When the molar fraction of $AlCl_3$ is below 0.5 (1:1 molar ratio of $AlCl_3$:EMIC), it results in a Lewis base.

By adding more $AlCl_3$ to EMIC such that the molar fraction of $AlCl_3$ is above 0.5, it results in a Lewis acid as indicated in Figure 2-76 that represents the phase diagram of EMIC-$AlCl_3$ ionic liquid. It is noticeable that EMIC-$AlCl_3$ can be tuned as a room temperature ionic liquid (RTIL). This tuning copes with the use of this ionic liquid in the aluminum deposition since the deposition of aluminum does not take place in Lewis bases.

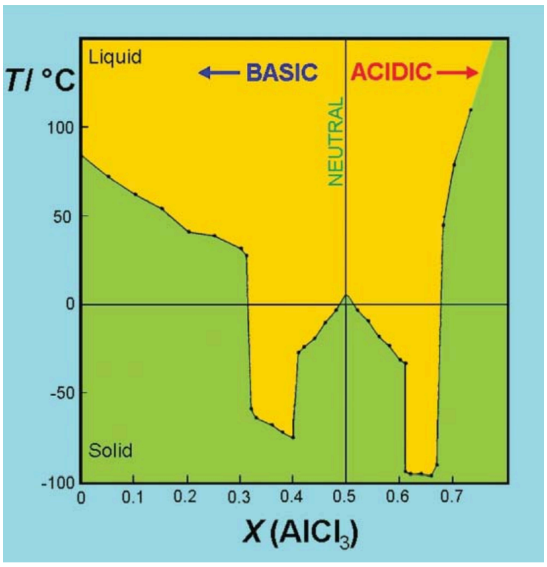

Figure 2-76 The phase diagram of $AlCl_3$-EMIC ionic liquid.[164], [165]

The increase in the molar fraction of $AlCl_3$ in the ionic liquid results in a tremendous increase in $AlCl_4^-$ ions until a threshold point is reached at which adding extra $AlCl_3$ results in a rapid conversion of $AlCl_4^-$ ions to $Al_2Cl_7^-$ ions as illustrated Figure 2-77. This conversion is governed by Equation 2-14.[166], [167][166][176]

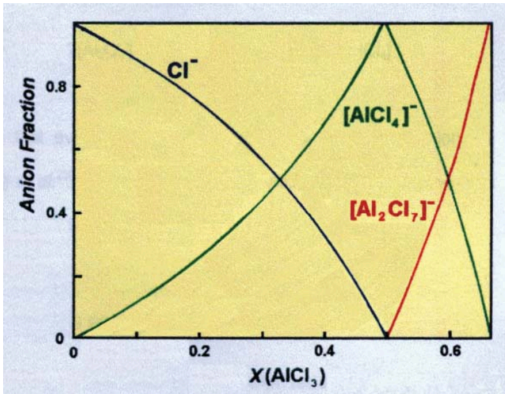

Figure 2-77 Effect of adding $AlCl_3$ on the change of $[AlCl_4]^-$ and $[Al_2Cl_7]^-$ anions fraction.[165], [168]

$$2[AlCl_4]^- \leftrightarrow [Al_2Cl_7]^- + Cl^- \qquad \text{Equation 2-14}$$

Recent research has proven that the mechanism of aluminum electrodeposition is more dependent on the presence of $Al_2Cl_7^-$ ions than $AlCl_4^-$ ions.[169] These ionic species are preferably generated when the molar ratio between $AlCl_3$: EMIC is above 1:1 (Lewis acid).[158] Aluminum deposition takes place when $Al_2Cl_7^-$ ions are reduced as illustrated in Equation 2-15.

$$4Al_2Cl_7^- + 3e^- \rightarrow 7AlCl_4^- + Al \qquad \text{Equation 2-15}$$

The reduction of $Al_2Cl_7^-$ ions can be done in both electroplating (requires an anode, a cathode,

and an external power source) and electroless plating (by adding a reducing agent) to provide the right electrochemical reduction potential of aluminum ions.

2.10.3 The mechanisms of reducing agents in aluminum electroless deposition

In electroless plating, a reducing agent such as diisobutylaluminum hydride (DIBAH), lithium hydride, or lithium aluminum hydride (LAH) must be added to the ionic liquid for the purpose of promoting the autocatalytic electrochemical reduction of $Al_2Cl_7^-$ anions.[20]–[22] When lithium hydride (LiH) was used as a reducing agent for the purpose of donating enough electrons for the electrochemical reduction reaction indicated previously in Equation 2-15, it was proven by experiment that hydrogen gas came out of the ionic liquid. In addition, lithium cations were found to exist in the ionic liquid. Therefore, the mechanism of LiH as a reducing agent was deduced as in Equation 2-16.[20]

$$LiH \rightarrow Li^+ + \frac{1}{2}H_2 + e^- \qquad \text{Equation 2-16}$$

Another type of reducing agents that can be used in the electroless plating of aluminum is DIBAH. This reducing agent is usually dissolved in toluene and used as a liquid reducing agent. In this case, hydrogen gas was also present as a product in the reaction indicated in Figure 2-78.[21], [22]

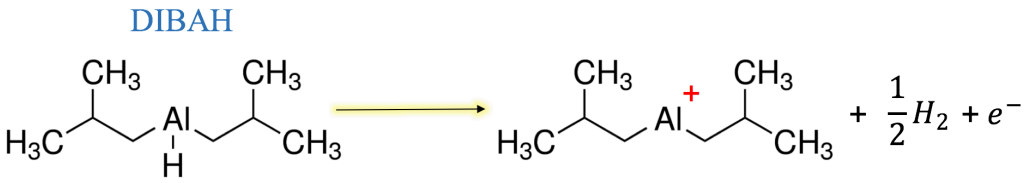

Figure 2-78 Mechanism of DIBAH as a reducing agent.[21]

Finally, LAH can also be used as a reducing agent. It was discovered that in the presence of catalytic nanoparticles, LAH decomposes at room temperature into 2 different steps as illustrated in Equation 2-17 followed by Equation 2-18.[170]

$$3LiAlH_4 \rightarrow Li_3AlH_6 + 2Al + 3H_2 \qquad \text{Equation 2-17}$$

$$2Li_3AlH_6 \rightarrow 6LiH + 2Al + 3H_2 \qquad \text{Equation 2-18}$$

The previous decomposition reactions lead to two desirable outcomes. The first outcome is related to the production of LiH that plays the same role of producing electrons as mentioned before in Equation 2-16. These electrons are essential to complete the electrochemical

reduction of $Al_2Cl_7^-$ ions essential for the deposition of aluminum as indicated before in Equation 2-15. The second beneficial outcome is related to the aluminum formed as a result of LAH decomposition reactions. This aluminum along with the aluminum reduced by electroless plating contribute to the growth of the aluminum film on top of the part to be plated.

The main challenge that faces EMIC-$AlCl_3$ system is the extremely high cost of EMIC. Therefore, it is important to find an alternative ionic liquid to reduce the cost of aluminum electroless deposition especially when high surface area to volume ratio materials such as CNTs are needed to be plated with aluminum.

2.10.4 Case studies for aluminum electroless plating

In 2008, researchers conducted an experiment for aluminum electroless plating using 66.5 mole % of $AlCl_3$ and 33.5 mole % of EMIC as an ionic liquid. A 0.1 mol L^{-1} of LiH was used as a solid reducing agent.[20] The plating was carried out at 35℃ for 2 hours. SEM imaging showed the growth of coarse aluminum crystals on top of the substrate as represented in Figure 2-79 (A). The XRD pattern shown in Figure 2-79 (B) indicated the crystallographic planes of the aluminum coated on the surface of the substrate.

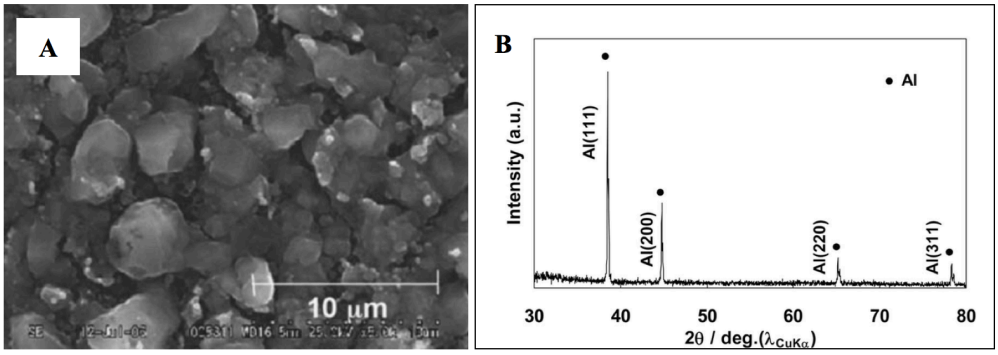

Figure 2-79 A) an SEM image of aluminum crystals obtained by electroless plating B) XRD pattern of the obtained Al-coat.[20]

In 2009, another research group in Japan performed aluminum electroless deposition in $AlCl_3$-EMIC RTIL with the same molar ratio used in the previous study.[21] Diisobutylaluminum hydride (DIBAH) dissolved in Toluene was used as a liquid reducing agent. The deposition was carried out on Pd activated glass substrate at 35℃ for 2 hours resulting in a less coarse aluminum structure than the previous study as shown in Figure 2-80 (A). The XRD analysis presented in Figure 2-80 (B) has proven the existence of aluminum in a crystalline form.

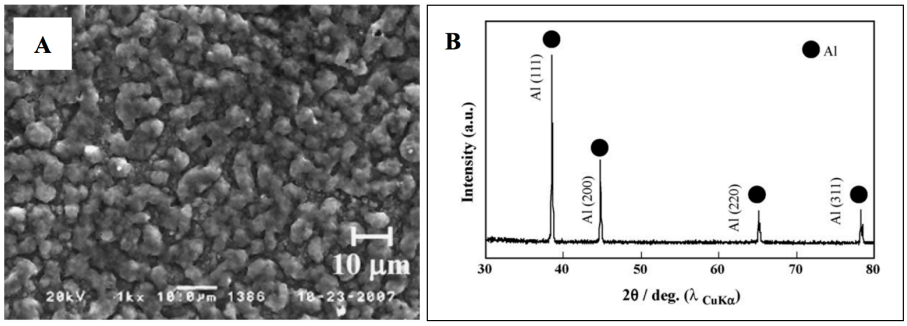

Figure 2-80 A) an SEM image of aluminum crystals obtained by electroless plating B) XRD pattern of the obtained Al-coat.[21]

The success of the electroless aluminum plating process has grabbed the attention of the current investigation to use this process in depositing aluminum on top of CNTs in order to improve their dispersion and wettability in molten aluminum during the casting of the Al-CNT composite. However, the high cost of EMIC as an ionic liquid makes this particular electroless plating approach the highest in cost among other techniques. Therefore, the current research work focused on finding cost effective ionic liquids that can generate $Al_2Cl_7^-$ ions. In 2016, a study of $AlCl_3$/Urea ionic liquid as a battery electrolyte was carried out.[171] The battery cell consisted of a graphite cathode and an aluminum anode. When the molar ratio of $AlCl_3$/Urea was 1.3, deposition of aluminum on the anode was observed as shown in Figure 2-81.

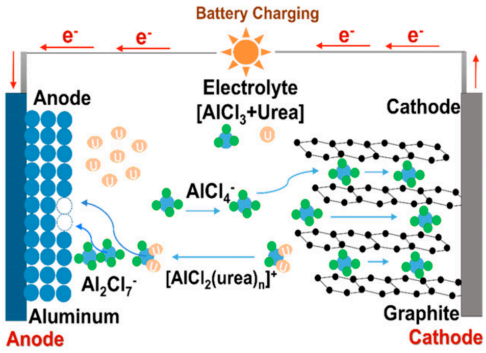

Figure 2-81 The deposition of aluminum at 1.3 molar ratio of AlCl3/Urea.[171]

Increasing the molar ratio of $AlCl_3$/Urea could lead to better ion conductivity. However, scientists concerned with studying this particular ionic liquid as a battery electrolyte tend to avoid using it at higher molar ratios of $AlCl_3$/Urea as it results in more aluminum deposition on the electrode of the battery depleting all the conducting ions in the electrolyte and making the ionic liquid useless. This phenomenon motivated the current study on the potential of $AlCl_3$/Urea RTIL as an ionic liquid for aluminum electroless deposition. Therefore, the current study is focused on tuning the molar ratio of $AlCl_3$/Urea RTIL and adding a reducing agent to create a cost effective aluminum electroless deposition process suitable for CNTs.

3. Problem statement

The main problem that this research tackles is the inability of CNTs to be dispersed and wetted in molten aluminum. This problem limits the production of Al-CNT bulk parts to powder metallurgical approaches and not casting. Therefore, success in resolving the wettability and dispersion issue of CNTs in molten aluminum will facilitate producing Al-CNT composites by casting and hence overcome many constraints associated with powder metallurgy such as complexity of shapes and the overall cost of processing. The wettability and dispersion issue of CNTs in molten aluminum could be resolved in the literature by conventional electroless plating of CNTs in aqueous solutions with metals that are different in nature than aluminum. When coating CNTs with copper, nickel, or silver, an alloying effect has been reported. The alloying effect that was observed made the process of studying the effect of adding CNTs to aluminum on the mechanical properties more complex. Therefore, this research work provides a process that can provide a pure aluminum coat on CNTs prior to being cast with pure aluminum to form Al-CNT composites.

This research work also tackles the problem of the low density of CNTs that makes them hard to disperse in molten aluminum. This can be solved by coating CNTs with aluminum to densify them before being added to molten aluminum.

Another problem that is common for Al-CNT composites is their high cost of production due to the high equipment cost of mechanical milling that is usually used in producing Al-CNT composite powders. In addition, the powder metallurgical approach involves a high cost of tooling. By producing Al-CNT composites using casting, these costs are going to be reduced tremendously. However, to be able to conduct aluminum electroless plating on CNTs prior to introducing them cast Al, the following problems will be tackled in the current research:

1- The requirement of an electroless plating electrolyte of a wide electrochemical window in order not to decompose easily during the deposition of Al on CNTs
2- The high cost of ionic liquids used for aluminum plating in the market.
3- The decomposition of ionic liquids due to excessive exothermic heat.
4- The catalyzation of CNTs required for electroless plating to work. This problem comes as a result of the small dimensions of CNTs and their high surface area to volume ratio that requires a special type of catalysis to completely cover the surface of CNTs prior to the aluminum electroless plating.

All the previous challenges, when tackled, will allow the production of a light weight and high performance Al-CNT composite by casting.

4. Aim of work

This work aims to develop a novel process by which CNTs can be coated with pure aluminum and to investigate the effectiveness of the aluminum-coated CNTs in reinforcing pure aluminum by the casting technique. Therefore, the study aims to provide good dispersion and wettability between CNTs and aluminum with minimal damage to CNTs. Unlike previous studies that focused on Ni and Cu coats in improving the dispersion and wettability of CNTs, the current study uses aluminum itself to coat CNTs. Coating CNTs by aluminum is expected to improve the wettability of CNTs in the molten aluminum matrix without involving external elements that shall affect the mechanical properties by alloying. In addition, the density of CNTs will be increased by the added coat in order to provide a better dispersion when CNTs are embedded in molten aluminum. Therefore, a series of experiments will be done to fulfil the following aims:

1- Optimizing the concentration and volume of the colloidal Pd-Sn solution needed for providing a complete coverage of a fixed weight of CNTs with catalytic nanoparticles prior to the electroless plating.
2- Optimizing a novel aluminum electroless plating process that is based on $AlCl_3$ and Urea mixture as a RTIL. This step involves investigating the right concentrations of the ionic liquid as well as the reducing agent (LAH) used in Al-electroless plating on CNTs. In addition to this, it is important to determine the volume of the ionic liquid needed for a known amount of the provided MWCNTs.
3- Dispersing Al-coated CNTs in molten aluminum such that the final percentage of CNTs in the sample is 2% by weight then testing the composite to obtain the mechanical properties of the composite.
4- Disperse Al-coated CNTs in pure aluminum powder and hot compacting the powder before being hot extruded. The produced Al-CNT samples by this technique will be compared to the cast samples.
5- Success in dispersing 2% by weight of CNTs in aluminum for both cast and hot compacted samples will open the way to compare the tensile strength of the produced composites to previously investigated Al-CNT composites containing the same weight percent of CNTs but produced via other casting and powder metallurgical ball milling approaches that are more expensive and complex to undertake.

5. Experimental

5.1 Materials used

Multi-wall carbon nanotubes having an average diameter of 10-15 nm were supplied by Thomas Swan corporation, UK. For the catalytic activation of CNTs, colloidal palladium-tin activator as well as the accelerator were supplied by Macdermid Enthony USA. For copper electroless plating, copper sulfate pentahydrate (98.5% Assay) and Sodium Carbonate Anhydrous (99.5% Assay) were supplied by Lobachemie India. Sodium hydroxide (99% Assay) was supplied by Chem-Lab Belgium. Pottasium sodium tartrate tetrahydrate or what is known as Rochelle salt (99% Assay) was supplied by CARLO ERBA Reagents Italy. Cobalt (II) Chloride Hexahydrate (99% Assay) was supplied by JHD Company China. Formaldehyde 37% in aqueous solution was supplied by Alfa Aeser Germany. For the aluminum electroless plating, anhydrous aluminum chloride was provided by Alfa-Aeser, Urea (99.9%) was provided by Lobachemie India, and lithium aluminum hydride was provided by Alfa-Aeser. For preparing bulk Al-CNT composite samples, pure aluminum ingots (99.7%) were donated by Egyptalum Company, Nagaa Hammadi, Egypt.

5.2 Experimental procedure

The experiments took place on 4 different stages as illustrated in Figure 5-1.

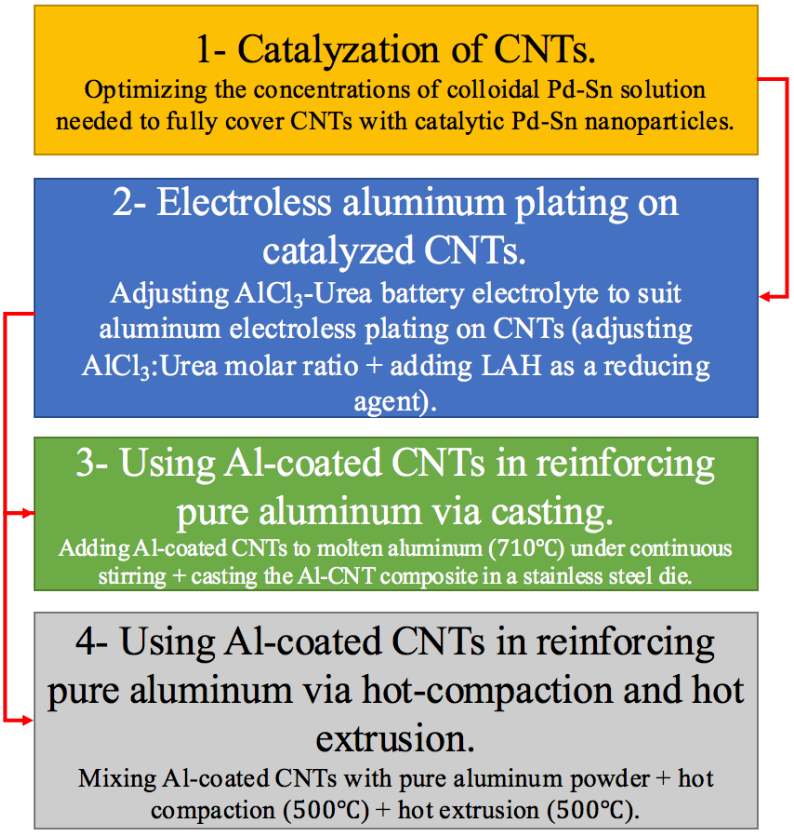

Figure 5-1 Flow chart of experiments done in the current research work.

5.2.1 Catalyzation of CNTs via Pd-Sn nanoparticles

This experiment aimed at determining the optimal concentration and volume of the colloidal Pd-Sn solution needed for a complete surface coverage of a fixed amount of MWCNTs by the catalytic Pd-Sn nanoparticles. This essential step is critical for ensuring the quality of the metal coats to be electroless plated on the catalyzed CNTs since the better the surface coverage of CNTs with the catalytic nanoparticles, the higher the quality of the metal coat provided on CNTs by electroless plating. Therefore, a standard Cu-Co electroless plating electrolyte proven to work with previous researchers was used to test the effectiveness of each experimented concentration of the colloidal Pd-Sn solution in providing a complete and conformal copper coat on top of CNTs. The quality of this copper coat will be the response that determines the best concentration of Pd-Sn solution.

This experiment was conducted in three steps shown in Figure 5-2. The process started by the activation of CNTs using a solution that contains colloidal Pd-Sn particles. Afterwards, an acceleration step was conducted to remove excess stannous hydroxide $Sn(OH)_2$ that exists on top of the activated surface. Finally, the electroless plating of copper on CNTs was performed in a Cu-Co electrolyte.

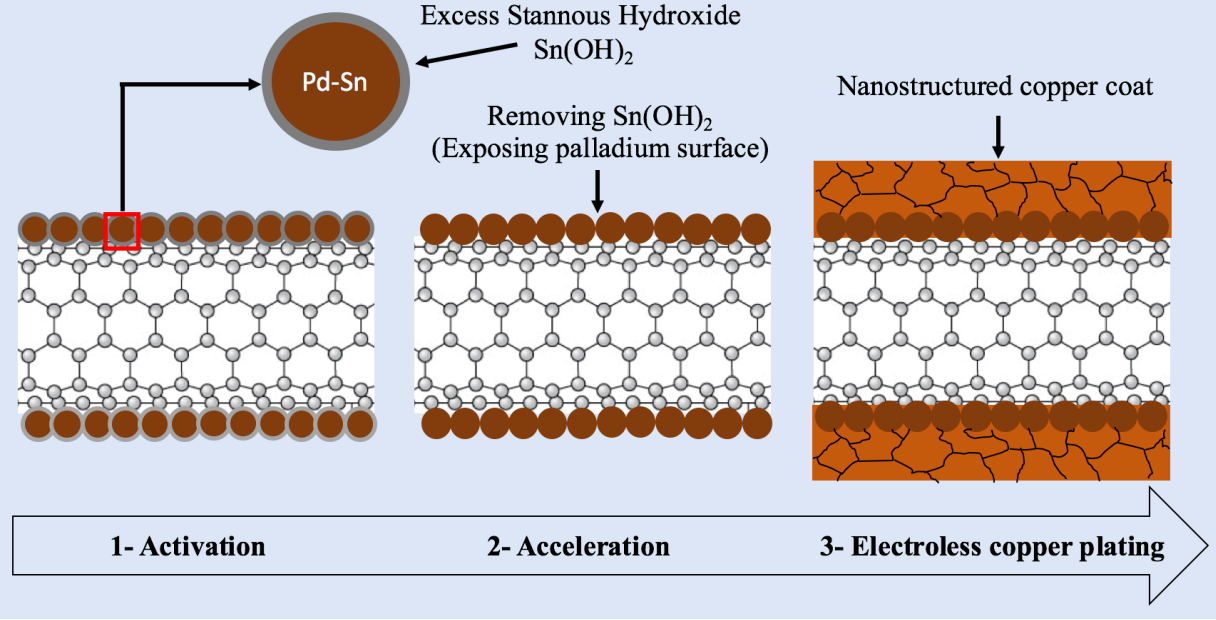

Figure 5-2 Steps for copper electroless plating of CNTs.

- **Activation step of CNTs**

The amount of MWCNTs used per run was 0.1 grams. The MWCNTs were used as received without any acid functionalization. The main precursor used in the activation was a commercial colloidal Pd-Sn concentrate adopted from the plating on plastics (POP) industry. The colloidal

Pd-Sn nanoparticles have an average size of 20-30 A° and an elemental ratio of 1:7 for Sn and Pd respectively.[137] The activation process was done in a mixture of colloidal Pd-Sn concentrate, DI water, and hydrochloric acid. The different compositions listed in Table 5-1 were investigated.

Table 5-1 Typical experimented concentrations of the activation solution.

Activation solution	A	B	C	D
Colloidal Pd-Sn (ml)	25	50	62.5	82.5
HCl (37%) (ml)	62.5	50	50	83.5
DI-water (ml)	162.5	150	137.5	84

To perform the activation step, CNTs were sonicated in the prepared activation solution for 1 minute. Afterwards, the solution was put under magnetic stir agitation for 2 extra minutes. Once activated, CNTs were filtered out from the activator solution using a filter membrane (0.22 µm PTFE) on a microfiltration kit that is schematically illustrated in Figure 5-3. After filtration, the activated CNTs were sonicated in DI water and filtered to remove any traces of the activator solution. Finally, CNTs were collected from the filter membrane by tweezers.

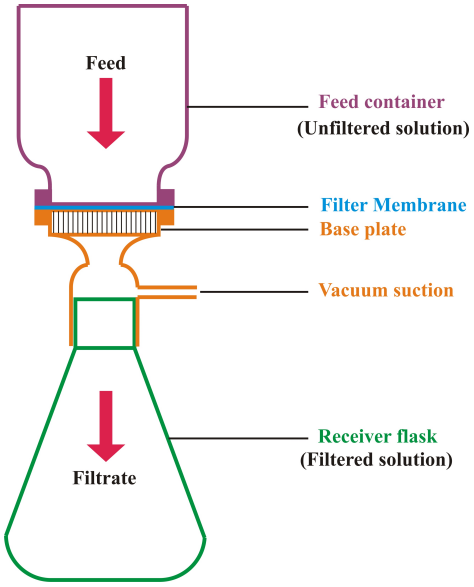

Figure 5-3 A schematic illustration of a microfiltration kit.

- **Acceleration of the activated CNTs**

This step was essential to remove excess $Sn(OH)_2$ from the surface of Pd-Sn particles deposited on CNTs for an increased catalytic activity. This acceleration step does not remove Sn from the core of colloidal Pd-Sn nanoparticles.[137] To perform acceleration of CNTs, the accelerator solution was prepared by dissolving 50 g/L of commercial accelerating acids in DI water. Afterwards, CNTs were added to the solution and put under sonication for 1 minute and

magnetic stirring for 2 extra minutes. The CNTs were then filtered out and redispersed in DI water to remove excess traces of the accelerator solution. Finally, CNTs were filtered and dried in a vacuum oven at 100℃.

- **Electroless Copper plating of CNTs**

To perform copper electroless plating on activated CNTs, one liter of copper-cobalt (Cu-Co) electrolyte was prepared using the concentrations listed in Table 5-2.

Table 5-2 Typical concentrations of the Cu-Co electrolyte constituents.

Cu-Co electrolyte constituents	Concentrations
$CuSO_4.6H_2O$	6.99 (g/l)
Na_2CO_3	2 (g/l)
$CoCl_2.6H_2O$	1.09 (g/l)
$KNaC_2H_4O_6.4H_2O$ (Rochelle Salt)	22.57 (g/l)
NaOH	4.5 (g/l)
Formaldehyde 37%	2.59 (ml/l)

All the chemicals were dissolved in DI water under sonication and manual stirring for 5 minutes using a glass rod. Cobalt chloride ($CoCl_2$) was used to help in the autocatalytic reduction of copper ions and to speed up the deposition rate. The formaldehyde (reducing agent) was added to the solution after making sure that all the solid chemicals were dissolved in water. Afterwards, the solution was put under magnetic stirring for an extra one minute. The color of the prepared solution was reported to be blue to green as a result of copper ions and cobalt ions. The activated MWCNTs were added to the prepared Cu-Co electrolyte and sonicated for 2 minutes. Once the CNTs were put in the solution, hydrogen bubbles started to appear in the entire solution as a result of the dissolved hydrogen from the surface of the catalytic Pd-Sn particles as well as the oxidation of formaldehyde. After sonication, the solution containing CNTs was left for 8 extra minutes under magnetic stirring. When the hydrogen bubbles stopped coming out of the solution, this indicated the coverage of CNTs with copper was complete. In this case, the solution turned dark brown indicating the color of the coated CNTs with a copper film in the nanoscale. After the stirring was completed, copper coated CNTs were filtered using the same filtration scheme used in the activation process of CNTs. The filtered out solution was reported to be light pink indicating that all the copper ions were consumed in the solution in the 10 minutes window of the reaction. The filtered out CNTs had a dark brown color as indicated in Figure 5-4.

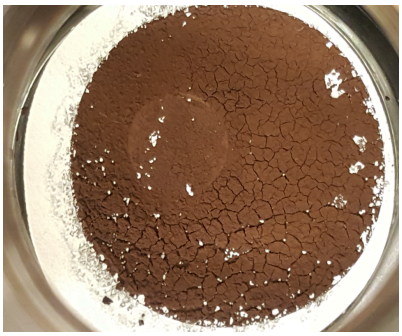

Figure 5-4 Filtered out copper coated CNTs with a dark brown color.

The optimal concentration of the activation solution that resulted in conformal and complete copper coats on top of CNTs was found to be concentration "C" mentioned in Table 5-1.

- **Characterization of Cu-coated CNTs**

The copper coated CNTs were characterized by means of scanning electron microscopy (SEM) using (LEO SUPRA 55VP FEG, Zeiss, equipped with Oxford EDS detector), transmission electron microscopy (TEM) using (JEM-2100 LaB6, JEOL, operating at 200 kV and equipped with Gatan SC200B CCD camera), energy dispersive X-ray (EDX) attached to the SEM, and X-ray diffraction (XRD) using (Cu Kα, Panalytical Xpert Pro diffractometer).

5.2.2 Electroless aluminum plating on CNTs

In this experiment, the optimized concentration of the colloidal Pd-Sn catalytic solution mentioned in section **Error! Reference source not found.** was used to activate MWCNTs to e used in optimizing a novel electroless aluminum plating process based on $AlCl_3$-Urea as a RTIL. The experiment was conducted on three different steps. The first step was done by the catalytic activation of CNTs using Pd-Sn nanoparticles. Then, excess stannous hydroxide was removed from the surface via a group of accelerating acids. Finally, the CNTs were electroless plated by aluminum as shown in Figure 5-5.

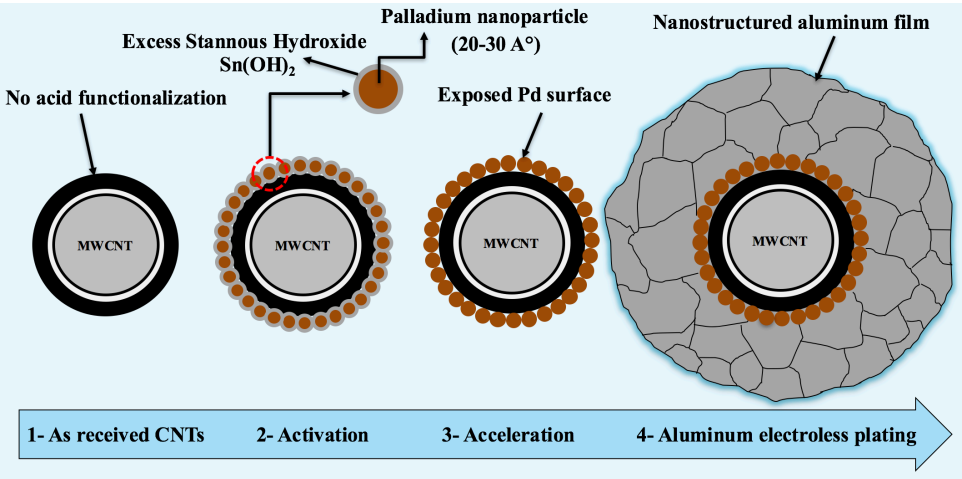

Figure 5-5 Procedures for electroless plating of aluminum on CNTs

For aluminum electroless deposition, the entire experiment was carried out in a glove box filled with dry argon gas at ambient conditions. To prepare the aluminum electroless deposition electrolyte, anhydrous aluminum chloride and urea (2:1) molar ratio were reacted together to form a room temperature ionic liquid (RTIL) that is rich in Al_2Cl_7- ions. The total volume prepared per run for the RTIL was 200 ml for each 0.1 grams of CNTs.

The aluminum chloride- urea reaction is an exothermic one. Therefore, excess heat may result in the decomposition of the entire electrolyte. Failure in controlling the exothermic heat of the reaction can lead to failure in the electroless deposition. For this reason, strict procedures were carried out to prevent the thermal decomposition of the electrolyte by preparing the volume needed on 4 separate parts in order to reduce the heat resulting from the exothermic reaction. However, the previous step was not sufficient in preventing the decomposition. Therefore, the volumetric flask was cooled with a sealed rubber ice bucket that also helped in preserving the dry environment of the chamber. An ideal electrolyte has a pale yellow color as a result of aluminum ions. If a light brown color is observed, this will be a sign of the electrolyte decomposition. After preparing the ionic liquid, lithium aluminum hydride (LAH) was dissolved in toluene, hexane, or diethyl ether and used as a reducing agent. Different amounts of 1.5, 1.9, 2.5, and 5 grams of LAH were tested. The concentration of 1.9 grams of LAH was found to give the best results from the point of view of the copper film continuity and uniformity. The activated CNTs were immersed in the electroless plating RTIL, sonicated for 5 minutes, and stirred magnetically for 10 extra minutes. The RTIL containing CNTs was viscous and it was hard to be filtered out without being diluted using an organic solvent. This solvent has to be the same type used in diluting LAH. Common successfully tested solvents are toluene, hexane or diethyl ether, and tetrahydrofuran (THF). After dilution, the CNTs were filtered and washed thoroughly with hexane.

- **Characterization of Al-coated CNTs**

SEM imaging using (LEO SUPRA 55VP FEG, Zeiss, equipped with Oxford EDS detector) and TEM imaging using (JEM-2100 LaB6, JEOL, operating at 200 kV and equipped with Gatan SC200B CCD camera) were used to investigate the aluminum coat on top of the CNTs. Chemical analysis was performed using EDX by means of the EDS detector attached to the SEM. Crystal structure of aluminum was confirmed using XRD (Cu Kα, Panalytical Xpert Pro diffractometer). Raman analysis using (ProRaman-L, ENWAVE OPTRONICS) was carried out to compare the intensities of the D-band and G-band (I_D/ I_G) of CNTs before and after being plated with aluminum.

5.2.3 Casting aluminum Samples (reinforced by Cu-coated CNTs)

This experiment was carried out for the purpose of making use of the prepared Cu-coated CNTs in section **Error! Reference source not found.** to gain a hands on experience in dispersing uch composite powders in molten aluminum without wasting the Al-coated CNTs prepared in section 5.2.2. Concentration of 0.5 wt.%, 1 wt. %, and 2 wt. % of Cu-coated CNTs were used as reinforcement for cast pure aluminum.

As CNTs start to oxidize in air in a temperature range of 440-450℃,[172] a melting flux was used to shield the surface of molten aluminum from oxidation during the expirement.[101] The copper coated CNTs were dispersed with a remelting flux in water via sonication. The mixture was then filtered and dried at 100℃ in a vacuum oven. Commercial pure aluminum slices were cut into small pieces from a 99.7% pure aluminum ingot as shown in Figure 5-6. The pieces were put in a silicon carbide crucible and melted in an induction melting furnace. The furnace was set at a temperature of 850℃. The actual temperature of the molten aluminum was monitored by an infrared detector and found to be 710℃.

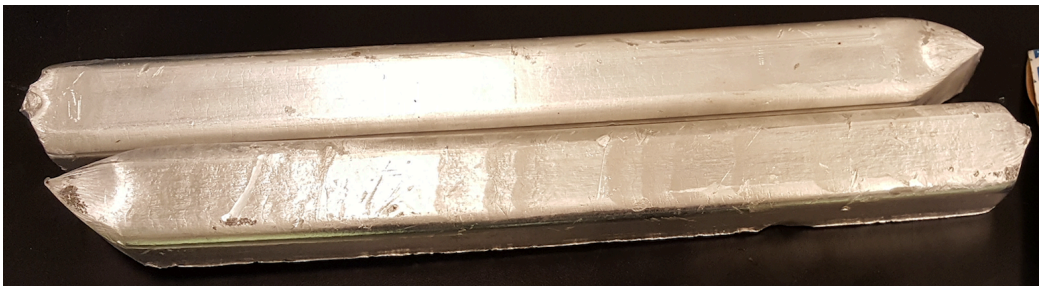

Figure 5-6 Pure aluminum ingot (99.7%).

To disperse the copper coated CNTs in molten aluminum, the powder mixture of the flux and Cu-coated CNTs was added to the molten aluminum and stirred by a ceramic stirring rod for 5 minutes. The excess flux floating on top of the crucible was then removed by a ceramic spoon. Afterwards, the molten composite was poured into a preheated steel mold (300 ℃) that has a cylindrical cavity of 15 mm diameter and length of 160 mm. The sample was left for cooling at room temperature.

- **Characterization of Cu-CNTs reinforced aluminum composite**

As this experiment was intended just for gaining knowledge about dispersing CNTs in molten aluminum, the only test done was the Vickers micro hardness using (Mitutoyo HM-112). To prepare the micro hardness samples, the produced cast cylindrical specimens were turned using a center lathe to reach a diameter of 10mm. The samples were then cut into slices using the isomet cutter. A polymeric mount was prepared for each sample before being grinded by means of 400-2500 grit size sand papers. A 3 microns diameter silica suspension was used for

polishing the samples. After obtaining a mirror finish of the sample without any microscratches, the samples were indented by the Vickers indenter using a 1 Kgf. Around 20 indentations were done for each sample.

5.2.4 Casting Aluminum samples reinforced by Al-coated CNTs

This experiment is considered the main experiment of this thesis work. As mentioned in section 5.2.2, aluminum coated CNTs could be achieved by the novel $AlCl_3$- Urea RTIL. Therefore, the produced Al-CNT powders were used to reinforce cast aluminum. The weight percent of CNTs needed to reinforce aluminum in this experiment was fixed to 2%. This percent was picked specifically for the purpose of establishing the right comparison between Al-CNTs composites produced by the casting technique and composites that were produced before in the literature using the ball milling technique containing 2 percent by weight of CNTs. In the experiment done in section 5.2.2. It was noticed that each gram of CNTs resulted in 8.73 grams of Al-coated CNTs. Therefore, the aluminum coat accounts for 7.73 grams of the total weight of Al-coated CNTs that happen to contain 1 gram of CNTs.

To insure that the total weight percent of CNTs in the sample is 2%, Equation 5-3 was deduced to calculate the weight of aluminum coated CNTs ($W_{Al-CNTs}$) needed in the sample. The only variable in the equation is the final weight of CNTs in the cast sample (W_{CNTs}).

$$W_{Al-cnts} = W_{CNTs} + (8.73 * W_{CNTs}) \quad \text{Equation 5-1}$$

$$W_{Al-cnts} = W_{CNTs} * (1 + 8.73) \quad \text{Equation 5-2}$$

$$W_{Al-cnts} = 9.73 * W_{CNTs} \quad \text{Equation 5-3}$$

Where, W_{CNTs} is the total weight of CNTs required in the final sample in grams. The weight of Al-CNTs that is required for a 100 gram cast sample is 19.46 grams. An amount of 10 grams of the remelting flux was mixed with the Al-coated CNTs and stored before being used in casting.

The weight of the pure aluminum to be melted in the crucible ($W_{Al-melt}$) can be calculated as mentioned in Equation 5-4.

$$W_{Al-melt} = W_F - W_{Al-CNTs} \quad \text{Equation 5-4}$$

Where, W_F is the final weight of the sample including the matrix and the reinforcement phases. The weight of pure aluminum needed for melting before adding the aluminum coated CNTs as a reinforcement was calculated to be 80.54 grams.

Preparing the cast sample of 2% by weight CNTs in pure aluminum

Five essential steps were carried out for the production of each cast sample. These procedures started by melting the 80.54 grams of pure aluminum pieces (99.7%) in a silicon carbide

crucible. The induction furnace was set at 850 °C. The actual measured temperature for the molten aluminum after 30 min was 710 °C. The second step involved adding the mixed aluminum coated CNTs and the flux in molten aluminum. Afterwards, the mixture was stirred with a graphite stirring rod for 5 minutes.

It was observed that the aluminum coat on CNTs helped them wet the molten aluminum and disperse very well in the matrix while the fluxes were kept at top of the crucible to shield the hot surface of molten aluminum from oxidation. After the stirring was done, it was time to remove excess fluxes from the top part of the crucible by means of a ceramic spoon. Immediately, the molten composite was cast into a preheated stainless steel mold (300°C) that has a cylindrical cavity of 15 mm inner diameter and 160 mm length. Finally, the cast was left for cooling at ambient conditions and was ready for testing. Figure 5-7 shows the procedures of preparing the cast Al-CNTs composite.

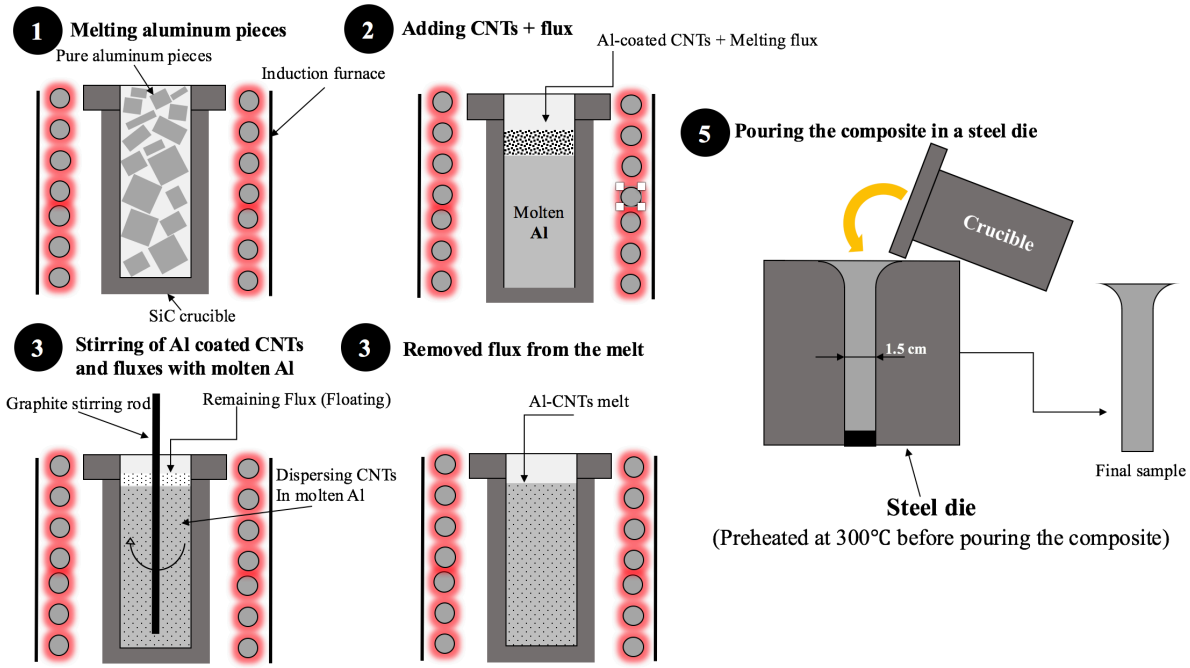

Figure 5-7 Procedures for casting Al-coated CNTs reinforced aluminum composite.

- **Characterization of cast Al-CNTs reinforced aluminum composite**

Tensile testing

Tensile testing of the pure vs. the reinforced samples was done on an Instron universal testing machine with a testing speed of 0.5 mm/s. The tensile test specimen had the dimensions specified in Figure 5-8.

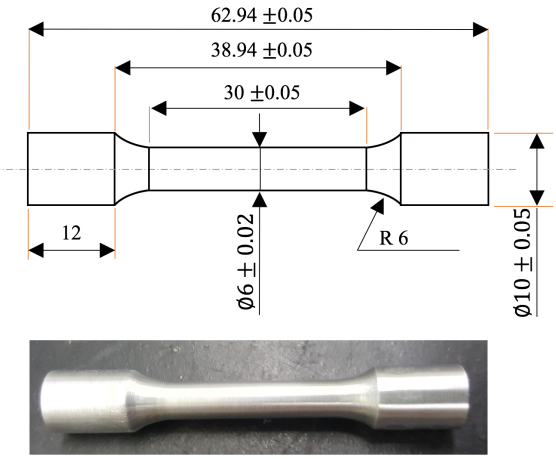

Figure 5-8 Dimensions of the tensile test specimen.

Fractography:
The fractography of the cast samples was carried out by SEM imaging using (LEO SUPRA 55VP FEG, Zeiss, equipped with Oxford EDS detector) to determine the failure modes as well as the ductility of each sample.

Chemical analysis and crystal structure:

The chemical analysis was performed using the EDX analysis by means of an EDS detector attached to the SEM. Crystal structure of aluminum was confirmed using XRD (Cu Kα, Panalytical Xpert Pro diffractometer). Raman analysis using (ProRaman-L, ENWAVE OPTRONICS) was carried out to determine the intensity of the D-band to the intensity of the G-band (I_D/ I_G) of CNTs in the cast samples in order to put them in comparison with the aluminum coated CNTs before being subjected to heat.

Hardness testing and nanoindentation:

Vickers micro hardness test using (Mitutoyo HM-112 tester) was carried out for the pure and the 2% by weight samples. More than 50 indentations were done all over the surface of each sample. The test specimens were prepared by cutting the cylindrical sample (15 mm) by an isomet cutter. The specimens were then fixed by a polymer mount, ground using 600 to 2500 grit size sand papers, and polished using a silica polishing compound.

The modulus of elasticity was measured on (MTS nanoindenter XP). The samples were prepared with the same technique used in Vickers testing.

5.2.5 Preparing a powder metallurgical sample of Al-coated CNTs with aluminum powder (Hot pressing, Hot extrusion)

The aim of this experiment is to use the prepared Al-coated CNTs in reinforcing pure aluminum using the powder metallurgical hot compaction technique followed by hot extrusion. This experiment uses the same calculations done in the experiment mentioned in section 5.2.4 for

the weights needed of both the matrix and the reinforcement. The only difference is that the aluminum matrix here is in powder form. Therefore, the weight of the aluminum powder needed for the experiment was 80.54 grams and the weight of aluminum coated CNTs was 19.46 grams. Figure 5-9 illustrates the steps undertaken to achieve the Al-CNT composite by hot compaction and hot extrusion. The experiment started by mixing the aluminum powder with the aluminum coated CNTs using a turbula mixer at 96 RPM for 60 minutes. After the powder was mixed, it was transferred to a custom made die that was insulated from all sides by a graphitic grease. After the die cavity was filled with the powder mixture, it was cold pressed at 475 MPa for an hour using a compression piston on a hydraulic press. The lower stopper was removed from the die and then the extrusion die was mounted to the compaction die. The entire setup was then put in a resistive heating coil and heated at 500℃ for an hour. The entire setup was isolated thermally by fiber glass yarn to prevent any sudden cooling from changing the mechanical properties of the composite. After the powder consolidation was completed. The compressed powder was hot extruded at 500 ℃ and left for cooling at ambient conditions without removing the insulation. Finally, the sample was ejected from the die and become ready for testing.

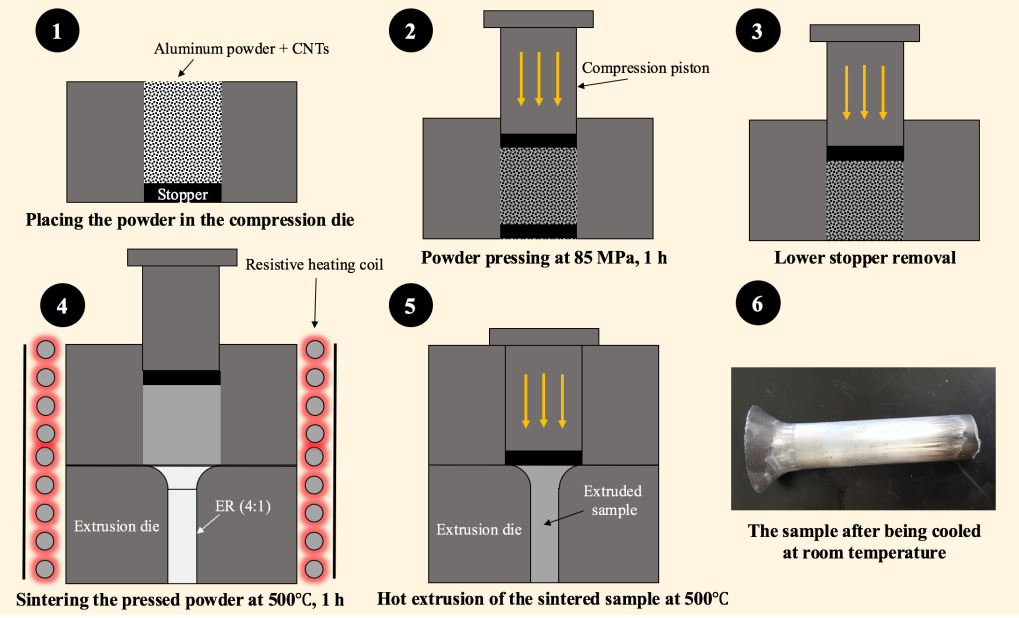

Figure 5-9 Preparation of Al-CNT reinforced aluminum composite by powder compaction and hot extrusion.

- **Characterization of hot pressed-hot extruded Al-CNTs reinforced aluminum composite**

The samples produced by this technique were subjected to the same types of testing that were done to the cast samples.

6. Results and discussion

6.1 Results for Pd-Sn catalyst optimization experiment

By conducting SEM imaging on the copper electroless plated CNTs, a noticeable increase in the diameter of CNTs was noticed when concentration "C" mentioned in Table 5-1 was used. Figure 6-1 shows copper coated CNTs with an average diameter of 130 nm. The original diameter of the as-received MWCNTs was from 10-15 nm. Therefore, a thick copper coat has been achieved. It is worth noting that CNTs were used as received without any acid functionalization and without being milled. Therefore, Cu-coated CNTs were neither individual nor clustered but rather grouped in a branched way, as shown in Figure 6-1.

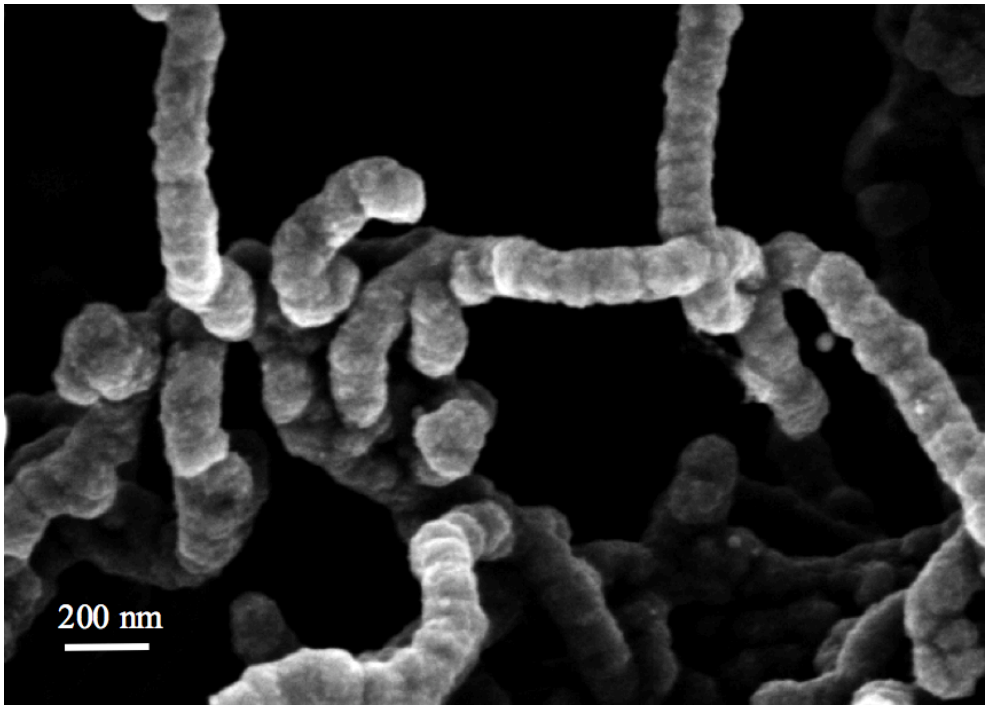

Figure 6-1 A high resolution SEM image of copper coated CNTs.

The high quality conformal copper coats grown on CNTs came as an indication to the proper catalyzation of CNTs using Pd-Sn nanoparticles of a narrow size distribution (2-3 nm). The presence of these catalytic nanoparticles in a size that is a fraction of the average diameter of CNTs made them able to uniformly cover the surface of CNTs and render it catalytic prior to the copper electroless plating.

Using a mortar and pestle, the copper coated CNTs were crushed to induce a fracture in the copper coat for the purpose of differentiating between the coated and uncoated part of CNTs that can be clearly seen by the TEM and SEM imaging in Figure 6-2.

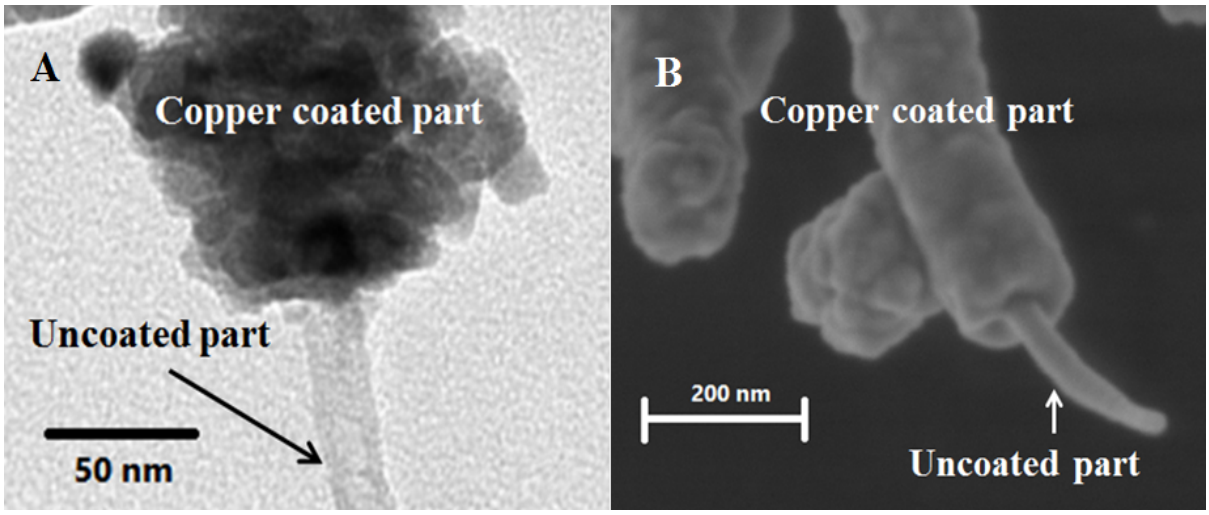

Figure 6-2 High resolution imaging of coated and uncoated parts of CNTs with copper using A) SEM imaging and B) TEM imaging.

The TEM image shown in Figure 6-3 revealed that the copper coat on top of the CNTs has a nanostructure. This can be attributed to the growth of copper on top of catalytic Pd-Sn nanoparticles wrapping the walls and tips of CNTs. Therefore, it appears that copper growth has mimicked the structure of these catalytic nanoparticles.

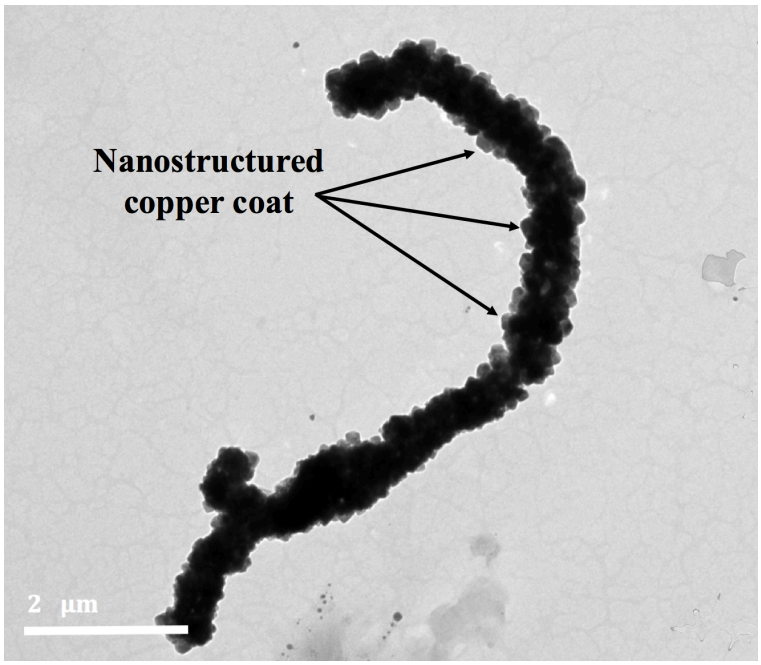

Figure 6-3 TEM imaging of the nanostructured copper coat on CNTs.

The chemical analysis of Cu-coated CNTs was conducted via energy dispersive X-ray (EDX). The EDX spectrum shown in Figure 6-4 represents the elements found on the surface of copper coated CNTs during SEM imaging.

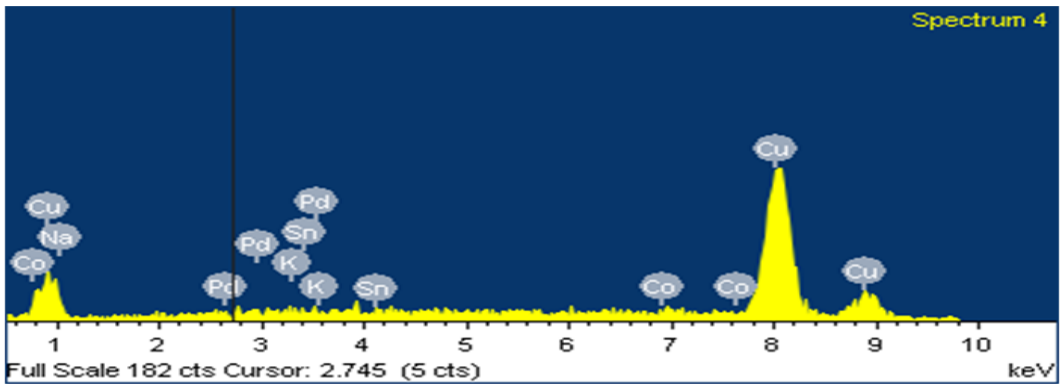

Figure 6-4 EDX spectrum of Cu-coated CNTs.

The copper coat represented 98.56% by weight of the elements on the surface. The other elements such as Na, Co, K, Pd, and Sn were found existing as traces from the electroless copper solution and the activation precursor as listen in Table 6-1.

Table 6-1 Elemental analysis of the Cu-coated CNTs sample.

Element	Weight %	Atomic%
Cu	98.56	98.32
Na	0.2	0.55
Co	0.66	0.71
K	0.08	0.13
Pd	0.43	0.26
Sn	0.07	0.04
Total	100 %	

To confirm the presence of copper in a crystalline form, X-ray diffraction (XRD) was conducted on the Cu-coated CNTs as shown in Figure 6-5. Different crystallographic planes of the face centered cubic (FCC) crystal structure of copper such as (111), (200), and (220) were clearly found in the XRD pattern.

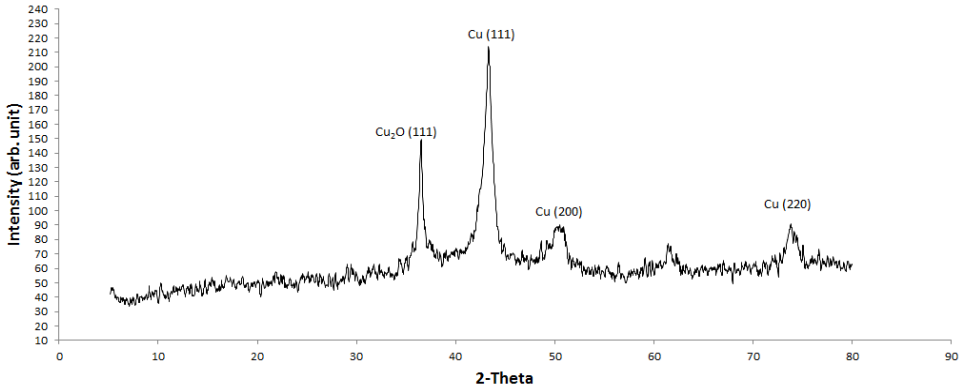

Figure 6-5 XRD pattern of Cu-coated CNTs.

The copper coated CNTs have high surface area to volume ratio. Being filtered out from an aqueous mother liquor has led to some copper oxides being formed and confirmed by the existence of the (111) crystallographic plane of copper at 36.5° in the XRD pattern. However, the XRD pattern in the present study showed much stronger peaks of copper compared to the copper oxide peak unlike XRD patterns of electroless copper coats obtained by other researchers.[173] This confirms that the electroless plating methodology used and the drying of the sample in a vacuum oven at 100°C in an inert N_2 environment has helped in lowering the amount of oxides in favor of the copper coat.

Interestingly, the (002) peak of CNTs (at 2θ=26 deg) was found absent in the XRD pattern. This can be attributed to different factors such as the difference in the atomic weight between copper and CNTs that makes it difficult for the electron to bend around the carbon atoms, the limited detection depth limit of the XRD technique especially that the CNTs were covered by a thick coat of a heavy element such as copper, the relatively small weight percent of CNTs compared to the weight percent of the thick coat on top of them (i.e. each 0.1 gram of CNT was coated by 2.9 grams of copper), and finally the interference between the high intensity peaks of copper and the low intensity peak of CNTs.

6.2 Results of Aluminum electroless plating on CNTs

The electrochemical window (EW) of the prepared RTIL was measured on a potensiostat and compared to ($AlCl_3$-EMIC) RTIL with the same molar ratio of 2:1. Figure 6-6 shows the actual measurements of the electrochemical reduction and oxidation potential limits for both $AlCl_3$-Urea and $AlCl_3$-EMIC. It can be noticed that the new $AlCl_3$-Urea RTIL has succeeded in displaying a wide EW that is similar in the characteristics to the EW of EMIC with a little shift in the oxidation and reduction potentials. The redline in the voltammogram indicates that the electrode potential of aluminum exists inside the EW of the new developed RTIL. Therefore, $AlCl_3$-Urea can be widely used in the electroplating and electroless plating of aluminum without being decomposed.

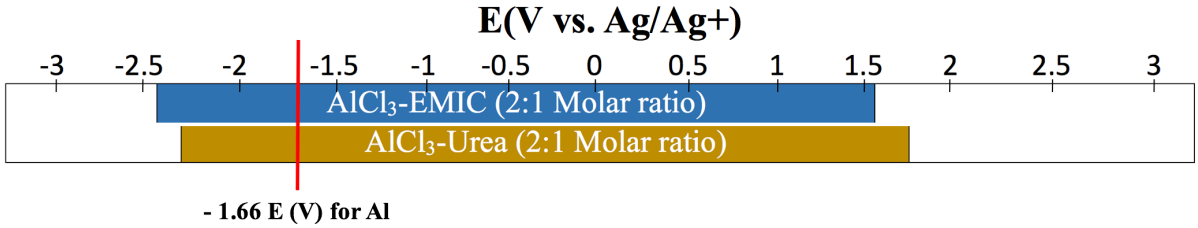

Figure 6-6 Voltammogram representing the EW of $AlCl_3$-Urea compared to $AlCl_3$-EMIC RTIL.

The electroless aluminum plating by the newly developed $AlCl_3$-Urea RTIL followed the reaction mechanisms that researchers have found when $AlCl_3$-Urea was used as a battery electrolyte causing aluminum to deposit on the cathode of the battery.[171] The only difference in this case is that the reduction of aluminum ions into their metallic form took place due to the presence of electrons donated by the reducing agent in the anodic partial reaction. These electrons have met the electrochemical reduction potential requirement for aluminum to be deposited on the catalyzed CNTs. Therefore, no external power source was needed for the reduction reaction. This was beneficial in depositing aluminum on top of an uncountable number of CNTs that are impossible to be connected to an external power source for plating. The aluminum electroless plating on CNTs took place through a series of reactions. In the presence of palladium as a catalyst on CNTs at room temperature, LAH decomposes on 3 steps as shown in , Equation 6-1, Equation 6-2, and Equation 6-3.

$$3LiAlH_4 \rightarrow Li_3AlH_6 + 2Al + 3H_2 \qquad \text{Equation 6-1}$$

$$2Li_3AlH_6 \rightarrow 6LiH + 2Al + 3H_2 \qquad \text{Equation 6-2}$$

$$LiH \rightarrow Li^+ + 1/2H_2 + e^- \qquad \text{Equation 6-3}$$

Simultaneously with the decomposition reactions of LAH, a group of reactions take place between $AlCl_3$ and Urea to generate Al_2Cl_7- ions responsible for the aluminum deposition as follows:

$$[AlCl_2.(Urea)_n]^+ \rightarrow AlCl_4^- + 2(Urea) + Al \qquad \text{Equation 6-4}$$

At 2:1 molar ratio of $AlCl_3$ and Urea respectively, the high amount of $AlCl_3$ results in generating more Al_2Cl_7- ions as shown in Equation 6-5.

$$AlCl_4^- + AlCl_3 \rightarrow Al_2Cl_7^- \qquad \text{Equation 6-5}$$

Using electrons donated by the reducing agent in Equation 6-3, Al_2Cl_7- ions are reduced into aluminum as shown in Equation 6-6.

$$4Al_2Cl_7^- + 3e^- \rightarrow 7AlCl_4^- + Al \qquad \text{Equation 6-6}$$

By implementing the previous chemical reactions, aluminum was plated on top of the CNTs from three different sources represented by the reduction reaction of Al_2Cl_7- ions, the reduction reaction of $[AlCl_2^{\cdot}(Urea)_n]^+$ ions, and the decomposition of LAH. The addition of extra $AlCl_3$ has promoted the production of Al_2Cl_7- ions which are the main source of aluminum ions.

It was confirmed by the high resolution TEM imaging shown in Figure 6-7 (A) and SEM imaging shown in Figure 6-7 (B) that there was a considerable increase in the diameter of CNTs indicating the presence of the aluminum coat. The CNTs were also grouped in a branched way.

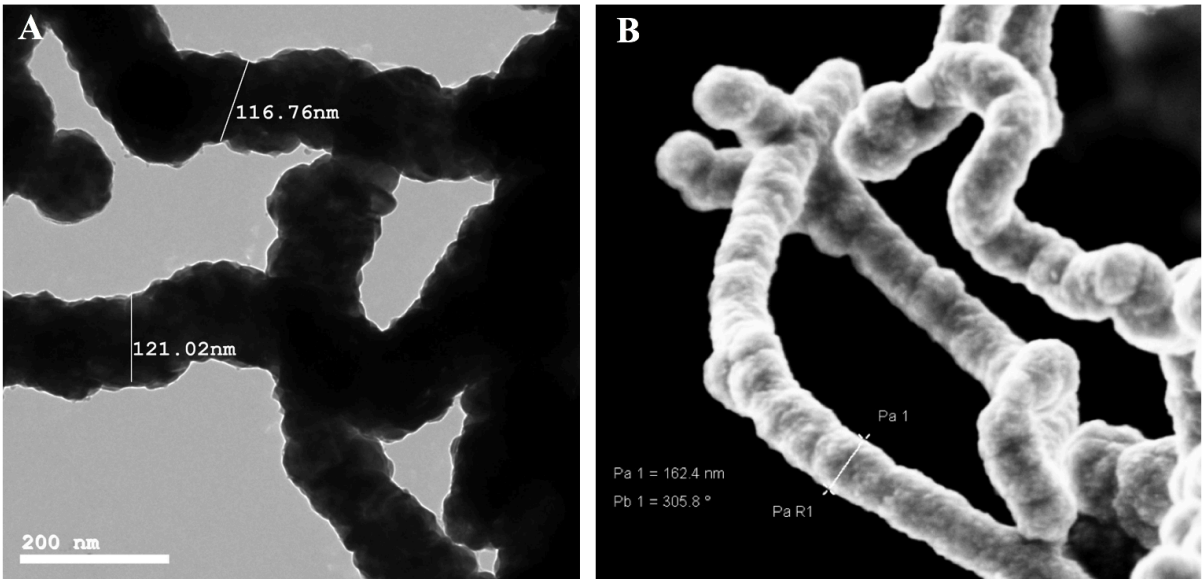

Figure 6-7 A) TEM image of Al-coated CNTs B) SEM image of Al-coated CNT.

It was also noticeable that the aluminum coated on CNTs is nanostructured as shown in Figure 6-8 (A).

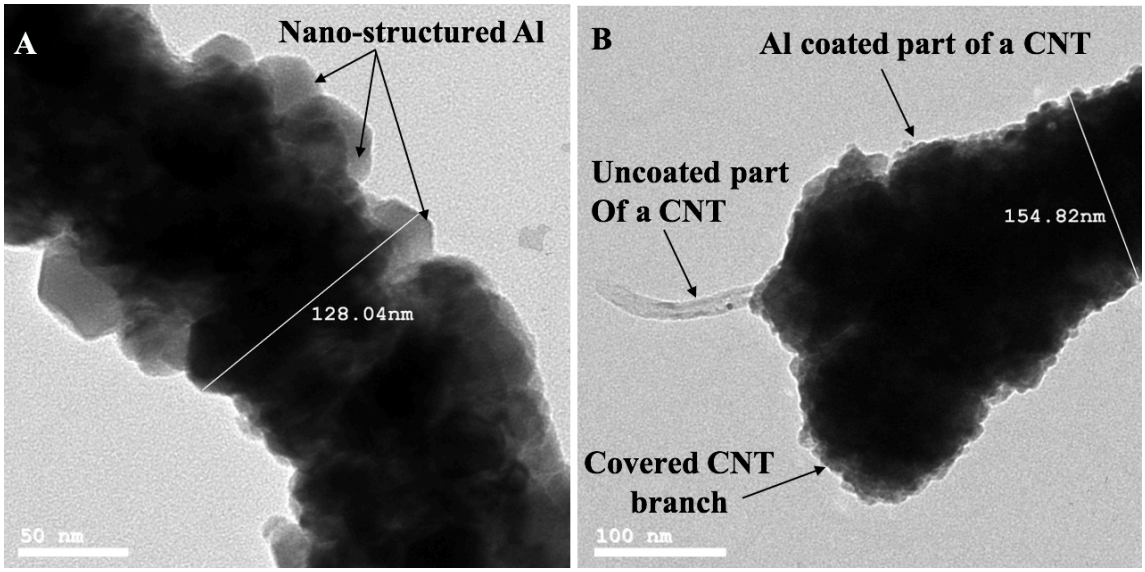

Figure 6-8 Surface morphology of Al-coated CNTs A) TEM image of the nanostructured aluminum on a CNT B) SEM image showing a coated and uncoated part of a CNT.

When the aluminum-coated CNTs were crushed by a mortar and pestle, it was possible to break some of the aluminum coating on the CNTs. Therefore, the difference between the coated and uncoated parts of a CNT that has two branches can be clearly shown in Figure 6-8 (B). The aluminum coat is much thicker than the CNT itself which is preferable in such a composite material.

It was important to conduct some chemical analysis to the sample in order to confirm the existence of aluminum on top of CNTs. The EDX spectrum shown in Figure 6-9 indicates the presence of aluminum, carbon as well as some aluminum oxides in the tested sample.

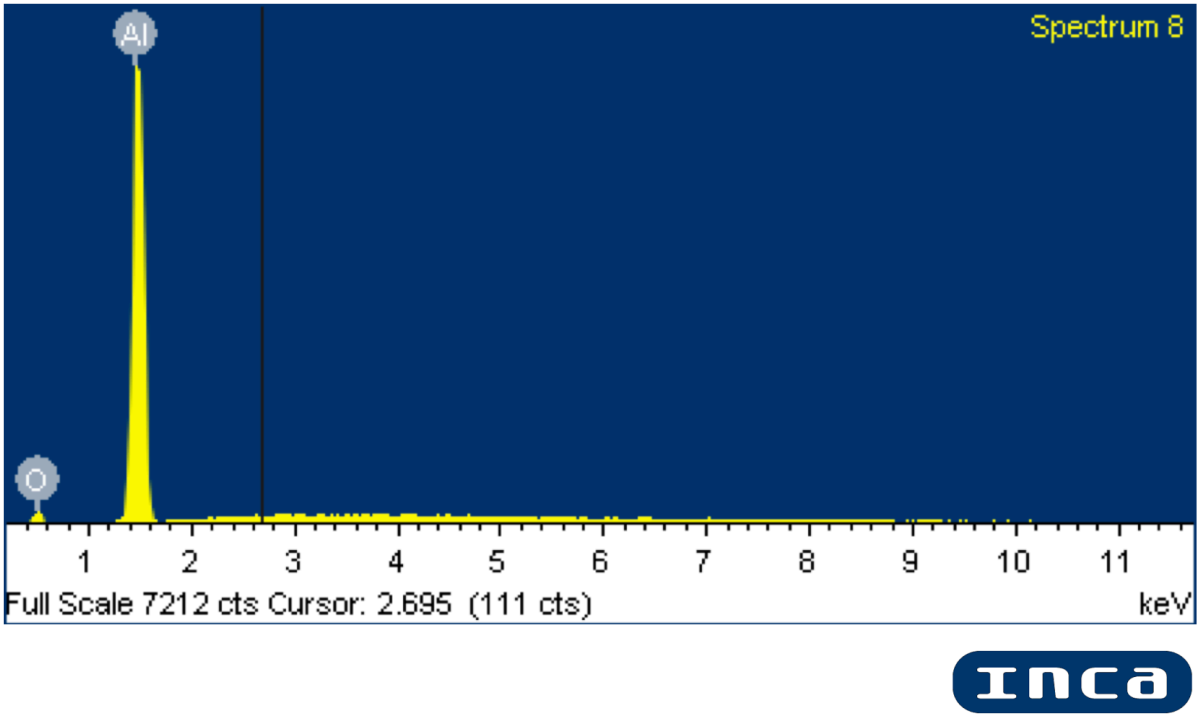

Figure 6-9 EDX analysis of Al-coated CNTs.

According to the EDX spectrum, 84.67% aluminum was present in the prepared sample. However, some parts of the sample were oxidized due to being exposed to the air in the sample preparation step as indicated in Table 6-2**.**

Table 6-2 Wt.% of aluminum, aluminum oxide and carbon in the sample.

Element	Weight %
Aluminum	84.67
Oxygen	13.67 (due to Al activity)
Carbon	1.67
Totals	100

Aluminum in nature cannot be formed in an amorphous form. So, it was important to confirm the FCC crystal structure of aluminum by conducting the XRD analysis as well as the SAED indexing done on the TEM. The diffraction circles on the TEM graph came in agreement with the XRD pattern as shown in Figure 6-10(A-B) confirming the existence of all the crystallographic planes of aluminum in the sample. As the diffraction depends on how heavy

the atoms are, it was difficult to observe the CNT peak (200) at 26° because of their low percentage in the sample as well as the big difference in the atomic weight between aluminum and carbon. The same observation was reported for the Cu-coated CNTs.

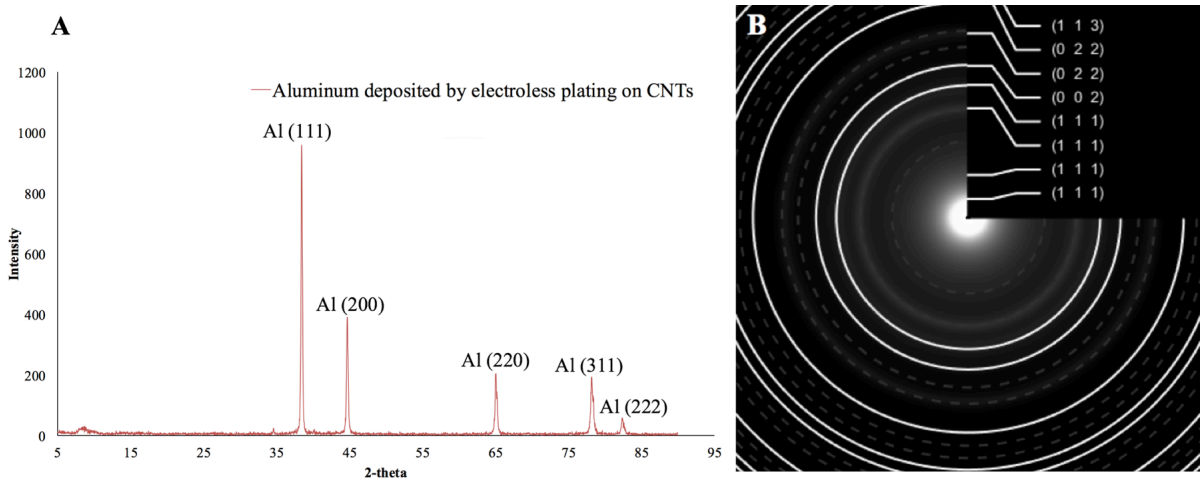

Figure 6-10 A) XRD diffraction pattern of Al-coated CNTs B) SAED indexing by TEM for Al-coated CNTs.

The Raman analysis of the aluminum coated CNTs shown in Figure 6-11 reveals that the ratio of the intensity of the D-band (I_D) to the intensity of the G-band (I_G) of CNTs is 1.015. To put that into perspective, the I_D:I_G ratio of as received MWCNTs is equal to 1.012. Therefore, the electroless deposition of aluminum on CNTs did not affect the structural integrity of CNTs.

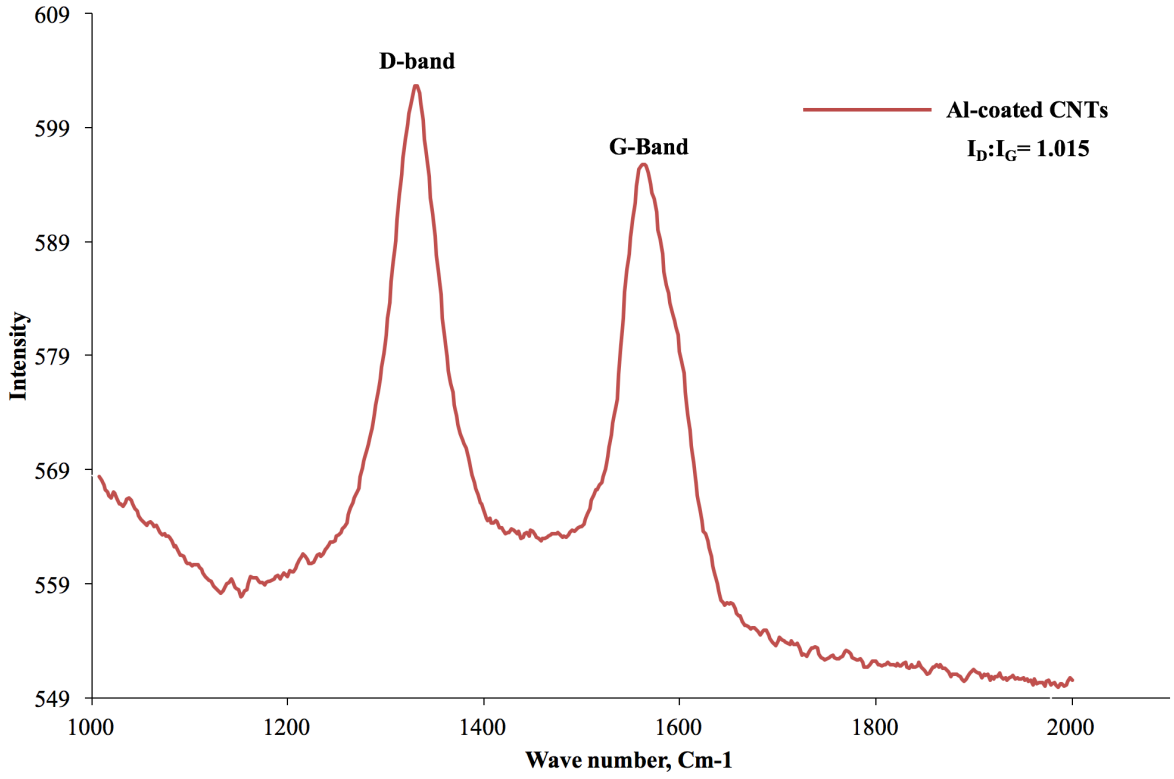

Figure 6-11 Raman analysis of Al-coated CNTs.

6.3 Analysis of bulk samples

6.3.1 Raman spectroscopy

The Raman analysis shown in Figure 6-12 for the cast sample indicates that the intensity ratio between the D-band and the G-band of CNTs did not undergo a significant change compared to the as-received CNTs. Therefore, it can be concluded that the quality of CNTs was preserved after the samples were cast.

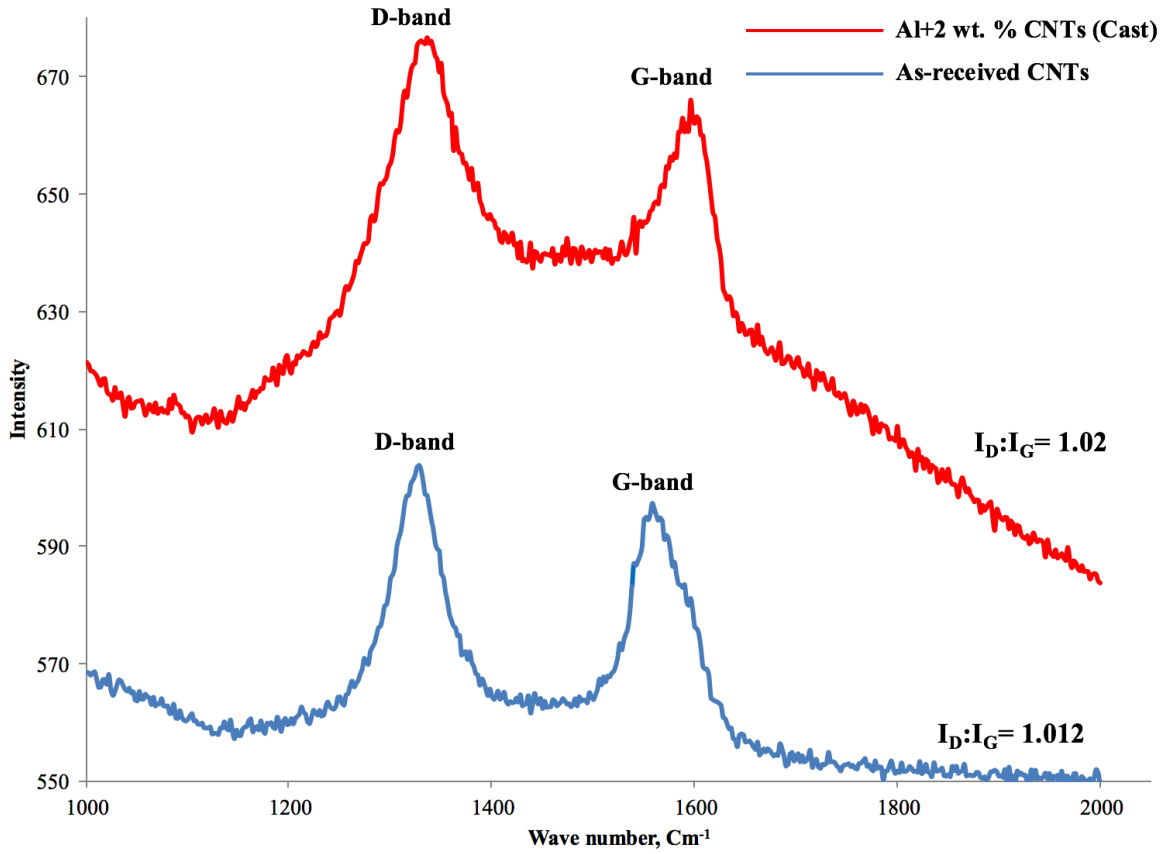

Figure 6-12 Raman spectra of cast Al-CNTs sample compared to the as-received CNTs.

It was also observed that a shift in the D-band and the G-band of CNTs took place when Al-coated CNTs were added to the molten aluminum. This can be attributed to the interaction between CNTs and the aluminum matrix.

In the hot compacted-hot extruded Al-CNT sample, the (I_D/I_G) ratio increased slightly as shown in Figure 6-13. This came as a result of the harsh mechanical work done on the sample. This mechanical work such as hot compaction and hot extrusion probably resulted in some amorphous carbon that was generated in the sample as noticeable in the intensity of the D-band. It was also observed that a similar shift to that happened in the Raman bands of CNTs during casting took place in the hot compacted-hot extruded sample due to the interaction between the aluminum matrix and CNTs.

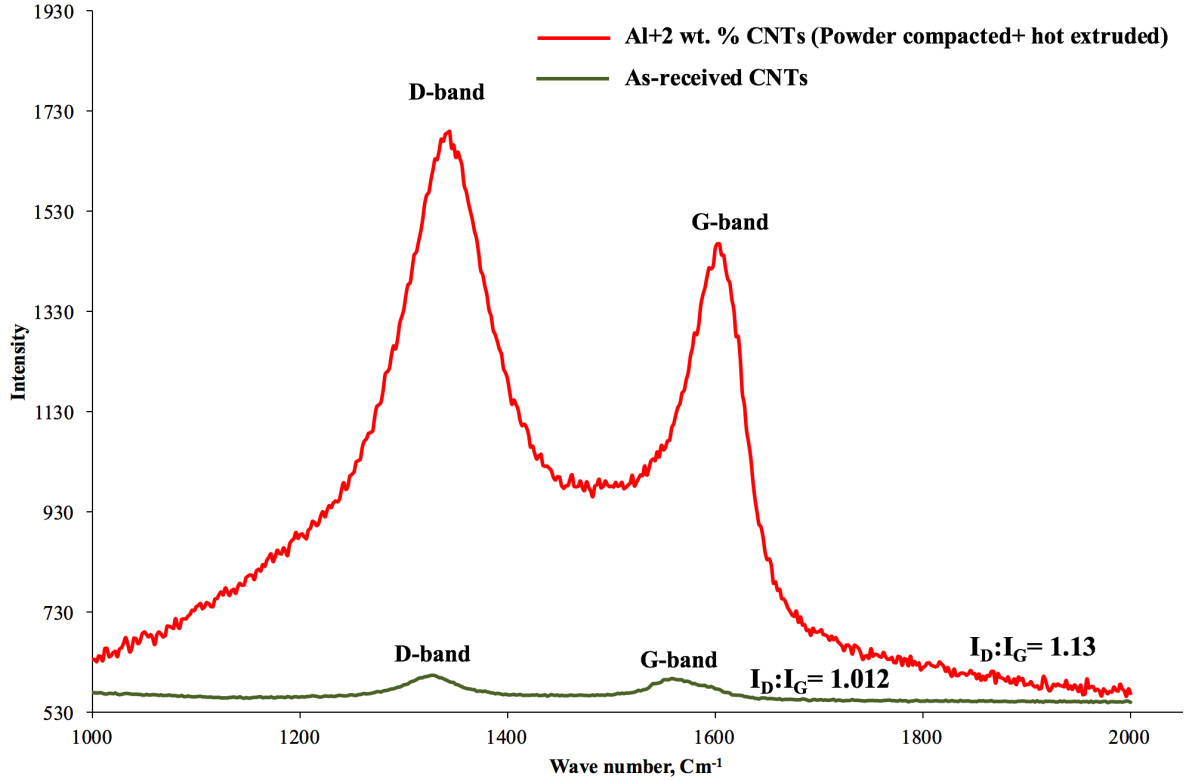

Figure 6-13 Raman spectra of the hot compacted-hot extruded Al-CNT sample compared to the as received CNTs.

6.3.2 X-Ray diffraction

XRD analysis was mainly conducted for the detection of any aluminum carbides (Al_4C_3) that may have formed in the aluminum matrix during the fabrication of the composite. Figure 6-14 shows the XRD pattern of Al-CNT composites fabricated by either casting or hot compaction followed by hot extrusion. The pattern of each composite is compared to the pure element fabricated by the same technique. In addition to the diffraction peaks for the aluminum FCC crystal structure such as (111), (200), (220), (311), and (222) which were apparent in the patterns of all samples, small traces of Al_4C_3 were observed in the XRD patterns of both the hot compacted-hot extruded and the cast Al-CNT composites. Those traces have intensities that are doubled in the hot compacted-hot extruded Al-CNT sample compared to the cast sample. This behavior contradicts with the experimental results obtained previously by researchers who investigated the interfacial behavior between MWCNTs and aluminum at elevated temperatures stating that the amount of carbides increases as a result of the increase in the process temperature. [93] However, when Al-coated CNTs were used in the current research work, this behavior came in a different manner because of the presence of catalytic

particles on CNTs. These particles shielded the surface of CNTs and prevented it from interacting with aluminum during casting.

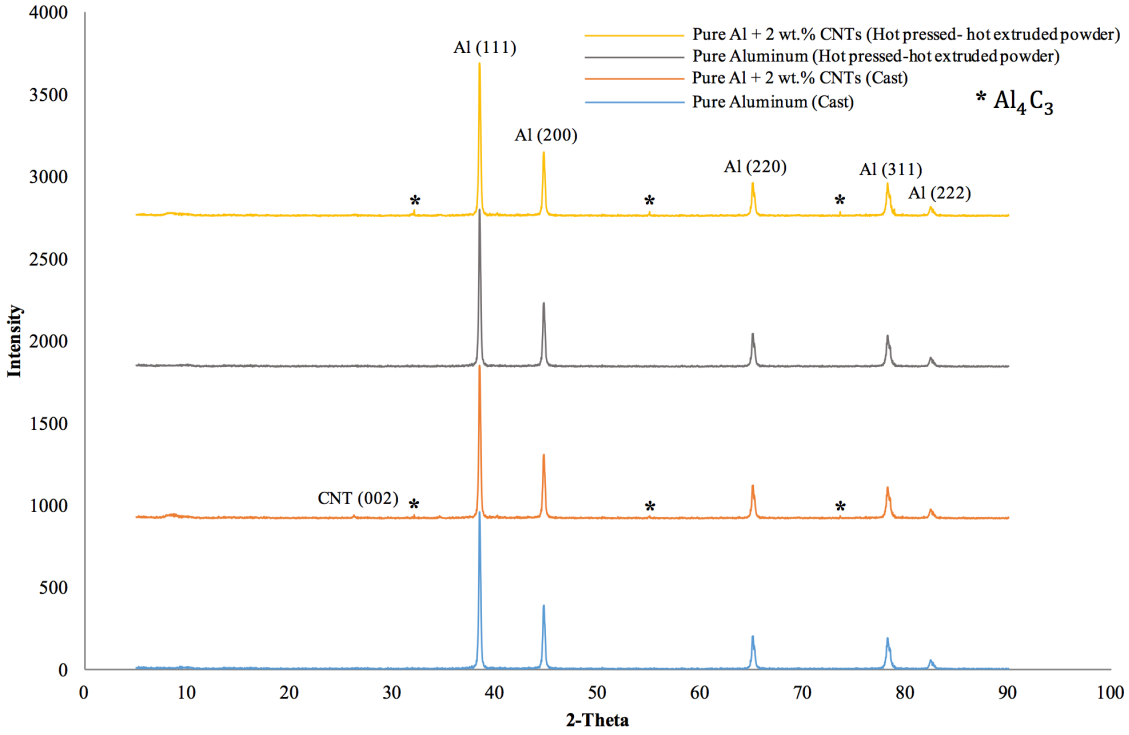

Figure 6-14 XRD pattern of both the hot pressed-hot compacted and cast Al-CNTs samples compared to their pure element.

For the hot compacted-hot extruded samples processed at only 500°C, the carbide peaks were higher due to the effect of compaction on imparting a minimal fracturing in the aluminum coat located on top of CNTs as well as wiping off the some of the catalytic nanoparticles that are electrostatically attached to the surface of CNTs. This fracturing allowed the aluminum matrix to interact chemically with carbon causing the formation of carbides. This reason was one of the factors why the hot pressed-hot compacted sample displayed a lower percentage of elongation than the cast one besides the work hardening of Al during compaction and extrusion. The increase in the ratio of the D-band to the G-band intensities in the powder compacted composite shown previously in the Raman spectra gives another reasonable explanation to the formation of more carbides due to the presence of a little amount of CNTs that have undergone some distortion in their structure forming amorphous carbon. The amorphous carbon is believed to have reacted chemically with aluminum at elevated temperatures forming aluminum carbides in the matrix.

6.4 Results of mechanical testing for bulk samples

For all the tested samples, the overall mechanical properties were measured and averaged from 3 different replicates for each sample. Properties such as tensile strength (TS) in mega pascals (MPa), percent of elongation (EL%), and Vickers hardness number (HV) were measured and listed in Table 6-3 for the cast samples and Table 6-4 for the hot compacted-hot extruded samples. All the samples displayed a standard error (SE) that is less than 1 indicating the consistency of results.

Table 6-3 Mechanical properties of cast samples.

Processing technique	Casting at (710℃)					
Type of sample	Pure aluminum (ingot)			Al+ 2% by weight CNTs		
Mechanical properties (Mean)	TS (MPa)	EL%	HV	TS (MPa)	EL%	HV
Values	58	36.5	36.76	263	6.5	161.046
Standard Error (SE)	0.34	0.3	0.644	0.58	0.37	0.364

Table 6-4 Mechanical properties of hot compacted-hot extruded samples.

Processing technique	Hot compacted (powder) -hot extruded (550℃)					
Type of sample	Pure aluminum			Al+ 2% by weight CNTs		
Mechanical properties (Mean)	TS (MPa)	EL%	HV	TS (MPa)	EL%	HV
Values	105	26.2	72.35	278	4.7	178.82
Standard Error (SE)	0.39	0.24	0.75	0.7	0.58	0.5675

6.4.1 Tensile testing

The tensile testing was done on Al-CNT samples prepared by both casting and hot-compaction followed by hot extrusion. The stress-strain diagrams of all the samples are shown in Figure 6-15. The tensile strength of the hot compacted-hot extruded Al-CNT powder sample was found to be higher than the reinforced cast sample by 5.7%. However, the percent improvement in the tensile strength after adding the 2% by weight of CNTs was 164.76% compared to the pure element fabricated by the same technique. This happened despite of the higher strength of the hot compacted-hot extruded pure aluminum powder sample (105 MPa) compared to the pure cast sample that was expected to be an additional factor in increasing the percentage of improvement in the tensile strength. This might be attributed to the effect of hot compaction and hot extrusion in breaking CNTs and making them less effective in reinforcing the composite.

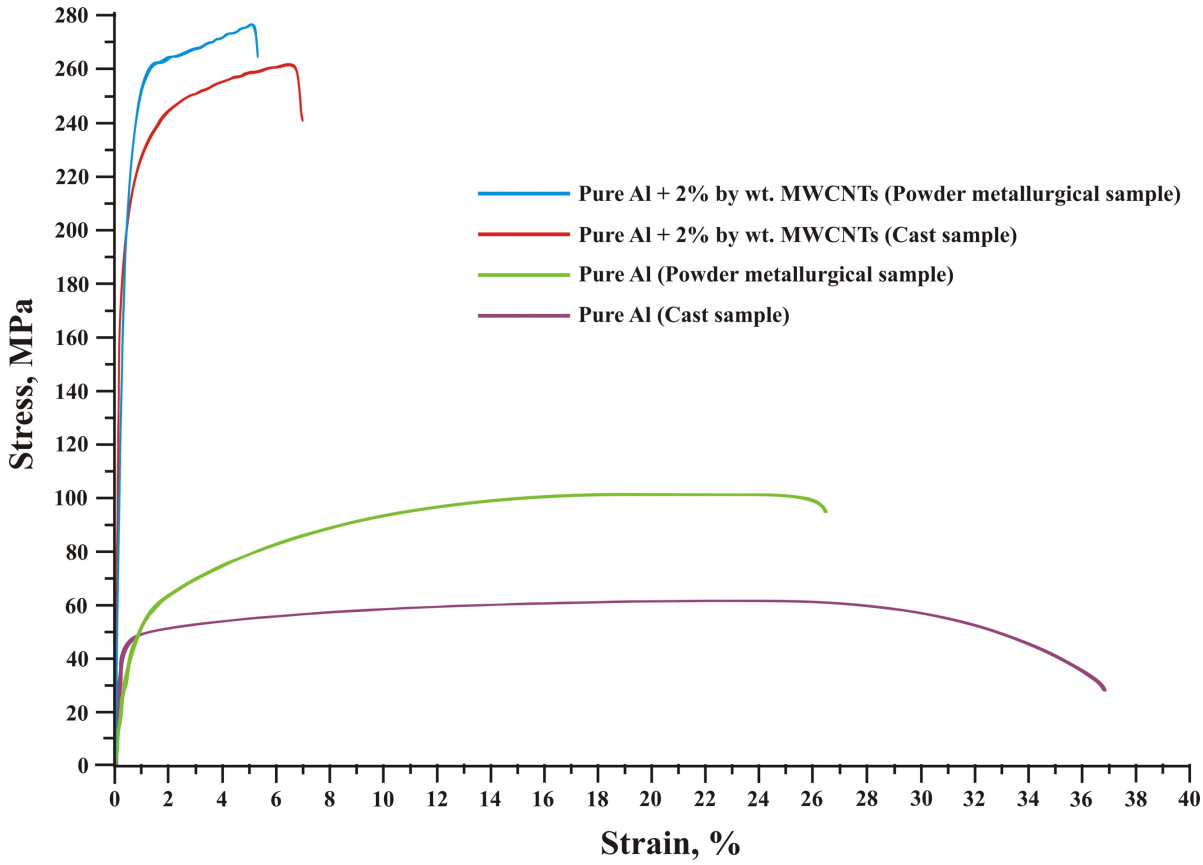

Figure 6-15 Stress-strain diagram of the tested Al-CNT samples and their pure element.

The significant enhancement observed in the tensile strength of all the reinforced samples, however, came at the cost of sacrificing the ductility. The cast Al-CNT sample displayed 6.5 percent of elongation while the hot compacted-hot extruded sample displayed only 4.7 percent of elongation. The reason for this decrease in ductility for the hot compacted-hot extruded Al-CNT sample may be attributed to several factors such as the strain hardening of aluminum during extrusion and the presence of carbides that were present in the XRD pattern as a result of the amorphous carbon formed during the mechanical processing. These low quality carbons were confirmed by the increase of the D-band in the Raman spectrum of the sample.

To compare the tensile strength of the obtained cast and hot compacted samples with samples reported in the literature which are produced by nearly the same processes, Table 6-5 presents two studies in comparison with the produced research work. Study (A) is related to a sample prepared by ball milling of aluminum powder with CNTs followed by pressureless sintering at 550℃ and hot extrusion at 500℃.[118] Study (B) represents a sample prepared by ball milling of Al with CNTs followed by cold compaction (2 Ton/Cm^2), sintering at 580℃ for 90 min, and cold extrusion.[133] Study (C) is related to a sample prepared by mixing MWCNTs with

pure Al and Mg powders in NR followed by melting of aluminum slab on top of the mixture at 800℃.[102]

Table 6-5 Comparison between tensile strength of the obtained samples and samples done with nearly the same methodology.

	Hot compacted Al-CNT sample (current study)	**Study (A) [118]**	**Study (B) [133]**	**Cast sample (current study)**	**Study (C) [102]**
Wt. % of CNTs	2%	2%	2%	2%	2%
TS (MPa)	278	243	184	263	280
Comments	14.4% higher than in study (A). The aluminum powder was not milled with CNTs	Despite of milling CNTs with Al powder	Despite of being cold worked	6% lower than in study (B). No alloying elements were added	Adding of Mg increased the tensile strength

To compare the results of the hot compacted-hot extruded Al-CNT sample to study (A), despite of containing unmilled aluminum powder, the sample in the current study has shown 14.4% increase in the tensile strength compared to study (A). This confirms that adding Al-coated CNTs has improved the tensile strength significantly without any milling to the aluminum matrix. Comparing the same sample to study (B), the sample in the current study has shown 51% increase in tensile strength than in study (B). Therefore, CNTs can lead to a better strengthening effect to the pure aluminum matrix if coated by Al prior to processing.

For the cast sample compared to study (C), the tensile strength of the sample was 6% lower than in study (C). However, the strengthening happened in study (C) could not only be attributed to the presence of CNTs as Mg powder was also mixed with the aluminum powder in the prepared sample.

6.4.2 Hardness measurements

More than fifty micro-indents for each replicate of the samples were used to calculate the Vickers hardness. The results are presented in Figure 6-16. The observed increase in hardness in the composite samples is in agreement with the tensile testing results, i.e., the hot compacted-hot extruded Al-CNT composite had higher hardness than the cast sample.

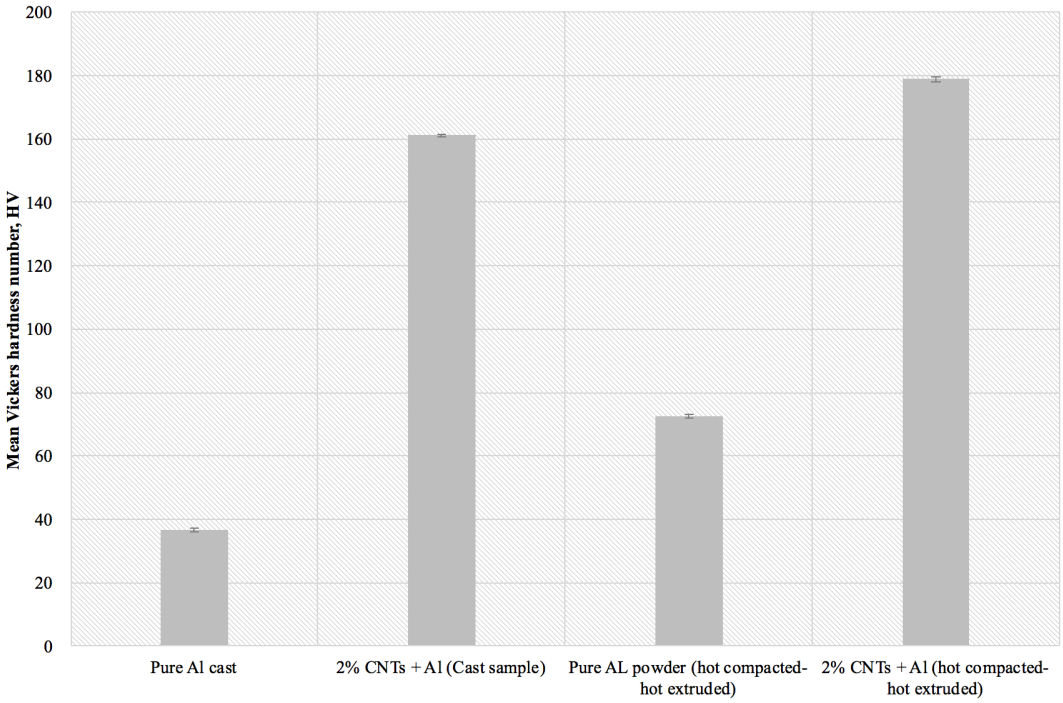

Figure 6-16 Vickers hardness number of the tested Al-CNT samples compared to their pure element.

6.4.3 Nano-scale mechanical properties

- **Nano-hardness**

To conduct nanoindentation, 9 different indents were done on each sample. The distance between indentations was kept fixed at 50 microns. The Nano-hardness measurements for all the samples are shown in Figure 6-17.

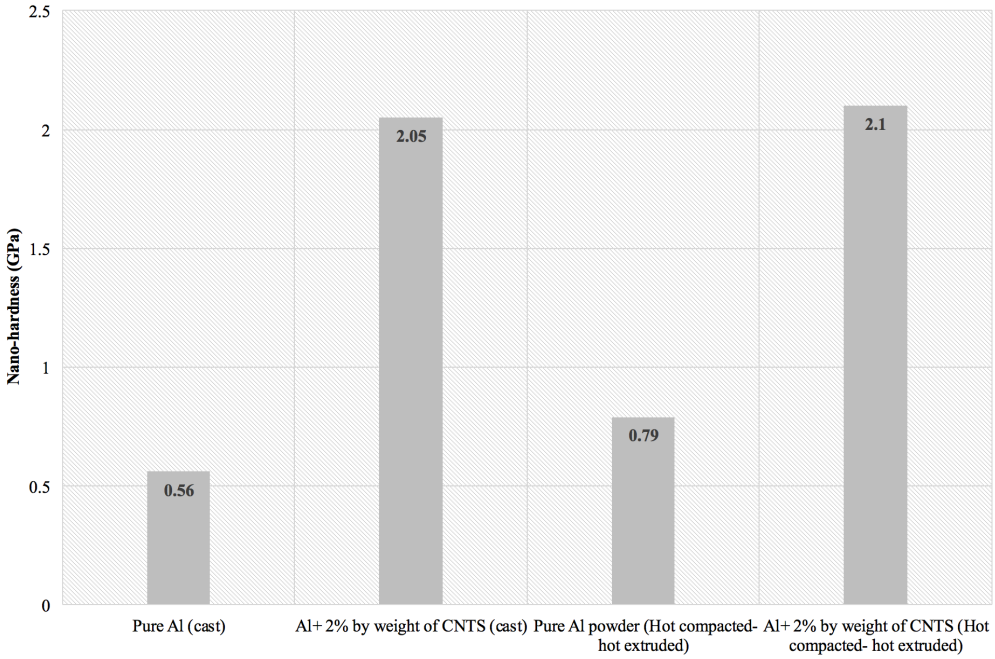

Figure 6-17 Nano-hardness results of the Al-CNT samples in comparison with their pure element.

The results show an improvement in the hardness of both the cast and the hot pressed-hot extruded Al-CNT samples in comparison to the results obtained from the micro-hardness test. One of the main reasons to explain this behavior is that a part of the nanostructured aluminum coat on CNTs was found present in the fracture surface as will be discussed in section 6.4.4 related to the fractography of the tested samples. The nanostructured Al-coats on CNTs are of a higher tensile strength due to their refined structure. Therefore, conducting the nanoindentation on a smaller scale magnified the effect of the refined Al-coats in strengthening the aluminum matrix. The overall improvement in the bulk properties of the composites shows how effective the presence of Al-coated CNTs in the aluminum matrix.

- **Modulus of elasticity**

By conducting nanoindentation of the samples, the modulus of elasticity in gigaPascals (GPa) could be obtained as shown in Figure 6-18. As anticipated, the powder compacted Al-CNT sample displayed a higher elastic modulus than the cast sample. The results came in consistency with the tensile strength values obtained from the tensile test.

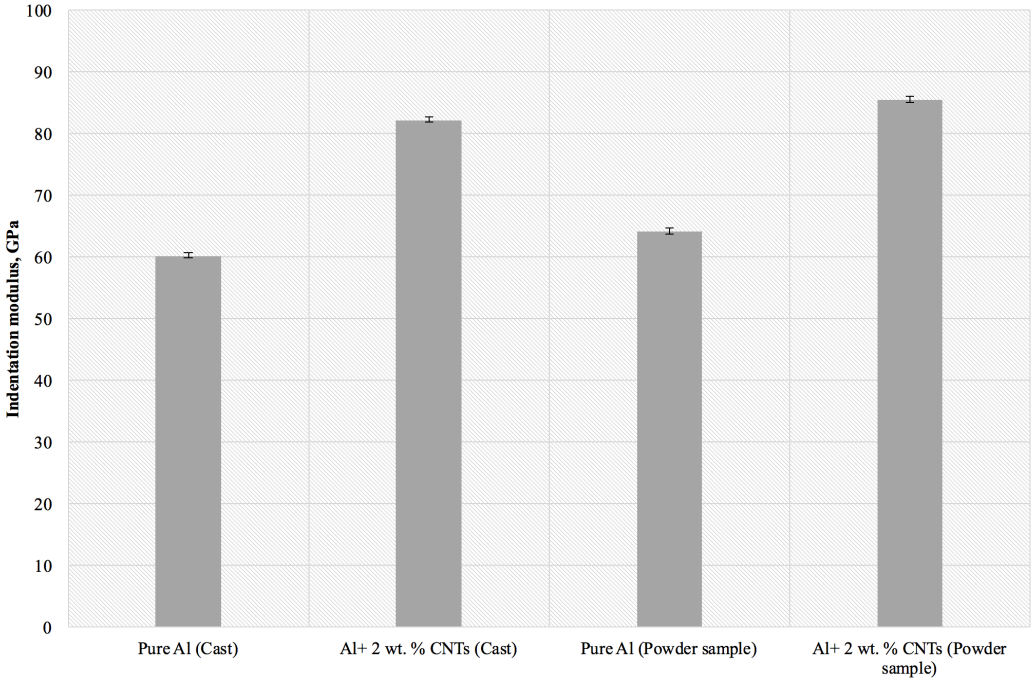

Figure 6-18 Modulus of elasticity of the samples obtained from the nano-indentation test.

The hot compacted-hot extruded Al-CNT samples displayed 36% increase in the nano-indentation modulus compared to pure hot compacted-hot extruded aluminum while the cast Al-CNT sample displayed 37.5% increase in the indentation modulus compared to pure cast aluminum. All these results reflect the effectiveness of adding Al-coated CNTs in reinforcing pure aluminum without being milled in the case of the powder sample and without being annealed or alloyed in the case of casting.

6.4.4 Fractography of the tensile test samples

Failure modes in the 2% CNT reinforced aluminum cast sample in comparison to its pure element:

Figure 6-19 (A) shows the low magnification imaging of the fracture surface of the pure aluminum cast sample suggesting that the fracture is purely ductile. The high percent of elongation obtained in the tensile testing can be validated by looking at the increased flatness of the fracture surface. This flatness suggests that the high purity of the aluminum used in addition to the use of casting in preparing the sample were the key reasons for the high ductility of the sample. Another sign of ductility is the presence of dimples in Figure 6-19 (B).

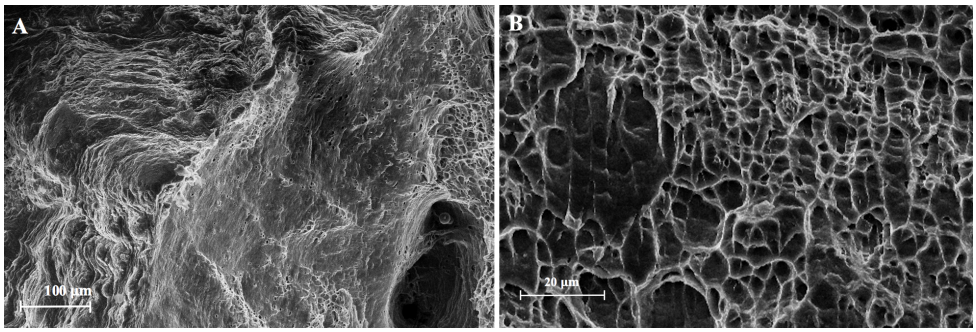

Figure 6-19 Fracture surface of the pure cast aluminum at A) low magnification B) higher magnification.

By conducting high and low magnification SEM imaging on the fracture surface of the CNT reinforced aluminum cast sample, it can be clearly seen that a ductile fracture took place as shown in Figure 6-20 (A-B). The dimples shown in Figure 6-20 (A) are not as deep as the ones displayed in Figure 6-20 (B) for the pure element despite of being imaged at a higher magnification. Therefore, an expected decrease of ductility took place after the Al-coated CNTs were added to the pure matrix. This explanation also matches the stress strain diagram of the cast Al-CNT sample.

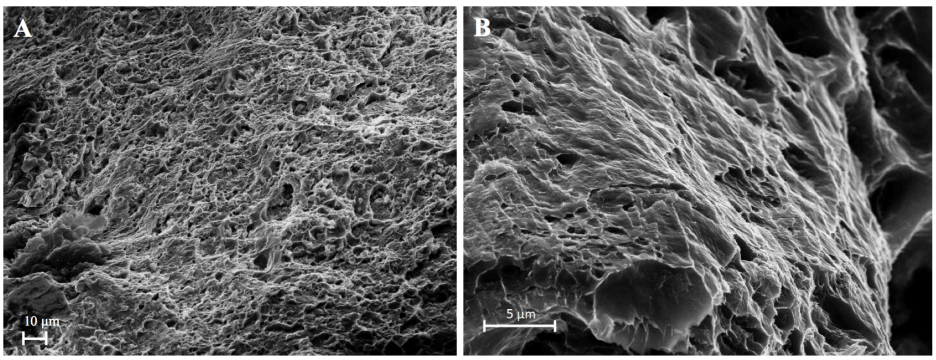

Figure 6-20 Fracture surface of the 2% by weight CNT reinforced Al cast sample at A) low magnification B) higher magnification.

Taking a closer look on the fracture surface of the Al-CNT cast sample as seen in Figure 6-21, a number of protrusions in the aluminum matrix can be noticeable which confirms that the matrix did not undergo brittle fracture.

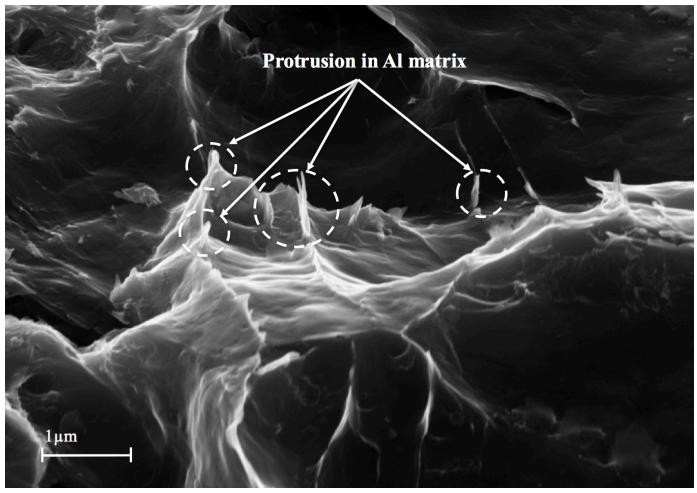

Figure 6-21 SEM image showing protrusion in the aluminum matrix.

In certain regions in the fracture surface of the composite, Al-CNT particulates were found embedded in the aluminum matrix as shown in Figure 6-22. As mentioned before, the Al-coated CNTs used in reinforcing the pure aluminum were not formed as individual CNTs but rather branched CNTs with their original length in the order of tens of microns. Therefore, it is believed that the molten aluminum wetted those branched groups of CNTs through the aluminum coat as a new interface between the molten pure aluminum and CNTs. This wetting resulted in the formation of composite particulates of Al-CNT that has the aluminum coat melted and emerged with the molten aluminum matrix. The length of each group of aluminum coated CNTs is nearly 20-30 μm which is similar to the original length of CNTs that were used as received before being coated with aluminum.

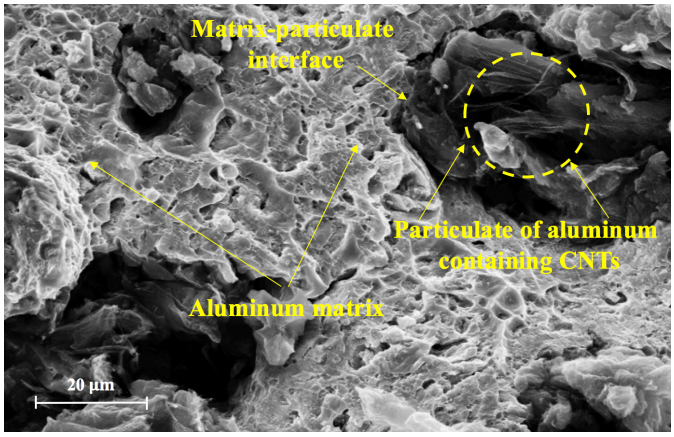

Figure 6-22 SEM image showing the position of AL-CNTs particulates in the Al-CNTs composite.

By imaging the interface between the composite Al-CNT particulate and the aluminum matrix as shown in Figure 6-23, it can be clearly seen that the interfacial area has a continuous phase of the aluminum matrix bonded with the Al-CNT particulate.

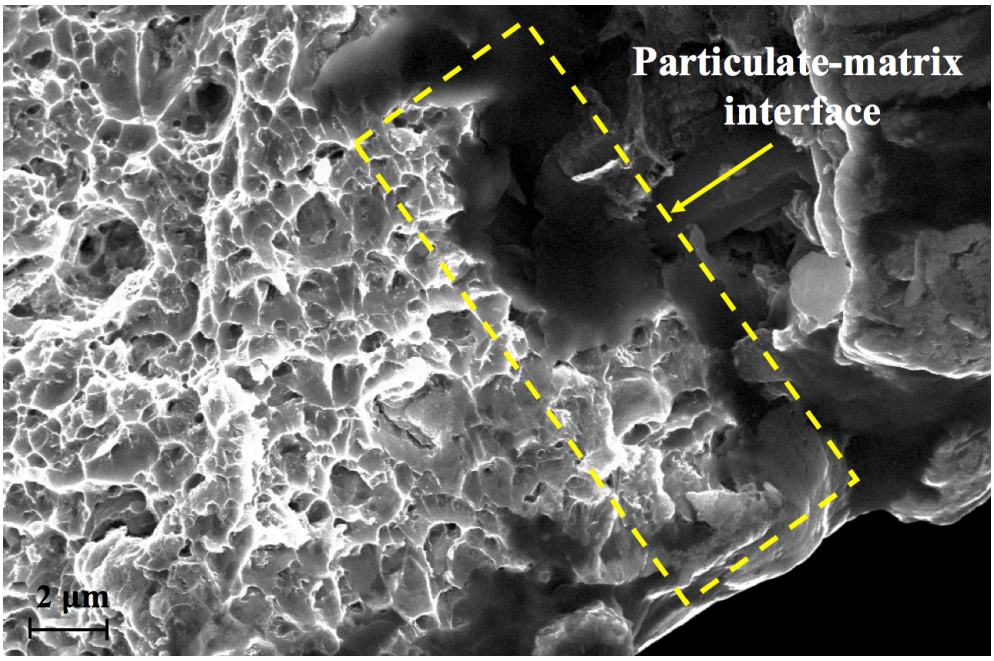

Figure 6-23 A high magnification SEM image showing the interface between an Al-CNT particulate and the aluminum matrix.

The structure of the aluminum matrix looks similar to the ductile structure of the pure sample shown before in Figure 6-19. While the structure of aluminum in the Al-CNT particulate is most probably a mixture between the pure molten aluminum matrix and a part of the aluminum coat that was previously applied on CNTs by electroless deposition. This structure is higher in the hardness and strength since it did not form small protrusions as in the pure aluminum matrix. This could be due to the observed nanostructure of the Al-coat that possesses a higher strength than the aluminum matrix.

- **Al-CNT particulates fracture modes**

Since CNTs are randomly distributed in the matrix, the fracture can be interpreted in both the radial and the axial directions of CNTs.

Radial direction of CNTs

In this fracture mode, the tension applied on the sample came in the radial direction of CNTs causing the fracture to take place in the aluminum-CNT interface as shown in Figure 6-24 (A). The tension applied in the radial direction of the CNT does not result in fracturing the CNT but rather fractures the aluminum matrix around it as illustrated in Figure 6-24(B). As a matter of fact, the aluminum coat produced by electroless plating on CNTs is not chemically bonded to

the CNTs and the only way this coat was held together with each CNT is by mechanical interlocking. Therefore, in the radial direction of a CNT, this Al-CNT interface is most likely to fracture. The energy consumed in fracturing this interface makes the material tougher and prevents the catastrophic failure of the composite.

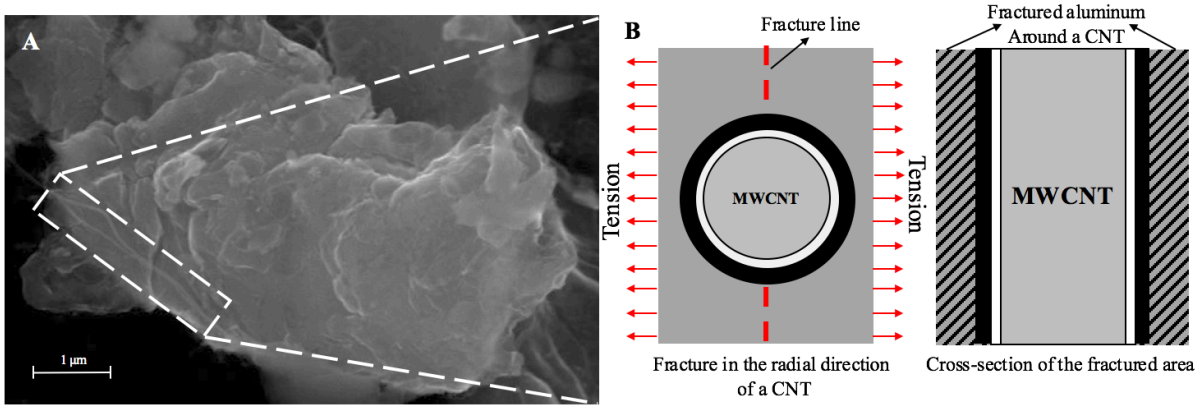

Figure 6-24 A) A high magnification SEM image of Al-CNTs particulate B) explanation of the failure mode in the radial direction of a CNT.

Axial direction of CNTs

This fracture mode supposes that the fracture of the Al-CNT composite took place in the axial direction of a CNT. This means that CNTs are most likely to handle the load after the matrix is fractured causing an increase of tensile strength in the overall composite structure. Figure 6-25 (A) shows an SEM image for a part of the Al-CNT composite where the fracture happened in the axial direction of a CNT. A part of the aluminum coat can be clearly seen on top of a fractured CNT.

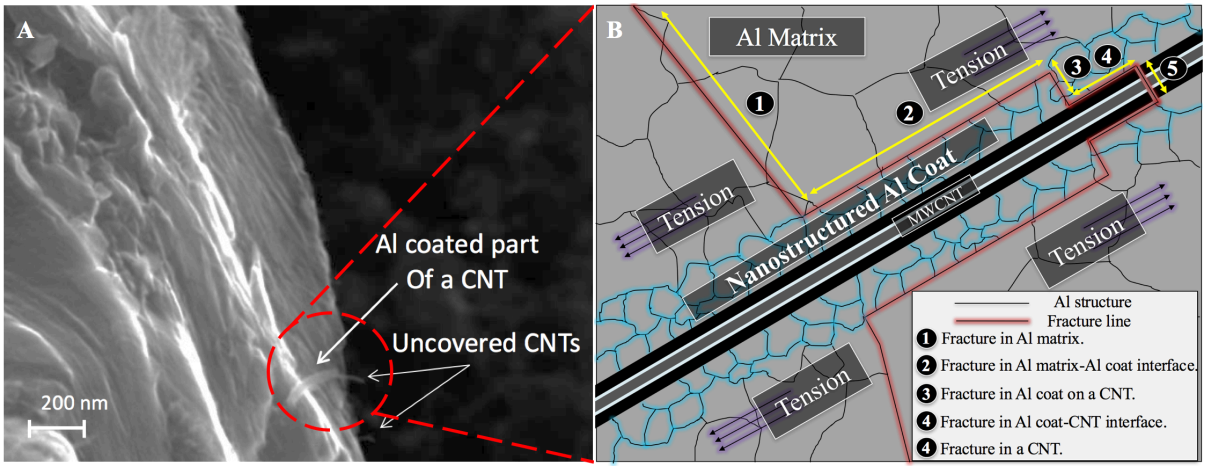

Figure 6-25 A) A high magnification SEM image showing an Al-coated CNT on the fracture surface of the sample B) explanation of the failure mode in the axial direction of a CNT.

The high magnification SEM image revealed an aluminum coated CNT that has a missing part of the aluminum coat. This suggests that the fracture took place on five different modes as illustrated in Figure 6-25 (B). The fracture started primarily in the soft aluminum matrix until it reached the refined aluminum coat that was electroless plated on top of the CNT. Then, the fracture continued on the interface between the aluminum matrix and the refined aluminum coat. Afterwards, the fracture took place in the nanostructured coat until the crack reached the surface of CNTs. Since CNTs have an extremely high tensile strength, the crack fractured the interface between the CNT and the nanostructured aluminum coat. Finally, the CNTs started to handle the entire load before being fractured.

Comparing the dimension of the aluminum coated CNTs shown in figure Figure 6-25 (A) to the originally obtained aluminum coated CNTs, it can be noticed that a part of the aluminum coat has been melted and merged with the molten aluminum matrix while another part of it kept its refined nanostructure that is expected to be slightly higher in strength than the aluminum matrix.

- **Discussion of mechanical properties in relation to the fractography**

The presence of CNTs in their as received form made the reinforcement so effective that the tensile strength increased by 353.4% compared to the pure cast element. The aluminum coat provided on the CNTs helped the molten pure aluminum to penetrate the groups of branched Al-coated CNTs. This resulted in forming composite Al-CNT particulates that are well distributed in the matrix causing a significant improvement in the tensile strength with an adequate percent of elongation.

The 6.5% elongation displayed in the reinforced cast sample reflects that the sample could keep an adequate percent of elongation that might be as a result of using the CNTs as received without subjecting them to harsh mechanical milling. The evidence of that can be seen in the lower intensity of the Al-carbide peaks in the reinforced cast sample.

Failure modes of the 2% CNT reinforced aluminum sample (powder compacted sample) compared to its pure element:

Taking an in-depth look at the high and low magnification images of the fracture surface for the pure hot compacted-hot extruded aluminum sample shown in Figure 6-26 (A-B), it is noticeable that the sample is ductile but less ductile than the pure cast sample. The absence of flatness in the sample can be attributed to the refined aluminum structure that came as a result of the hot compaction of fine aluminum particles.

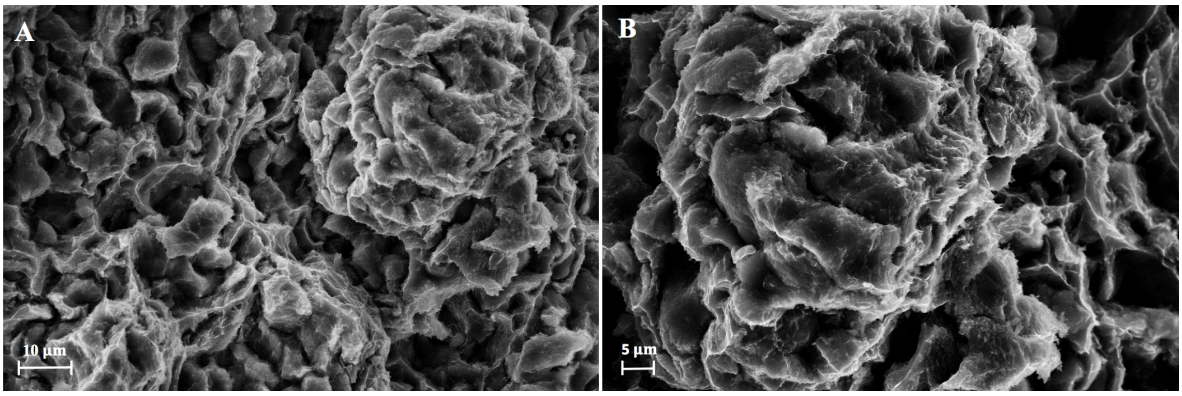

Figure 6-26 Fracture surface of the pure hot compacted-hot extruded aluminum powder at A) low magnification B) higher magnification.

By adding CNTs to pure aluminum, the presence of micro-voids suggests an increase in the brittleness of the sample. However, the cup-cone structures of aluminum can also be seen which suggests that the aluminum matrix has retained its ductility as seen in Figure 6-27 (A-B).

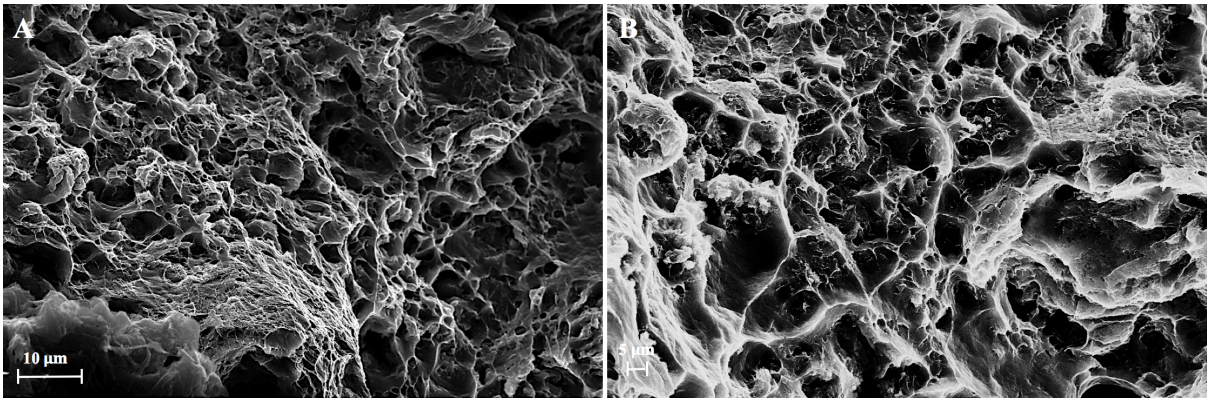

Figure 6-27 Fracture surface of the 2% by weight CNT reinforced hot pressed-hot extruded Al powder sample at A) low magnification, B) higher magnification.

Taking a closer magnification at the sample fractography shown in Figure 6-28, CNTs can be clearly seen in the matrix.

The absence of the aluminum coat on CNTs indicates that the hot compaction and hot extrusion processes have possibly caused the aluminum coat to totally merge with the aluminum matrix. The flatness of the refined aluminum structure at high magnification gives a valid reason for the adequate percent of elongation obtained in the tensile testing of the sample.

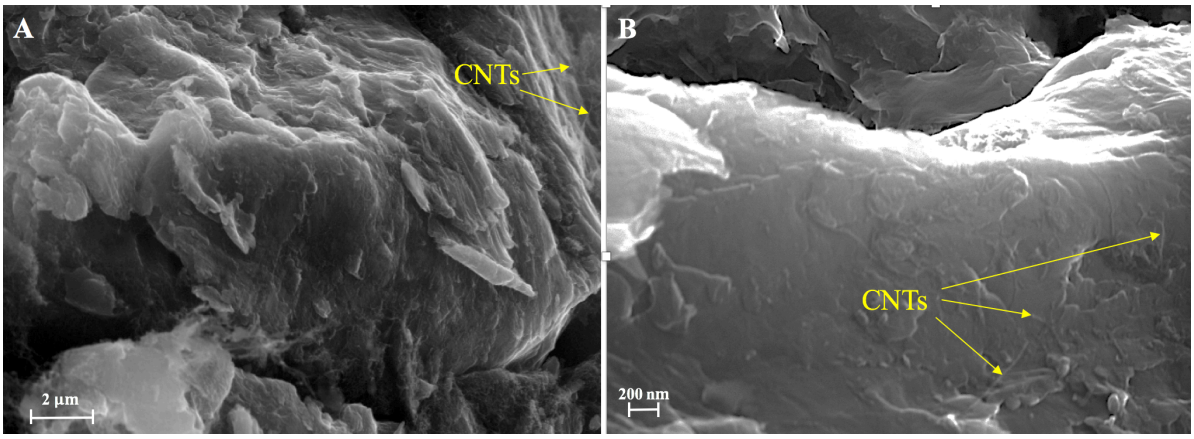

Figure 6-28 High resolution imaging of the fracture surface at A) low magnification, B) higher magnification.

The high elastic modulus and tensile strength of the sample came as a result of the uniform dispersion of CNTs in the matrix. It must be taken into consideration that the aluminum powder used was not subjected to any mechanical milling. Therefore, any strengthening effect shall be as a result of the added Al-coated CNTs and the mechanical work done on the bulk sample such as the hot compaction and hot extrusion. Figure 6-28 (B) shows that CNTs are well dispersed in the matrix. This indicates how effective the aluminum coat was in keeping CNTs apart and helping in their dispersion in the aluminum powder. The nanostructured aluminum coat provided on CNTs could be a considerable factor in increasing the modulus of elasticity for the sample.

7. Summary

1- A novel cost effective aluminum electroless plating process could be achieved by using a 2:1 molar ratio of aluminum chloride and urea respectively in addition to the use of LAH as a reducing agent.

2- Colloidal Pd-Sn one step catalyzation approach was conducted on CNTs to render their surface catalytic prior to being electroless plated.

3- The aluminum electroless plating on catalyzed CNTs resulted in a nanostructured aluminum coat on their surface.

4- The Raman analysis, EDX analysis, and XRD analysis were conducted on Al-coated CNTs to identify the characteristics of both the aluminum coat and the CNTs after being coated. The Raman spectra showed that there was no significant change in the structure of CNTs. The EDX analysis showed that there was a great percent of aluminum present on the surface of CNTs.

5- The Al-coated CNTs were used as a reinforcement for pure aluminum to form Al-CNT composites by both the casting technique and the powder compaction followed by hot extrusion techniques.

6- The Al-coated CNTs were added to the aluminum matrix such that the overall percent of CNTs in the final composite is 2% by weight in both fabrication methods.

7- The cast Al-CNT composites were prepared by melting pure aluminum pieces (99.7%) in a crucible followed by adding a mixture of Al-coated CNTs and a melting flux with continuous stirring. Afterwards, the composite was cast in a stainless steel die.

8- The hot compacted-hot extruded sample was prepared by mixing pure aluminum powder with the Al-coated CNTs in a turbula mixer followed by the hot compaction and hot extrusion in a steel die at 500℃.

9- Mechanical testing was done to determine the change in tensile strength, modulus of elasticity, Vickers hardness, Nano-hardness, and percent of elongation after the Al-coated CNTs were added to the pure aluminum matrix.

10- The mechanical testing showed an increase of 353.4 %, 338.7%, and 266.1% in the tensile strength, Vickers hardness, and nanoindentation hardness of the reinforced cast sample in addition to an increase of 164.8 %, 147.2 %, and 165.8% of the sample properties for the hot compacted-hot extruded reinforced sample.

11- The overall cost and time reduction in producing Al-CNT composite was achieved.

8. Conclusions and recommendations

- By adjusting $AlCl_3$-Urea RTIL adopted from a battery electrolyte, a novel cost effective aluminum electroless deposition process could be achieved. The newly developed RTIL succeeded in coating CNTs uniformly with aluminum despite of their high surface area to volume ratio.
- The cost reduction in the newly developed RTIL helped in preparing sufficient volumes of the electrolyte required for depositing a suitable thickness of aluminum on CNTs.
- The one step colloidal Pd-Sn catalyzation approach was beneficial in limiting the optimization factors of the catalyzation process to only two factors (volume of solution needed for a fixed amount of CNTs and the concentration of the colloidal Pd-Sn concentrate in the final catalyzation solution) instead of four factors in the predecessor two-step tin-chloride sensitization and palladium-chloride activation approach used by previous researchers. Therefore, a significant reduction in the optimization time could be achieved.
- The use of a standard copper-cobalt electroless copper plating electrolyte in optimizing the catalytic solution resulted in reaching the right concentrations and volume of Pd-Sn solution needed for a fixed amount of CNTs by testing the quality of the produced film against each concentration used.
- The narrow size distribution of the colloidal Pd-Sn catalytic nanoparticles in addition to their dimensions that is a fraction of a CNT dimension have led to an effective catalyzation and hence provided an electroless plated film of a great quality.
- The aluminum coat on CNTs grew in a nanostructured manner proving that the colloidal Pd-Sn nanoparticles used in the activation step were effective in the nucleation and film growth.
- The use of Al-coated CNTs in reinforcing pure aluminum has eliminated at least 2 undesirable processing steps along its way in obtaining Al-coated CNT powder. The first undesirable step was the acid functionalization of CNTs that researchers usually do for reducing clustering of CNTs. Secondly, the mechanical milling of CNTs with aluminum powder to get CNTs mechanically interlocked inside aluminum particles. Instead, electroless plating could mechanically interlock CNTs inside aluminum without imparting any damage on the structure of CNTs as concluded from the Raman analysis. These cuts in the processing steps have helped in reducing time and cost of processing.

- The aluminum coat on CNTs could make them dispersible and wettable with molten aluminum as apparent in the fracture surface of the reinforced cast sample.
- The increase in the ratio of the D-band to the G-band of CNTs in the hot compacted-hot extruded sample proves that these two processing steps made some damage to the structure of CNTs resulting in the reduction in ductility and the increase in the formation of aluminum carbide.
- Both the cast and the powder compacted Al-CNT samples have undergone a noticeable strengthening to their structure by the addition of Al-coated CNTs compared to their pure element. However, preserving CNTs in their original form without being damaged made the increase of the tensile strength for the cast sample more effective than in the case of the hot-compacted hot-extruded sample.
- The significant increase of the tensile strength and the elastic modulus of both the cast composite and the hot compacted-hot extruded composite confirmed that Al-CNT composites can be produced by the use of plain aluminum matrices without being annealed, milled, or alloyed.
- The outstanding mechanical properties achieved also give an indication that CNTs on their own if preserved in their original form without being damaged can impart a great improvement in the mechanical characteristics of the composite.
- The use of commercially available supplies such as the colloidal Pd-Sn solution as well as the commercial pure aluminum donated by EgyptAlum company proves that these Al-CNT composites can be produced on an industrial scale in a cost effective manner.

Future recommendations

The new aluminum electroless plating approach was done at room temperature. Therefore, this room temperature technique can be used potentially in thin-film deposition of Al on different substrates especially the temperature sensitive ones.

- Since Al-CNT particulates were formed in the cast sample, it is suggested to conduct acid functionalization of CNTs prior to the electroless plating to help in breaking the branched structure and to make their dispersion better in molten aluminum. However, this is expected to lower the quality of CNTs produced. Therefore, there must be a tradeoff between the quality of CNTs and their dispersion in the matrix.
- The future research work suggests the use of Al-coated CNTs in additive manufacturing (AM) of Al-CNT composites with an expectation that the aluminum coat will help in embedding CNTs in AM layers for aluminum and aluminum alloys. The presence of

Al-coated CNTs in this tiny scale is expected to reduce the laser reflection and scattering on the surface during AM.

- For future applications, aluminum thin films can be electroless plated on conductive and non-conductive substrates for metal cladding. The low capital and running cost of the process makes it an ideal alternative for aluminum PVD and CVD thin film deposition. Finally, electroless aluminum plating can be conducted on ABS plastics after being protected with copper coats. The aluminum coat can be then anodized and filled with different colors that preserve the aesthetic look as well as the functional wear resistance value of the coat.

9. References

[1] O. Carvalho, G. Miranda, D. Soares, and F. S. Silva, "Carbon nanotube dispersion in aluminum matrix composites—Quantification and influence on strength," *Mech. Adv. Mater. Struct.*, vol. 23, no. 1, pp. 66–73, Jan. 2016.

[2] P. Cavaliere, B. Sadeghi, and A. Shabani, "Carbon nanotube reinforced aluminum matrix composites produced by spark plasma sintering," *J. Mater. Sci.*, vol. 52, no. 14, pp. 8618–8629, Jul. 2017.

[3] A. AGARWAL, *CARBON NANOTUBES: reinforced metal matrix composites.* S.l.: CRC PRESS, 2017.

[4] H. Kwon, M. Estili, K. Takagi, T. Miyazaki, and A. Kawasaki, "Combination of hot extrusion and spark plasma sintering for producing carbon nanotube reinforced aluminum matrix composites," *Carbon*, vol. 47, no. 3, pp. 570–577, Mar. 2009.

[5] Z. Y. Liu, S. J. Xu, B. L. Xiao, P. Xue, W. G. Wang, and Z. Y. Ma, "Effect of ball-milling time on mechanical properties of carbon nanotubes reinforced aluminum matrix composites," *Compos. Part Appl. Sci. Manuf.*, vol. 43, no. 12, pp. 2161–2168, Dec. 2012.

[6] A. M. K. Esawi, K. Morsi, A. Sayed, M. Taher, and S. Lanka, "Effect of carbon nanotube (CNT) content on the mechanical properties of CNT-reinforced aluminium composites," *Compos. Sci. Technol.*, vol. 70, no. 16, pp. 2237–2241, Dec. 2010.

[7] A. M. K. Esawi, K. Morsi, A. Sayed, A. A. Gawad, and P. Borah, "Fabrication and properties of dispersed carbon nanotube–aluminum composites," *Mater. Sci. Eng. A*, vol. 508, no. 1–2, pp. 167–173, May 2009.

[8] H. Kwon and M. Leparoux, "Hot extruded carbon nanotube reinforced aluminum matrix composite materials," *Nanotechnology*, vol. 23, no. 41, p. 415701, Oct. 2012.

[9] C. L. Xu, B. Q. Wei, R. Z. Ma, J. Liang, X. K. Ma, and D. H. Wu, "Fabrication of aluminum–carbon nanotube composites and their electrical properties," *Carbon*, vol. 37, no. 5, pp. 855–858, Apr. 1999.

[10] H. Kwon, D. H. Park, J. F. Silvain, and A. Kawasaki, "Investigation of carbon nanotube reinforced aluminum matrix composite materials," *Compos. Sci. Technol.*, vol. 70, no. 3, pp. 546–550, Mar. 2010.

[11] S. Simões, F. Viana, M. A. L. Reis, and M. F. Vieira, "Improved dispersion of carbon nanotubes in aluminum nanocomposites," *Compos. Struct.*, vol. 108, pp. 992–1000, Feb. 2014.

[12] ASM International, P. W. Lee, and ASM International, Eds., *Powder metal technologies and applications*, [10. ed.], 2. print. Materials Park, Ohio: ASM International, 2002.

[13] S. A. Tsukerman, *Powder Metallurgy.* Burlington: Elsevier Science, 2013.

[14] E. Dujardin, T. W. Ebbesen, H. Hiura, and K. Tanigaki, "Capillarity and Wetting of Carbon Nanotubes," *Science*, vol. 265, no. 5180, pp. 1850–1852, Sep. 1994.

[15] S. Arai, Y. Suzuki, J. Nakagawa, T. Yamamoto, and M. Endo, "Fabrication of metal coated carbon nanotubes by electroless deposition for improved wettability with molten aluminum," *Surf. Coat. Technol.*, vol. 212, pp. 207–213, Nov. 2012.

[16] Q. Li, S. Fan, W. Han, C. Sun, and W. Liang, "Coating of Carbon Nanotube with Nickel by Electroless Plating Method," *Jpn. J. Appl. Phys.*, vol. 36, no. Part 2, No. 4B, pp. L501–L503, Apr. 1997.

[17] M. Elsharkawi and A. M. K. Esawi, "Development of an Electroless Plating Process for Multi-wall Carbon Nanotubes (MWCNTS) to Improve Their Dispersion and Wettability in Molten Aluminum," in *Metal-Matrix Composites Innovations, Advances and Applications*, T. S. Srivatsan, Y. Zhang, and W. C. Harrigan, Eds. Cham: Springer International Publishing, 2018, pp. 29–39.

[18] Y. Feng and H. Yuan, “Electroless plating of carbon nanotubes with silver,” *J. Mater. Sci.*, vol. 39, no. 9, pp. 3241–3243, May 2004.
[19] L.-M. Ang, T. S. A. Hor, G.-Q. Xu, C. Tung, S. Zhao, and J. L. S. Wang, “Electroless Plating of Metals onto Carbon Nanotubes Activated by a Single-Step Activation Method,” *Chem. Mater.*, vol. 11, no. 8, pp. 2115–2118, Aug. 1999.
[20] N. Koura *et al.*, “Electroless Plating of Aluminum from a Room-Temperature Ionic Liquid Electrolyte,” *J. Electrochem. Soc.*, vol. 155, no. 2, p. D155, 2008.
[21] I. Shitanda, A. Sato, M. Itagaki, K. Watanabe, and N. Koura, “Electroless plating of aluminum using diisobutyl aluminum hydride as liquid reducing agent in room-temperature ionic liquid,” *Electrochimica Acta*, vol. 54, no. 24, pp. 5889–5893, Oct. 2009.
[22] J. H. Martin, J. A. Kolodziejska, J. J. Vajo, J. A. Graetz, and C. S. Roper, “Method of electroless deposition of aluminum or aluminum alloy, an electroless plating composition, and an article including the same,” US9803283B1, 31-Oct-2017.
[23] S. Iijima, “Helical microtubules of graphitic carbon,” *Nature*, vol. 354, no. 6348, pp. 56–58, Nov. 1991.
[24] null Mintmire, null Dunlap, and null White, “Are fullerene tubules metallic?,” *Phys. Rev. Lett.*, vol. 68, no. 5, pp. 631–634, Feb. 1992.
[25] R. Saito, M. Fujita, G. Dresselhaus, and M. S. Dresselhaus, “Electronic structure of graphene tubules based on C 60,” *Phys. Rev. B*, vol. 46, no. 3, pp. 1804–1811, Jul. 1992.
[26] N. Hamada, S. Sawada, and A. Oshiyama, “New one-dimensional conductors: Graphitic microtubules,” *Phys. Rev. Lett.*, vol. 68, no. 10, pp. 1579–1581, Mar. 1992.
[27] S. Iijima and T. Ichihashi, “Single-shell carbon nanotubes of 1-nm diameter,” *Nature*, vol. 363, no. 6430, pp. 603–605, Jun. 1993.
[28] D. S. Bethune *et al.*, “Cobalt-catalysed growth of carbon nanotubes with single-atomic-layer walls,” *Nature*, vol. 363, no. 6430, pp. 605–607, Jun. 1993.
[29] H. O. Pierson, *Handbook of carbon, graphite, diamond, and fullerenes properties, processing, and applications*. Park Ridge, N.J.: Noyes Publications, 1993.
[30] J. E. Proctor, D. A. Melendrez Armada, and A. Vijayaraghavan, *An introduction to graphene and carbon nanotubes*. Boca Raton: CRC Press, Taylor & Francis Group, 2017.
[31] “Why doesn’t carbon make a tetravalent bond with another carbon atom? - Quora.” [Online]. Available: https://www.quora.com/Why-doesn%E2%80%99t-carbon-make-a-tetravalent-bond-with-another-carbon-atom. [Accessed: 14-Jan-2017].
[32] G. Gunawardena, “Excited-State Atom | OChemPal.” [Online]. Available: http://www.ochempal.org/index.php/alphabetical/e-f/excited-state-atom/. [Accessed: 14-Aug-2018].
[33] M. Endo, T. Hayashi, Y. Ahm Kim, M. Terrones, and M. S. Dresselhaus, “Applications of carbon nanotubes in the twenty-first century,” *Philos. Trans. R. Soc. Math. Phys. Eng. Sci.*, vol. 362, no. 1823, pp. 2223–2238, Oct. 2004.
[34] A. Jorio, Ed., *Raman spectroscopy in graphene related systems*. Weinheim, Germany: Wiley-VCH, 2011.
[35] E. Boysen and N. Boysen, *Nanotechnology for dummies*, 2nd edition. Hoboken, NJ: Wiley Publishing, Inc, 2011.
[36] J. Prasek *et al.*, “Methods for carbon nanotubes synthesis—review,” *J. Mater. Chem.*, vol. 21, no. 40, p. 15872, 2011.
[37] Gore and A. Sane, “Flame Synthesis of Carbon Nanotubes,” in *Carbon Nanotubes - Synthesis, Characterization, Applications*, S. Yellampalli, Ed. InTech, 2011.
[38] “Multi Walled Carbon Nanotubes Products,” *Cheap Tubes*. .

[39] D. Sadyraliev, "Double-Walled Carbon Nanotubes Overview," *Nanografi Nano Technology*. [Online]. Available: https://nanografi.com/blog/doublewalled-carbon-nanotubes-overview/. [Accessed: 14-Aug-2018].
[40] M. S. Dresselhaus, G. Dresselhaus, P. Avouris, and LINK (Online service), *Carbon nanotubes: synthesis, structure, properties, and applications*. Berlin: Springer-Verlag, 2001.
[41] M. Yu, "Strength and Breaking Mechanism of Multiwalled Carbon Nanotubes Under Tensile Load," *Science*, vol. 287, no. 5453, pp. 637–640, Jan. 2000.
[42] W. Ding, L. Calabri, K. M. Kohlhaas, X. Chen, D. A. Dikin, and R. S. Ruoff, "Modulus, Fracture Strength, and Brittle vs. Plastic Response of the Outer Shell of Arc-grown Multi-walled Carbon Nanotubes," *Exp. Mech.*, vol. 47, no. 1, pp. 25–36, Feb. 2007.
[43] B. Peng *et al.*, "Measurements of near-ultimate strength for multiwalled carbon nanotubes and irradiation-induced crosslinking improvements," *Nat. Nanotechnol.*, vol. 3, no. 10, pp. 626–631, Oct. 2008.
[44] S. H. Kim, G. W. Mulholland, and M. R. Zachariah, "Density measurement of size selected multiwalled carbon nanotubes by mobility-mass characterization," *Carbon*, vol. 47, no. 5, pp. 1297–1302, Apr. 2009.
[45] M. Loos, *Carbon nanotube reinforced composites*, First edition. Amsterdam: Elsevier, 2015.
[46] "Kuraray Vectran™ Properties: Tensile Properties." [Online]. Available: http://www.vectranfiber.com/properties/tensile-properties/. [Accessed: 24-Feb-2018].
[47] admin, "Kevlar® Properties | Kevlar® Technical Guide | DuPont USA." [Online]. Available: http://www.dupont.com/products-and-services/fabrics-fibers-nonwovens/fibers/articles/kevlar-properties.html. [Accessed: 18-Mar-2018].
[48] "Steels, General Properties." [Online]. Available: http://www.matweb.com/search/datasheet.aspx?matguid=10e1c14130cd4ed6ae64b85723be53af&n=1. [Accessed: 30-Mar-2018].
[49] "Aluminium - Specifications, Properties, Classifications and Classes." [Online]. Available: https://www.azom.com/article.aspx?ArticleID=2863. [Accessed: 18-Aug-2018].
[50] Q. Han and H. Xi, "Elastic Properties of Carbon Nanotubes," in *Carbon Nanotubes - Polymer Nanocomposites*, S. Yellampalli, Ed. InTech, 2011.
[51] T. Dumitrică, T. Belytschko, and B. I. Yakobson, "Bond-breaking bifurcation states in carbon nanotube fracture," *J. Chem. Phys.*, vol. 118, no. 21, pp. 9485–9488, Jun. 2003.
[52] R. M. Stevens, "New carbon nanotube AFM probe technology," *Mater. Today*, vol. 12, no. 10, pp. 42–45, Oct. 2009.
[53] T. Nishino, T. Ito, and Y. Umezawa, "Carbon Nanotube Scanning Tunneling Microscopy Tips for Chemically Selective Imaging," *Anal. Chem.*, vol. 74, no. 16, pp. 4275–4278, Aug. 2002.
[54] Y. Ando, X. Zhao, H. Shimoyama, G. Sakai, and K. Kaneto, "Physical properties of multiwalled carbon nanotubes," *Int. J. Inorg. Mater.*, vol. 1, no. 1, pp. 77–82, Apr. 1999.
[55] A. Thess *et al.*, "Crystalline Ropes of Metallic Carbon Nanotubes," *Science*, vol. 273, no. 5274, pp. 483–487, Jul. 1996.
[56] H. Dai, A. Javey, E. Pop, D. Mann, W. Kim, and Y. Lu, "Electrical transport properties and field effect transistors of carbon nanotubes," *Nano*, vol. 01, no. 01, pp. 1–13, Jul. 2006.
[57] W. A. de Heer, A. Ch telain, and D. Ugarte, "A Carbon Nanotube Field-Emission Electron Source," *Science*, vol. 270, no. 5239, pp. 1179–1180, Nov. 1995.
[58] A. G. Rinzler *et al.*, "Unraveling Nanotubes: Field Emission from an Atomic Wire," *Science*, vol. 269, no. 5230, pp. 1550–1553, Sep. 1995.

[59] Z. Yao, H. W. C. Postma, L. Balents, and C. Dekker, “Carbon nanotube intramolecular junctions,” *Nature*, vol. 402, no. 6759, pp. 273–276, Nov. 1999.
[60] S. J. Tans, A. R. M. Verschueren, and C. Dekker, “Room-temperature transistor based on a single carbon nanotube,” *Nature*, vol. 393, no. 6680, pp. 49–52, May 1998.
[61] E. D. Cobas, S. M. Anlage, and M. S. Fuhrer, “Single Carbon Nanotube Schottky Diode Microwave Rectifiers,” *IEEE Trans. Microw. Theory Tech.*, vol. 59, no. 10, pp. 2726–2732, Oct. 2011.
[62] A. Jorio, *Raman spectroscopy in graphene related systems*. 2011.
[63] L. M. Malard, M. A. Pimenta, G. Dresselhaus, and M. S. Dresselhaus, “Raman spectroscopy in graphene,” *Phys. Rep.*, vol. 473, no. 5–6, pp. 51–87, Apr. 2009.
[64] M. S. Dresselhaus, G. Dresselhaus, R. Saito, and A. Jorio, “Raman spectroscopy of carbon nanotubes,” *Phys. Rep.*, vol. 409, no. 2, pp. 47–99, Mar. 2005.
[65] V. T. Le, C. L. Ngo, Q. T. Le, T. T. Ngo, D. N. Nguyen, and M. T. Vu, “Surface modification and functionalization of carbon nanotube with some organic compounds,” *Adv. Nat. Sci. Nanosci. Nanotechnol.*, vol. 4, no. 3, p. 035017, Jul. 2013.
[66] J. Zhu *et al.*, “Reinforcing Epoxy Polymer Composites Through Covalent Integration of Functionalized Nanotubes,” *Adv. Funct. Mater.*, vol. 14, no. 7, pp. 643–648, Jul. 2004.
[67] J. Zhu, J. Kim, H. Peng, J. L. Margrave, V. N. Khabashesku, and E. V. Barrera, “Improving the Dispersion and Integration of Single-Walled Carbon Nanotubes in Epoxy Composites through Functionalization,” *Nano Lett.*, vol. 3, no. 8, pp. 1107–1113, Aug. 2003.
[68] H. Fayazfar, A. Afshar, and A. Dolati, “Controlled Growth of Well-Aligned Carbon Nanotubes, Electrochemical Modification and Electrodeposition of Multiple Shapes of Gold Nanostructures,” *Mater. Sci. Appl.*, vol. 04, no. 11, pp. 667–678, 2013.
[69] E. Pop, D. Mann, Q. Wang, K. Goodson, and H. Dai, “Thermal Conductance of an Individual Single-Wall Carbon Nanotube above Room Temperature,” *Nano Lett.*, vol. 6, no. 1, pp. 96–100, Jan. 2006.
[70] S. Sinha, S. Barjami, G. Iannacchione, A. Schwab, and G. Muench, “Off-axis Thermal Properties of Carbon Nanotube Films,” *J. Nanoparticle Res.*, vol. 7, no. 6, pp. 651–657, Dec. 2005.
[71] K. K. Koziol, D. Janas, E. Brown, and L. Hao, “Thermal properties of continuously spun carbon nanotube fibres,” *Phys. E Low-Dimens. Syst. Nanostructures*, vol. 88, pp. 104–108, Apr. 2017.
[72] N. Mingo, D. A. Stewart, D. A. Broido, and D. Srivastava, “Phonon transmission through defects in carbon nanotubes from first principles,” *Phys. Rev. B*, vol. 77, no. 3, Jan. 2008.
[73] J. Mäklin, N. Halonen, O. Pitkänen, G. Tóth, and K. Kordás, “Solder transfer of carbon nanotube microfin coolers to ceramic chips,” *Appl. Therm. Eng.*, vol. 65, no. 1–2, pp. 539–543, Apr. 2014.
[74] E. Thostenson, C. Li, and T. Chou, “Nanocomposites in context,” *Compos. Sci. Technol.*, vol. 65, no. 3–4, pp. 491–516, Mar. 2005.
[75] A. C. Dillon, K. M. Jones, T. A. Bekkedahl, C. H. Kiang, D. S. Bethune, and M. J. Heben, “Storage of hydrogen in single-walled carbon nanotubes,” *Nature*, vol. 386, no. 6623, pp. 377–379, Mar. 1997.
[76] M. Wang, X. Zhao, M. Ohkohchi, and Y. Ando, “Carbon Nanotubes Grown on the Surface of Cathode Deposit by Arc Discharge,” *Fuller. Sci. Technol.*, vol. 4, no. 5, pp. 1027–1039, Sep. 1996.
[77] Y. Ando, X. Zhao, T. Sugai, and M. Kumar, “Growing carbon nanotubes,” *Mater. Today*, vol. 7, no. 10, pp. 22–29, Oct. 2004.

[78] Y. Ando and S. Iijima, “Preparation of Carbon Nanotubes by Arc-Discharge Evaporation,” *Jpn. J. Appl. Phys.*, vol. 32, no. Part 2, No.1A/B, pp. L107–L109, Jan. 1993.
[79] G. G. Tibbetts, “Vapor-grown carbon fibers: Status and prospects,” *Carbon*, vol. 27, no. 5, pp. 745–747, 1989.
[80] R. T. K. Baker, “Catalytic growth of carbon filaments,” *Carbon*, vol. 27, no. 3, pp. 315–323, 1989.
[81] M. Escobar *et al.*, “Synthesis of carbon nanotubes by CVD: Effect of acetylene pressure on nanotubes characteristics,” *Appl. Surf. Sci.*, vol. 254, no. 1, pp. 251–256, Oct. 2007.
[82] T. Guo, P. Nikolaev, A. G. Rinzler, D. Tomanek, D. T. Colbert, and R. E. Smalley, “Self-Assembly of Tubular Fullerenes,” *J. Phys. Chem.*, vol. 99, no. 27, pp. 10694–10697, Jul. 1995.
[83] W. K. Hsu, J. P. Hare, M. Terrones, H. W. Kroto, D. R. M. Walton, and P. J. F. Harris, “Condensed-phase nanotubes,” *Nature*, vol. 377, no. 6551, pp. 687–687, Oct. 1995.
[84] M. Terrones, “Science and Technology of the Twenty-First Century: Synthesis, Properties, and Applications of Carbon Nanotubes,” *Annu. Rev. Mater. Res.*, vol. 33, no. 1, pp. 419–501, Aug. 2003.
[85] I. A. Novoselova *et al.*, “Electrolytic synthesis of carbon nanotubes from carbon dioxide in molten salts and their characterization,” *Phys. E Low-Dimens. Syst. Nanostructures*, vol. 40, no. 7, pp. 2231–2237, May 2008.
[86] S. Manafi, H. Nadali, and H. R. Irani, “Low temperature synthesis of multi-walled carbon nanotubes via a sonochemical/hydrothermal method,” *Mater. Lett.*, vol. 62, no. 26, pp. 4175–4176, Oct. 2008.
[87] Y. Gogotsi, J. A. Libera, and M. Yoshimura, “Hydrothermal synthesis of multiwall carbon nanotubes,” *J. Mater. Res.*, vol. 15, no. 12, pp. 2591–2594, Dec. 2000.
[88] “Teflon Chamber Of Teflon Lined Hydrothermal Synthesis Autoclave Reactor.” [Online]. Available: http://www.toptionlab.com/blogdetail/teflon-chamber-hydrothermal-autoclave-re.html. [Accessed: 19-Jul-2017].
[89] S. R. Bakshi and A. Agarwal, “An analysis of the factors affecting strengthening in carbon nanotube reinforced aluminum composites,” *Carbon*, vol. 49, no. 2, pp. 533–544, Feb. 2011.
[90] T. Kuzumaki, K. Miyazawa, H. Ichinose, and K. Ito, “Processing of Carbon Nanotube Reinforced Aluminum Composite,” *J. Mater. Res.*, vol. 13, no. 09, pp. 2445–2449, Sep. 1998.
[91] A. M. K. Esawi and M. A. El Borady, “Carbon nanotube-reinforced aluminium strips,” *Compos. Sci. Technol.*, vol. 68, no. 2, pp. 486–492, Feb. 2008.
[92] H. Kwon and A. Kawasaki, “Extrusion of spark plasma sintered aluminum-carbon nanotube composites at various sintering temperatures,” *J. Nanosci. Nanotechnol.*, vol. 9, no. 11, pp. 6542–6548, Nov. 2009.
[93] L. Ci, Z. Ryu, N. Y. Jin-Phillipp, and M. Rühle, “Investigation of the interfacial reaction between multi-walled carbon nanotubes and aluminum,” *Acta Mater.*, vol. 54, no. 20, pp. 5367–5375, Dec. 2006.
[94] A. M. K. Esawi, K. Morsi, A. Sayed, M. Taher, and S. Lanka, “The influence of carbon nanotube (CNT) morphology and diameter on the processing and properties of CNT-reinforced aluminium composites,” *Compos. Part Appl. Sci. Manuf.*, vol. 42, no. 3, pp. 234–243, Mar. 2011.
[95] R. Pérez-Bustamante, F. Pérez-Bustamante, I. Estrada-Guel, L. Licea-Jiménez, M. Miki-Yoshida, and R. Martínez-Sánchez, “Effect of milling time and CNT concentration on hardness of CNT/Al2024 composites produced by mechanical alloying,” *Mater. Charact.*, vol. 75, pp. 13–19, Jan. 2013.

[96] H. Kwon, M. Takamichi, A. Kawasaki, and M. Leparoux, "Investigation of the interfacial phases formed between carbon nanotubes and aluminum in a bulk material," *Mater. Chem. Phys.*, vol. 138, no. 2–3, pp. 787–793, Mar. 2013.
[97] T. Laha, S. Kuchibhatla, S. Seal, W. Li, and A. Agarwal, "Interfacial phenomena in thermally sprayed multiwalled carbon nanotube reinforced aluminum nanocomposite," *Acta Mater.*, vol. 55, no. 3, pp. 1059–1066, Feb. 2007.
[98] H. Choi, J. Shin, B. Min, J. Park, and D. Bae, "Reinforcing effects of carbon nanotubes in structural aluminum matrix nanocomposites," *J. Mater. Res.*, vol. 24, no. 08, pp. 2610–2616, Aug. 2009.
[99] Q. Han, R. Setchi, and S. L. Evans, "Characterisation and milling time optimisation of nanocrystalline aluminium powder for selective laser melting," *Int. J. Adv. Manuf. Technol.*, vol. 88, no. 5–8, pp. 1429–1438, Feb. 2017.
[100] A. Maqbool, F. A. Khalid, M. A. Hussain, and N. Bakhsh, "Synthesis of copper coated carbon nanotubes for aluminium matrix composites," *IOP Conf. Ser. Mater. Sci. Eng.*, vol. 60, p. 012040, Jun. 2014.
[101] M. Mansoor and M. Shahid, "Carbon nanotube-reinforced aluminum composite produced by induction melting," *J. Appl. Res. Technol.*, vol. 14, no. 4, pp. 215–224, Aug. 2016.
[102] T. Noguchi, A. Magario, S. Fukazawa, S. Shimizu, J. Beppu, and M. Seki, "Carbon Nanotube/Aluminium Composites with Uniform Dispersion," *Mater. Trans.*, vol. 45, no. 2, pp. 602–604, 2004.
[103] M. A. Maleque, U. Abdullah, I. Yaacob, and Y. Ali, "Characterization of ball-milled carbon nanotube dispersed aluminum mixed powders," *IOP Conf. Ser. Mater. Sci. Eng.*, vol. 123, p. 012011, Apr. 2016.
[104] H. Yan and H. Qiu, "Fabrication of carbon nanotube reinforced A356 nanocomposites," *J. Mater. Res.*, vol. 31, no. 15, pp. 2277–2283, Aug. 2016.
[105] K. P. So *et al.*, "Improving the wettability of aluminum on carbon nanotubes," *Acta Mater.*, vol. 59, no. 9, pp. 3313–3320, May 2011.
[106] T. S. Srivatsan, Y. Zhang, and W. C. Harrigan, Eds., *Metal-Matrix Composites Innovations, Advances and Applications*. Cham: Springer International Publishing, 2018.
[107] G. Xie *et al.*, "Effect of Interface Behavior between Particles on Properties of Pure Al Powder Compacts by Spark Plasma Sintering," *Mater. Trans.*, vol. 42, no. 9, pp. 1846–1849, 2001.
[108] G. Xie *et al.*, "Frequency effect on pulse electric current sintering process of pure aluminum powder," *Mater. Sci. Eng. A*, vol. 359, no. 1–2, pp. 384–390, Oct. 2003.
[109] M. Kubota, "Properties of nano-structured pure Al produced by mechanical grinding and spark plasma sintering," *J. Alloys Compd.*, vol. 434–435, pp. 294–297, May 2007.
[110] M. Zadra, F. Casari, L. Girardini, and A. Molinari, "Spark plasma sintering of pure aluminium powder: mechanical properties and fracture analysis," *Powder Metall.*, vol. 50, no. 1, pp. 40–45, Mar. 2007.
[111] F. A. Khalid, O. Beffort, U. E. Klotz, B. A. Keller, and P. Gasser, "Microstructure and interfacial characteristics of aluminium–diamond composite materials," *Diam. Relat. Mater.*, vol. 13, no. 3, pp. 393–400, Mar. 2004.
[112] R. George, K. T. Kashyap, R. Rahul, and S. Yamdagni, "Strengthening in carbon nanotube/aluminium (CNT/Al) composites," *Scr. Mater.*, vol. 53, no. 10, pp. 1159–1163, Nov. 2005.
[113] S. H. Oh, M. Legros, D. Kiener, and G. Dehm, "In situ observation of dislocation nucleation and escape in a submicrometre aluminium single crystal," *Nat. Mater.*, vol. 8, no. 2, pp. 95–100, Feb. 2009.

[114] S. Nuriel, L. Liu, A. H. Barber, and H. D. Wagner, "Direct measurement of multiwall nanotube surface tension," *Chem. Phys. Lett.*, vol. 404, no. 4–6, pp. 263–266, Mar. 2005.
[115] J. . Molina, R. . Saravanan, R. Arpón, C. García-Cordovilla, E. Louis, and J. Narciso, "Pressure infiltration of liquid aluminium into packed SiC particulate with a bimodal size distribution," *Acta Mater.*, vol. 50, no. 2, pp. 247–257, Jan. 2002.
[116] R. A. Saravanan, J. M. Molina, J. Narciso, C. García-Cordovilla, and E. Louis, "Surface tension of pure aluminum in argon/hydrogen and nitrogen/hydrogen atmospheres at high temperatures," *J. Mater. Sci. Lett.*, vol. 21, no. 4, pp. 309–311, Feb. 2002.
[117] S.-I. Oh *et al.*, "Fabrication of carbon nanofiber reinforced aluminum alloy nanocomposites by a liquid process," *J. Alloys Compd.*, vol. 542, pp. 111–117, Nov. 2012.
[118] R. Pérez-Bustamante *et al.*, "Microstructural and mechanical characterization of Al–MWCNT composites produced by mechanical milling," *Mater. Sci. Eng. A*, vol. 502, no. 1–2, pp. 159–163, Feb. 2009.
[119] K. Morsi and A. Esawi, "Effect of mechanical alloying time and carbon nanotube (CNT) content on the evolution of aluminum (Al)–CNT composite powders," *J. Mater. Sci.*, vol. 42, no. 13, pp. 4954–4959, Jun. 2007.
[120] A. Esawi and K. Morsi, "Dispersion of carbon nanotubes (CNTs) in aluminum powder," *Compos. Part Appl. Sci. Manuf.*, vol. 38, no. 2, pp. 646–650, Feb. 2007.
[121] H. Kwon and A. Kawasaki, "Effect of Spark Plasma Sintering in Fabricating Carbon Nanotube Reinforced Aluminum Matrix Composite Materials," in *Advances in Composite Materials for Medicine and Nanotechnology*, B. Attaf, Ed. InTech, 2011.
[122] H. Hu, "Squeeze casting of magnesium alloys and their composites," *J. Mater. Sci.*, vol. 33, no. 6, pp. 1579–1589, Mar. 1998.
[123] R. Etemadi, "Effect of Processing Parameters and Matrix Shrinkage on Porosity Formation During Synthesis of Metal Matrix Composites with Dual-scale Fiber Reinforcements Using Pressure Infiltration Process," Master thesis, University of Wisconsin Milwaukee, US, 2014.
[124] H. Uozumi *et al.*, "Fabrication process of carbon nanotube/light metal matrix composites by squeeze casting," *Mater. Sci. Eng. A*, vol. 495, no. 1–2, pp. 282–287, Nov. 2008.
[125] S. Zhou, X. Zhang, Z. Ding, C. Min, G. Xu, and W. Zhu, "Fabrication and tribological properties of carbon nanotubes reinforced Al composites prepared by pressureless infiltration technique," *Compos. Part Appl. Sci. Manuf.*, vol. 38, no. 2, pp. 301–306, Feb. 2007.
[126] B. Abbasipour, B. Niroumand, and S. M. Monir Vaghefi, "Compocasting of A356-CNT composite," *Trans. Nonferrous Met. Soc. China*, vol. 20, no. 9, pp. 1561–1566, Sep. 2010.
[127] L. Girisha and R. George, "Study on properties of multi walled carbon nanotube reinforced aluminum matrix composite through casting technique," *Int. J. Eng. Res. Technol.*, vol. 3, no. 4, pp. 1372–1375, Apr. 2014.
[128] K. P. So *et al.*, "SiC formation on carbon nanotube surface for improving wettability with aluminum," *Compos. Sci. Technol.*, vol. 74, pp. 6–13, Jan. 2013.
[129] M. Shahid and M. Mansoor, "Induction melting as a fabrication route for aluminum-carbon nanotubes nanocomposite," *Int. J. Mater. Metall. Eng.*, vol. 10, no. 6, pp. 682–687, 2016.
[130] W. A. Kaczmarek, A. Calka, and B. W. Ninham, "Evaluation of Fe contamination in ball milling of nonmagnetic materials by VSM," *Phys. Status Solidi A*, vol. 141, no. 2, pp. K123–K126, Feb. 1994.

[131] M. Abdellatief, M. Abele, M. Leoni, and P. Scardi, “Solid State Nuclear Magnetic Resonance and X-ray Diffraction Line Profile Analysis of heavily deformed fluorite,” *Thin Solid Films*, vol. 530, pp. 44–48, Mar. 2013.
[132] C. Probst, C. Goujon, R. Gauvin, and R. A. L. Drew, “Enhanced Wettability by Copper Electroless Coating of Carbon Nanotubes,” in *Ceramic Engineering and Science Proceedings*, vol. 26, D. Zhu and K. Plucknett, Eds. Hoboken, NJ, USA: John Wiley & Sons, Inc., 2005, pp. 263–270.
[133] I. Sridhar and K. R. Narayanan, “Processing and characterization of MWCNT reinforced aluminum matrix composites,” *J. Mater. Sci.*, vol. 44, no. 7, pp. 1750–1756, Apr. 2009.
[134] G. O. Mallory, J. B. Hajdu, and American Electroplaters and Surface Finishers Society, *Electroless plating: fundamentals and applications*. Norwich, NY: Knoyes Publications/William Andrew Publishing, 2009.
[135] T. Osaka, “An Electron Diffraction Study on Mixed $PdCl_2/SnCl_2$ Catalysts for Electroless Plating,” *J. Electrochem. Soc.*, vol. 127, no. 11, p. 2343, 1980.
[136] L. G. Svendsen, “Behavior of Pd/Sn and Pd Catalysts for Electroless Plating on Different Substrates Investigated by Means of Rutherford Backscattering Spectroscopy,” *J. Electrochem. Soc.*, vol. 130, no. 11, p. 2252, 1983.
[137] R. . Cohen and R. . Meek, “The chemistry of palladium—tin colloid sensitizing processes,” *J. Colloid Interface Sci.*, vol. 55, no. 1, pp. 156–162, Apr. 1976.
[138] “Classic Plating, Inc. - Redford, MI.” [Online]. Available: http://www.classicplating.com/En.html. [Accessed: 24-Aug-2018].
[139] X. Wei and D. K. Roper, “Tin Sensitization for Electroless Plating Review,” *J. Electrochem. Soc.*, vol. 161, no. 5, pp. D235–D242, 2014.
[140] R. Perumalraj and B. S. Dasaradan, “Electroless nickel plated composite textile materials for electromagnet compatibility,” *Indian J. Fibre Text. Res.*, vol. 36, no. 1, pp. 35–41, Mar. 2011.
[141] P. Bindra, “Mechanisms of Electroless Metal Plating,” *J. Electrochem. Soc.*, vol. 132, no. 11, p. 2581, 1985.
[142] C. K. Mital, P. B. Shrivastava, and R. G. Dhaneshwar, “Studies of electroless nickel deposition using electroanalytical techniques,” *Met. Finish.*, vol. 85, pp. 87–90, Jun. 1987.
[143] M. Paunovic, “Determination of Electroless Copper Deposition Rate from Polarization Data in the Vicinity of the Mixed Potential,” *J. Electrochem. Soc.*, vol. 126, no. 12, p. 2282, 1979.
[144] F. Nuzzi, “Accelearting the rate of electroless copper plating,” *Plat. Surf. Finish.*, vol. 70, pp. 51–54, 1983.
[145] C.-L. Lee, Y.-C. Huang, and L.-C. Kuo, “Catalytic effect of Pd nanoparticles on electroless copper deposition,” *J. Solid State Electrochem.*, vol. 11, no. 5, pp. 639–646, Feb. 2007.
[146] X. Cui, D. A. Hutt, D. J. Scurr, and P. P. Conway, “The Evolution of Pd/Sn Catalytic Surfaces in Electroless Copper Deposition,” *J. Electrochem. Soc.*, vol. 158, no. 3, p. D172, 2011.
[147] C. A. Loto, “Electroless Nickel Plating – A Review,” *Silicon*, vol. 8, no. 2, pp. 177–186, Apr. 2016.
[148] Y. Shacham, “Electroless plating for 2D and 3D printing technologies - Yosi Shacham Technion lecture - YouTube.” [Online]. Available: https://www.youtube.com/watch?v=buYHlNTeiD8. [Accessed: 23-Jan-2017].
[149] T. Ogura, M. Malcomson, and Q. Fernando, “Mechanism of copper deposition in electroless plating,” *Langmuir*, vol. 6, no. 11, pp. 1709–1710, Nov. 1990.

[150] L. M. Abrantes, “On the Mechanism of Electroless Ni-P Plating,” *J. Electrochem. Soc.*, vol. 141, no. 9, p. 2356, 1994.
[151] M. Hartings, “Reactions coupled to palladium,” *Nat. Chem.*, vol. 4, no. 9, pp. 764–764, Sep. 2012.
[152] J. Duffy, “The Effect of pH on Electroless Copper Deposition,” *J. Electrochem. Soc.*, vol. 130, no. 4, p. 876, 1983.
[153] Y. Lantasov, R. Palmans, and K. Maex, “New plating bath for electroless copper deposition on sputtered barrier layers,” *Microelectron. Eng.*, vol. 50, no. 1–4, pp. 441–447, Jan. 2000.
[154] L. M. Ang, T. S. A. Hor, G. Q. Xu, C. H. Tung, S. P. Zhao, and J. L. S. Wang, “Decoration of activated carbon nanotubes with copper and nickel,” *Carbon*, vol. 38, no. 3, pp. 363–372, 2000.
[155] P. Bindra, D. Light, and D. Rath, “Mechanisms of electroless metal plating: I. Mixed potential theory and the interdependence of partial reactions,” *IBM J. Res. Dev.*, vol. 28, no. 6, pp. 668–678, Nov. 1984.
[156] K. P. Yung, J. Wei, and B. K. Tay, “Electroless Plating of Nickel on Carbon Nanotubes Film,” in *2005 7th Electronic Packaging Technology Conference*, Singapore, 2005, vol. 2, pp. 636–638.
[157] J. Park, Y. Jung, P. Kusumah, J. Lee, K. Kwon, and C. Lee, “Application of Ionic Liquids in Hydrometallurgy,” *Int. J. Mol. Sci.*, vol. 15, no. 9, pp. 15320–15343, Aug. 2014.
[158] T. Jiang, M. J. Chollier Brym, G. Dubé, A. Lasia, and G. M. Brisard, “Electrodeposition of aluminium from ionic liquids: Part I—electrodeposition and surface morphology of aluminium from aluminium chloride (AlCl3)–1-ethyl-3-methylimidazolium chloride ([EMIm]Cl) ionic liquids,” *Surf. Coat. Technol.*, vol. 201, no. 1–2, pp. 1–9, Sep. 2006.
[159] T. C. Huynh, Q. P. D. Dao, T.-N. Truong, N.-G. Doan, and S.-L. Ho, “Electrodeposition of Aluminum on Cathodes in Ionic Liquid Based Choline Chloride/Urea/ALCL3,” *Environ. Pollut.*, vol. 3, no. 4, pp. 59–76, Sep. 2014.
[160] G. Yue, S. Zhang, Y. Zhu, X. Lu, S. Li, and Z. Li, “A promising method for electrodeposition of aluminium on stainless steel in ionic liquid,” *AIChE J.*, vol. 55, no. 3, pp. 783–796, Mar. 2009.
[161] M. Hayyan, F. S. Mjalli, M. A. Hashim, I. M. AlNashef, and T. X. Mei, “Investigating the electrochemical windows of ionic liquids,” *J. Ind. Eng. Chem.*, vol. 19, no. 1, pp. 106–112, Jan. 2013.
[162] M. Zhang, V. Kamavarum, and R. G. Reddy, “New electrolytes for aluminum production: Ionic liquids,” *JOM*, vol. 55, no. 11, pp. 54–57, Nov. 2003.
[163] P. Koronaios and R. A. Osteryoung, “Buffering of 1-Ethyl-3-methylimidazolium Chloride/Aluminum Chloride Ionic Liquids Using Alkali Metal Bromides and Iodides,” *J. Electrochem. Soc.*, vol. 148, no. 12, p. E483, 2001.
[164] A. A. Fannin *et al.*, “Properties of 1,3-dialkylimidazolium chloride-aluminum chloride ionic liquids. 2. Phase transitions, densities, electrical conductivities, and viscosities,” *J. Phys. Chem.*, vol. 88, no. 12, pp. 2614–2621, Jun. 1984.
[165] N. V. Plechkova and K. R. Seddon, “Applications of ionic liquids in the chemical industry,” *Chem Soc Rev*, vol. 37, no. 1, pp. 123–150, 2008.
[166] Y. Chryssoulakis, J.-C. Poignet, and G. Manoli, “Electrochemical study of aluminium ion reduction in acidic AlCl3-n-butyl-pyridinium chloride melts,” *J. Appl. Electrochem.*, vol. 17, no. 4, pp. 857–867, Jul. 1987.
[167] C. L. Hussey, “Chloroaluminate Equilibria in the Aluminum Chloride-1-Methyl-3-ethylimidazolium Chloride Ionic Liquid,” *J. Electrochem. Soc.*, vol. 133, no. 7, p. 1389, 1986.

[168] A. A. Fannin, L. A. King, J. A. Levisky, and J. S. Wilkes, “Properties of 1,3-dialkylimidazolium chloride-aluminum chloride ionic liquids. 1. Ion interactions by nuclear magnetic resonance spectroscopy,” *J. Phys. Chem.*, vol. 88, no. 12, pp. 2609–2614, Jun. 1984.
[169] S. Takahashi, L. A. Curtiss, D. Gosztola, N. Koura, and M.-L. Saboungi, “Molecular Orbital Calculations and Raman Measurements for 1-Ethyl-3-methylimidazolium Chloroaluminates,” *Inorg. Chem.*, vol. 34, no. 11, pp. 2990–2993, May 1995.
[170] J. Block and A. P. Gray, “The Thermal Decomposition of Lithium Aluminum Hydride,” *Inorg. Chem.*, vol. 4, no. 3, pp. 304–305, Mar. 1965.
[171] M. Angell *et al.*, “High Coulombic efficiency aluminum-ion battery using an $AlCl_3$ - urea ionic liquid analog electrolyte,” *Proc. Natl. Acad. Sci.*, vol. 114, no. 5, pp. 834–839, Jan. 2017.
[172] S. Osswald, M. Havel, and Y. Gogotsi, “Monitoring oxidation of multiwalled carbon nanotubes by Raman spectroscopy,” *J. Raman Spectrosc.*, vol. 38, no. 6, pp. 728–736, Jun. 2007.
[173] S. K. Singhal, M. Lal, I. Sharma, and R. B. Mathur, “Fabrication of copper matrix composites reinforced with carbon nanotubes using a combination of molecular-level-mixing and high energy ball milling,” *J. Compos. Mater.*, vol. 47, no. 5, pp. 613–621, Mar. 2013.